N–Cα Bond Cleavage Catalyzed by a Multinuclear Iron Oxygenase from a Divergent Methanobactin-like RiPP Gene Cluster

Vasiliki T. Chioti,[†] Kenzie A. Clark,[†] and Mohammad R. Seyedsayamdost[†,‡,*]

[†]Department of Chemistry, Princeton University, Princeton, NJ 08544, United States

[&]Department of Molecular Biology, Princeton University, Princeton, NJ 08544, United States

ABSTRACT: DUF692 multinuclear iron oxygenases (MNIOs) are an emerging family of tailoring enzymes involved in the biosynthesis of ribosomally synthesized and post-translationally modified peptides (RiPPs). Three members, MbnB, TglH, and ChrH, have been characterized to date and shown to catalyze unusual and complex transformations. Using a co-occurrence-based bioinformatic search strategy, we recently generated a sequence similarity network of MNIO-RiPP operons that encode one or more MNIOs adjacent to a transporter. The network revealed >1,000 unique gene clusters, evidence of an unexplored biosynthetic landscape. In this work, we assess an MNIO-RiPP cluster from the network that is encoded in proteobacteria and actinobacteria. The cluster, which we have termed *mov* (for methanobactin-like operon in *Vibrio*), encodes a 23-residue precursor peptide, two MNIOs, a RiPP recognition element, and a transporter. Using both *in vivo* and *in vitro* methods, we show that one MNIO, homologous to MbnB, installs an oxazolone-thioamide at a Thr-Cys dyad in the precursor. Subsequently, the second MNIO catalyzes N–Cα bond cleavage of the penultimate Asn to generate a *C*-terminally amidated peptide. This transformation expands the reaction scope of the enzyme family, marks the first example of an MNIO-catalyzed modification that does not involve Cys, and sets the stage for future exploration of other MNIO-RiPPs.

INTRODUCTION

Ribosomally synthesized and post-translationally modified peptides (RiPPs) are structurally diverse natural products with a range of biological activities.[1–3] Because the biosynthesis of all RiPPs begins with a precursor peptide containing the canonical twenty amino acids, the diversity in this natural product family is generated by tailoring enzymes, which install modifications onto the core region of the precursor, often leading to a variety of alterations that can blur their ribosomal origin.[3,4] A convenient means of categorizing RiPPs, therefore, is by the modifications, and the corresponding tailoring enzymes, involved in their biosynthesis. The ever-growing repository of bacterial genomes has especially benefitted the study of RiPPs through genome mining and prioritization of biosynthetic gene clusters (BGCs) that are predicted to produce novel chemotypes.[5–9] Application of genome mining to RiPPs has expanded the compound family and revealed numerous novel transformations, notably those that encode tailoring metalloenzymes, such as radical *S*-adenosylmethionine (SAM),[9–15] cytochrome P450,[16,17] or copper-dependent enzymes.[18]

An especially intriguing family of RiPPs are those synthesized by the emerging family of multinuclear iron oxygenases (MNIOs), previously known as DUF692 enzymes. Three MNIOs have been studied thus far, MbnB,[19–21] TglH,[22,23] and ChrH[24] from the methanobactin, pearlin, and chryseobasin biosynthetic pathways, respectively. The products of the former two are known, whereas the chryseobasin mature product remains to be characterized. A common theme among the characterized MNIOs is that they modify Cys-rich precursors via four-electron oxidative rearrangements in the absence of reductant, leading to heterocycle/macrocycle formation or β-carbon excision.[19,22,24] Specifically, MbnB in conjunction with its partner protein MbnC,[20] which acts as a scaffold for peptide binding, installs an oxazolone-thioamide at two Cys residues, thus generating the key motif that chelates copper in methanobactin (Figure 1A and S1A). Genes coding for MbnB, MbnC, and the precursor peptide MbnA have been found in several divergent BGCs, which have been categorized in Groups I–V (Figure S1B). Those in Group V contain an additional MNIO, MbnX, with yet unknown function. The second MNIO to be characterized, TglH, converts a terminal Cys residue to 2-mercaptoglycine, releasing the original Cys-Cβ as formic acid for a net four-electron oxidation (Figure 1A). The pearlin pathway is the first to utilize the precursor peptide catalytically, incorporating a Cys residue to be modified by TglH and then cleaving it to liberate the mature amino acid product. Finally, ChrH is the first SAM-dependent MNIO and has been shown to introduce a complex set of alterations onto its precursor including thioether macrocyclization, imidazolidinedione heterocycle formation, and thiomethylation. Over 10,000 MNIOs can be detected in microbial genomes, with the vast majority yet uncharacterized, evidence of a new chemical space that can be charted by focusing on this enzyme family.

Motivated by the biosynthetic promise of MNIOs, we recently generated a sequence similarity network (SSN)[25] of DUF692 enzymes in RiPP biosynthesis, using the near-ubiquitous feature of transporters in RiPP BGCs as a bioinformatic hook in a co-occurrence search.[26] After accounting for newly deposited sequences, the updated SSN consists of 1382 unique MNIO-RiPP BGCs, arranged in a net-

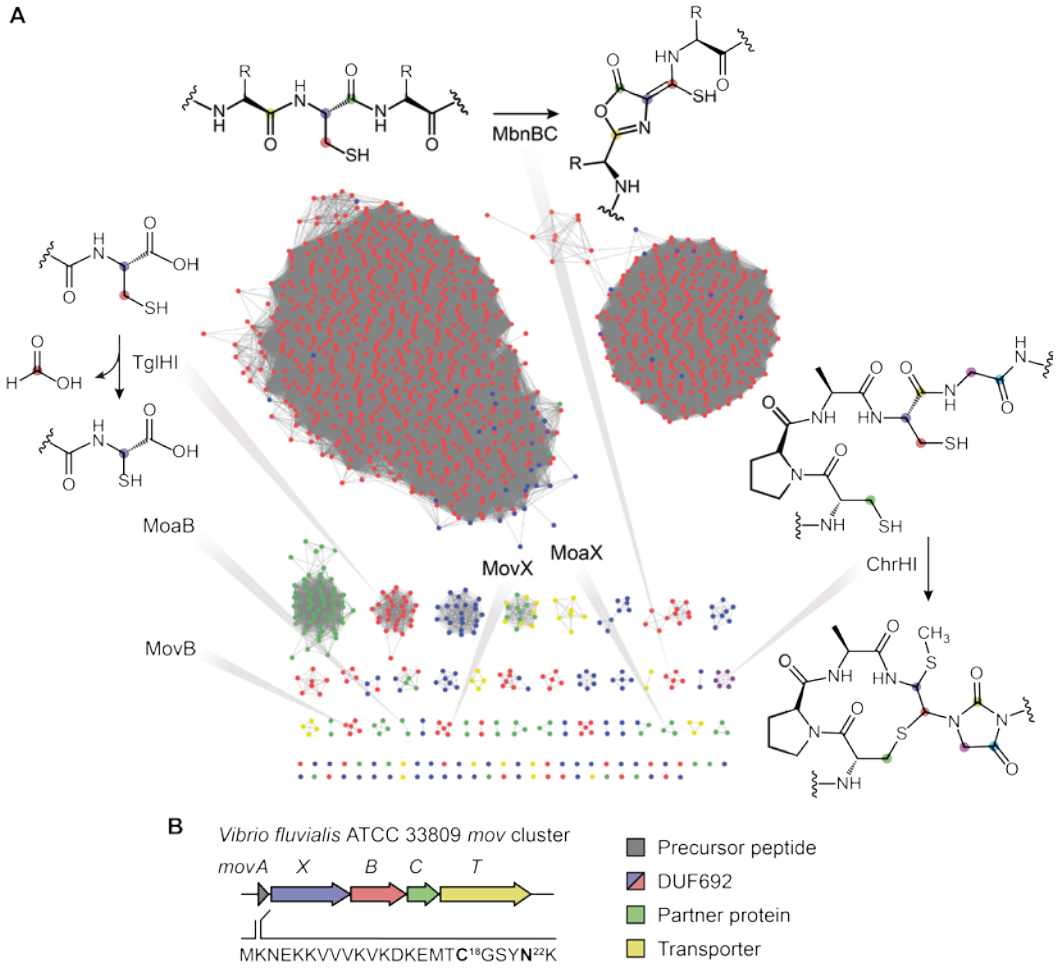

Figure 1. SSN of MNIO-RiPPs and the *mov* BGC studied herein. (A) SSN of RiPP BGCs that encode an MNIO and a neighboring transporter. Each node represents an individual MNIO enzyme, and lines connecting them indicate sequence similarity. Nodes are colored based on phyla: Proteobacteria (red), Actinobacteria (green), Firmicutes (yellow), Bacteroidetes (purple), and other phyla (blue). MNIO-RiPP families investigated in this work (MovX, MovB), related ones in Actinobacteria (MoaX, MoaB), and previously characterized ones (MbnB, TglH, and ChrH) are highlighted; reactions are shown for the latter. (B) The *mov* BGC from *Vibrio fluvialis*, which encodes a precursor peptide (MovA), two MNIOs (MovX, MovB), a discrete RRE (MovC), and a transporter (MovT). Genes are color-coded, and the sequence of the precursor peptide is shown.

work of 43 families with at least two homologous members and 57 singletons (Figure 1A). Notably, the three characterized MNIOs, MbnB, TglH, and ChrH, populate distinct families, affirming the validity of the network. Scanning the network also shows that MNIOs co-occur with various other biosynthetic enzymes, suggesting that complex and new modifications remain to be uncovered from MNIO-RiPPs. In the present work, we tackle a previously uncharacterized MNIO-RiPP BGC that is found in both proteobacterial and actinobacterial genomes and codes for two MNIOs, one that is homologous to MbnB and a divergent one with an extended sequence, previously termed MbnX. We show that the MbnB homolog installs an oxazolone-thioamide motif, much like the modification in methanobactin, while the other MNIO subsequently cleaves the N–Cα bond of the penultimate Asn to generate a *C*-terminally amidated peptide, a new reaction for a DUF692 enzyme. Our findings expand the scope and catalytic versatility of this emerging enzyme family in RiPP biogenesis.

RESULTS

The *mov* BGC from *Vibrio fluvialis*. To begin exploring the network of MNIO-RiPPs, we focused on an operon that encodes two MNIOs, an MbnB homolog and a distantly related and uncharacterized MNIO, previously termed MbnX. We selected the cluster from the commercially available strain *V. fluvialis* 33809 and have termed it *mov* (for methanobactin-like operon in *Vibrio*). The BGC encodes a precursor peptide (MovA), the two MNIOs (MovX and MovB), a discrete RiPP recognition element (RRE, MovC),[27] and a transporter (MovT) (Figure 1B). Compared to MbnAs from Groups I–IV, which contain two conserved Cys residues, Group V precursors contain only one Cys that is conserved in a TCG motif (Figure S1C and S2). Assuming that the Cys residue is modified by MovBC, MovX likely performs a new transformatin on an unprecedented residue for MNIOs. Sequence alignment of the Group V precursors reveals a conserved Tyr-Asn dipeptide motif, which may constitute the site of MovX catalysis (Figure S2).

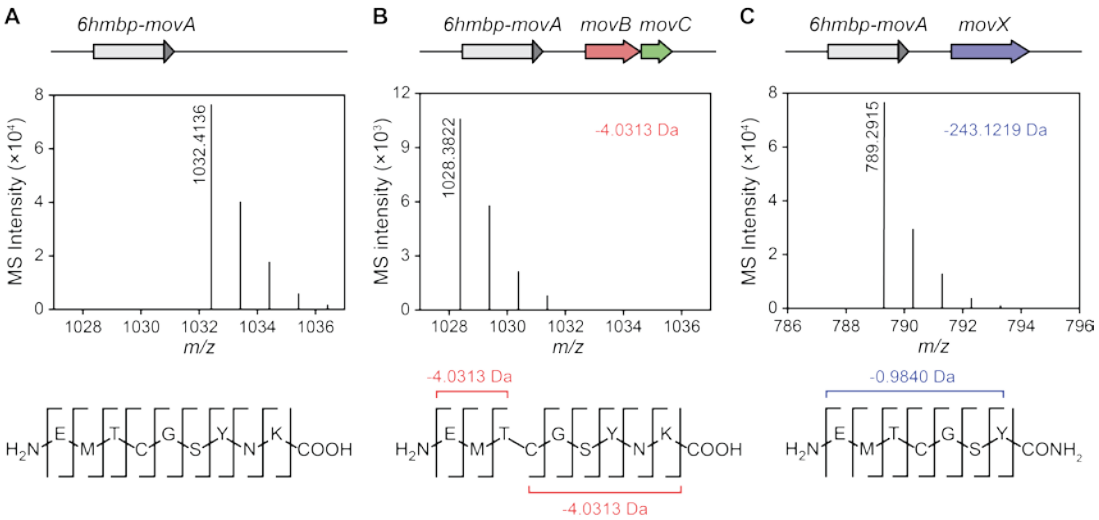

Figure 2. HR-MS and HR-MS/MS analyses of heterologous expression constructs. Shown are data for trypsin-cleaved MovA after co-expression with (A) no enzymes as control, (B) MovBC, and (C) MovX. The construct is shown above each HR-MS profile, which is zoomed in on the $[M+H]^+$ ion of the trypsin-cleaved peptide. Co-expression of MovA with MovBC and MovX gives product that is 4.0313 Da and 243.1219 Da lighter than the substrate, respectively. The HR-MS/MS fragmentation pattern of the MovBC product is consistent with an oxazolone-thioamide motif. HR-MS/MS analysis of the MovX product reveals that the peptide is devoid of the *C*-terminal Asn-Lys dipeptide; while b-ions are unaffected, all observed y-ions exhibit a −0.9840 Da shift relative to the unmodified peptide.

***In vivo* characterization of the *mov* BGC.** To characterize the transformations performed by each biosynthetic enzyme, we first followed a heterologous co-expression approach in *Escherichia coli*. The precursor peptide, MovA, was expressed with an *N*-terminal hexaHis maltose-binding protein (6HMBP) tag and an intervening HRV3C protease cleavage site. Following co-expression with either no enzyme, MovBC, or MovX, the 6HMBP-tagged MovA was purified, liberated by HRV3C proteolysis, and digested with trypsin. The products were then analyzed via HPLC-coupled high-resolution mass spectrometry (HR-MS) and tandem HR-MS (HR-MS/MS).

As expected, expression of 6HMBP-MovA alone, followed by purification and digestion with trypsin, afforded the unmodified *C*-terminal 9mer fragment (Figure 2A, Tables S3–4). Upon co-expression with MovBC, we observed a mass loss of 4.0313 Da accompanied with a shift in retention time (Figure 2B and S3, Table S3). HR-MS/MS analysis located the modification to the Thr-Cys dyad, consistent with an oxazolone-thioamide modification (Figure 2B, Table S5). We additionally observed side products 13.9793 Da heavier and 30.0105 Da lighter than unmodified substrate, reflecting hydrolysis and subsequent decarboxylation of the putative oxazolone ring (Figure S4A–B, Table S6). By contrast, co-expression of 6HMBP-MovA with MovX yielded a *C*-terminal fragment that was 243.1219 Da lighter than the unmodified 9mer peptide, suggesting cleavage of the *C*-terminal Asn-Lys dipeptide in addition to a mass loss of 0.9840 Da, consistent with an O-to-NH conversion (Figure 2C, Table S3). Intriguingly, all b-ions generated in the collision-induced dissociation of the MovX product were either unmodified or not observed, whereas all observed y-ions displayed a −0.9840 Da shift relative to unmodified 7mer peptide, indicating the presence of a *C*-terminal amide (Figure 2C, Table S7).

Repeated attempts to characterize the combined MovXBC-modified product failed as *E. coli* transformants were not viable unless mutations were introduced in the MovA *C*-terminus, suggesting that the co-expression plasmid, and therefore the MovXBC-modified product, was toxic to *E. coli* (Table S8). We thus assessed the products of select mutants that emerged, including two substitutions, C18S- and C18Y-MovA, as well as a deletion mutant that obliterated the *C*-terminal Tyr-Asn dyad of MovA. With both C18S- and C18Y-MovA, co-expression with MovXBC delivered *C*-terminal fragments that were 243.1219 Da lighter than the respective unmodified peptides, indicating that reaction with MovX had occurred (Tables S9–11). Meanwhile, co-expression of the deletion mutant with MovXBC yielded a fragment that was 4.0313 Da lighter than unmodified peptide, indicative of MovBC catalysis (Tables S9 and S12). Overall, the mutations abolished the function of either MovBC or MovX, suggesting that the modifications are mutually exclusive for these MovA variants, and confirming the discrete sites of post-translational tailoring by MovBC and MovX. The strong evolutionary pressure against the synthesis of MovXBC-modified product provides clues for the biological function of the mature *mov*-derived RiPP.

***In vitro* characterization of MovBC and MovX.** To access the MovXBC-modified product and further characterize the MovX reaction, we turned to *in vitro* enzymatic assays. MovX was expressed recombinantly as a hexaHis-tagged construct in *E. coli* and purified by metal affinity chromatography (Figure S5). Despite previous reports showing that MbnB and MbnC co-purify as a heterodimeric

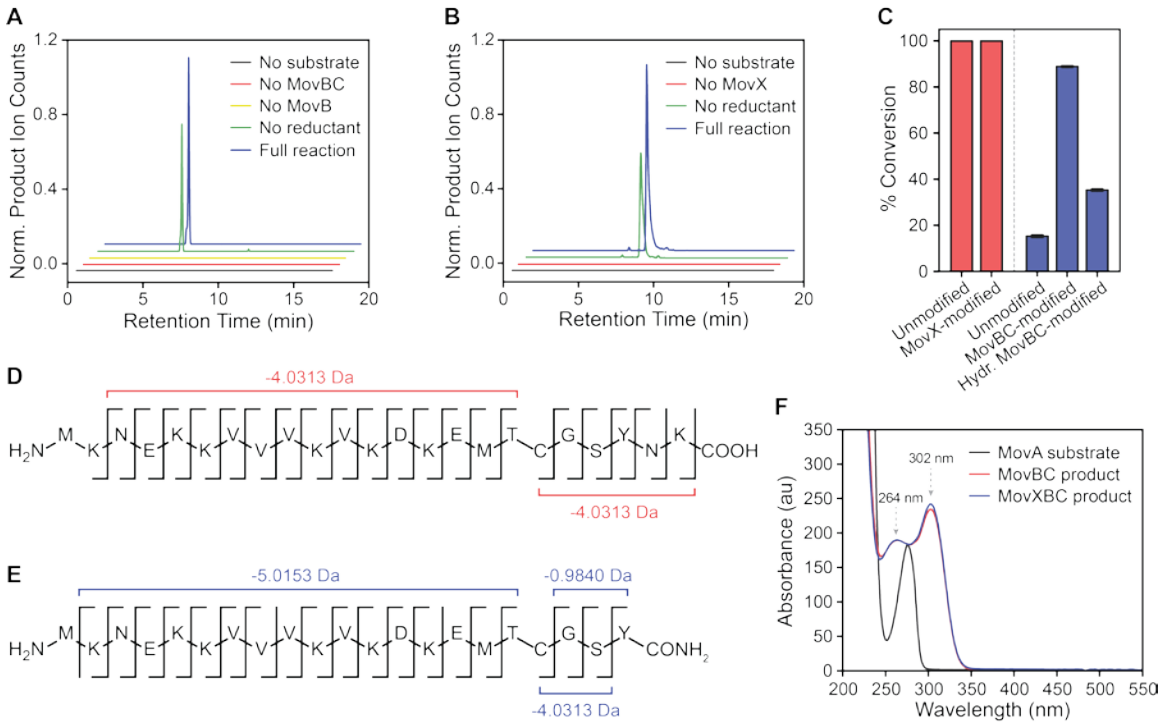

Figure 3. HR-MS and HR-MS/MS analyses of MovBC and MovX products. (A) Enzymatic activity assays of MovBC using MovA as substrate. Shown are extracted ion chromatograms for the −4.03130 Da product of MovBC. Product is not observed when MovB, MovBC, or substrate is omitted from the reaction, while addition of ascorbate increases turnover. (B) Enzymatic activity assays of MovX using MovBC-modified MovA, generated through co-expression of 6HMBP-MovA and MovBC in *E. coli*, as a substrate. Shown are extracted ion chromatograms for the −247.1532 Da product of MovXBC. Product is not observed when MovX or substrate is omitted from the reaction, while addition of ascorbate increases turnover. In panels (A) and (B), traces are offset in both axes for clarity and color-coded as indicated. (C) Substrate preference of MovBC (red) and MovX (blue), as assessed by monitoring conversion of MovA substrate variants by HPLC-coupled HR-MS. MovBC converts both unmodified and MovX-modified MovA to the same extent, while MovX displays a clear preference for MovBC-modified MovA, followed by hydrolyzed MovBC-modified MovA, and unmodified MovA. (D-E) HR-MS/MS analyses of (D) MovBC and (E) MovXBC products. (F) Ultraviolet-visible spectra of unmodified, MovBC-, and MovXBC-modified MovA. Unmodified MovA solely absorbs at 278 nm, while MovBC- and MovXBC-modified MovA exhibit additional absorption features at 264 nm and 302 nm.

complex,[19–21] in our hands MovB purified as a discrete protein when co-expressed with MovC. We therefore expressed and purified MovC separately. MovB and MovX were co-expressed with the GroEL/ES chaperone system and purified anaerobically. Use of molecular chaperones was required for obtaining soluble MovX, likely because it harbors an additional domain with a winged helix-turn-helix (wHTH) topology that is predicted to serve as an RRE (Figure S6A).[27] Iron quantification revealed that MovB and MovX contain 0.7 ± 0.1 and 1.2 ± 0.1 iron atoms per protomer, respectively, reflecting partial incorporation of the metal cofactor (Table S13). As substrates for enzymatic assays, we generated MovA by solid-phase peptide synthesis (SPPS, Figure S7, Table S14), and acquired the MovBC- and MovX-modified variants via co-expression in *E. coli*.

Upon incubation of synthetic MovA with MovBC under aerobic conditions, we observed time-dependent formation of a −4.0313 Da product (Figure 3A and S8A, Tables S15–16). This species was not observed in the absence of MovBC, while incubation with ascorbate increased turnover. HR-MS/MS analysis located the modification to the Thr-Cys dyad, once again consistent with the presence of the oxazolone-thioamide motif (Figure 3D). The MovBC product displayed sharp absorption features at 264 nm and 302 nm, diagnostic of a conjugated ring system (Figure 3F). We also observed side products that were 13.9793 Da heavier and 30.0105 Da lighter than unmodified substrate, reflecting hydrolysis and subsequent decarboxylation of the oxazolone ring, in agreement with the heterologous expression data (Figure S4C). Similar results were obtained with MovX-modified MovA (Figure 3C, Table S15), indicating that MovBC can install its modification on both MovA and MovX-reacted MovA. This result is consistent with a recent crystal structure of MbnABC from *V. caribbenthicus* BAA-2122 (PDB 7DZ9), which shows that the MbnA *C*-terminus extends out of the MbnB active site and minimally interacts with MbnBC.[20]

In contrast to MovB, MovX displayed a clear preference for MovBC-reacted MovA, followed by hydrolyzed MovBC-modified MovA, and finally unmodified MovA (Figure 3C, Tables S15 and S17–18). Upon incubation of MovX with MovBC-modified MovA under aerobic conditions, we observed time-dependent formation of a −243.1219 Da species relative to substrate (Figure 3B and S8B), a product

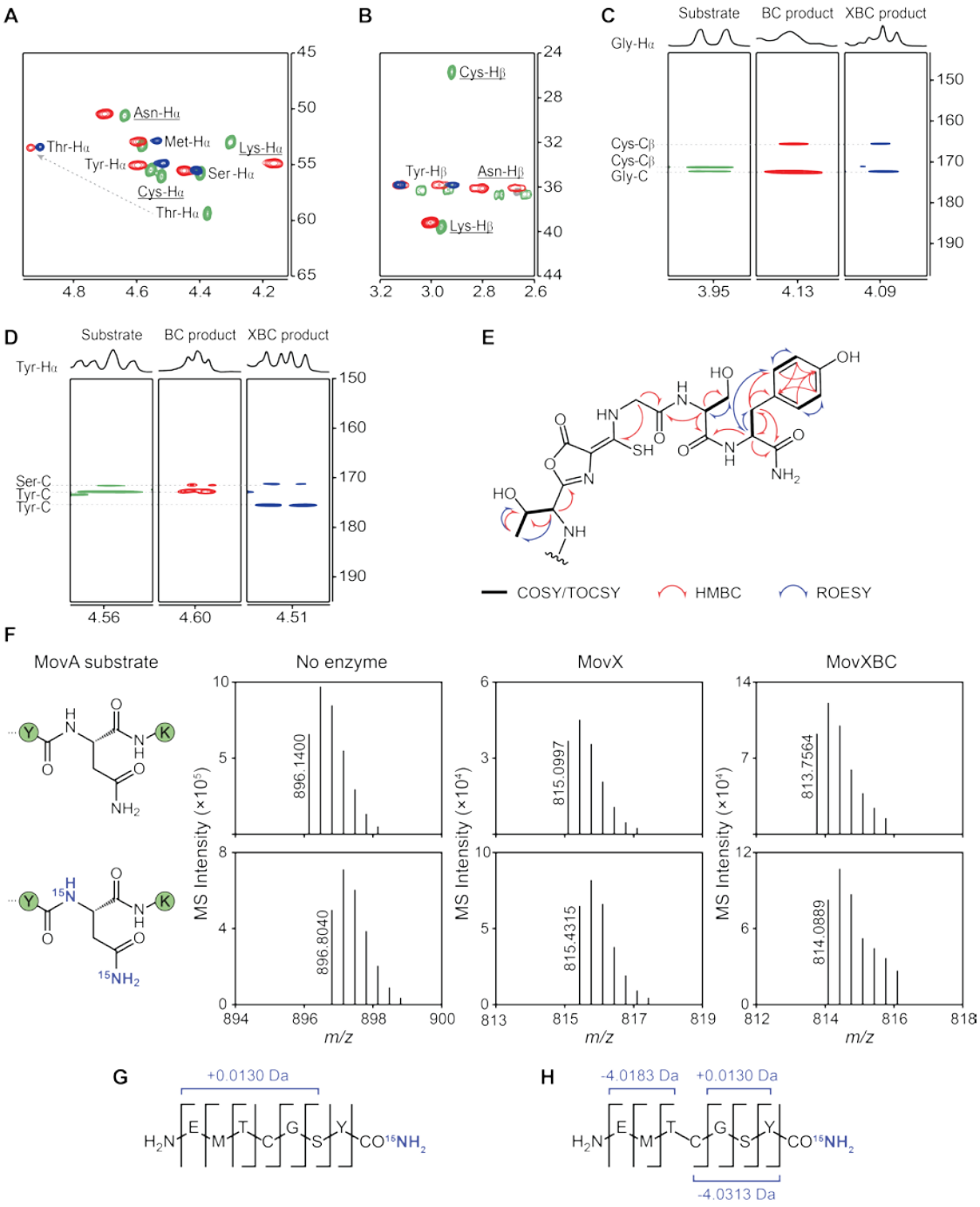

Figure 4. Structural elucidation of the MovBC and MovXBC products by 2D NMR and ^{15}N labeling studies. (A-D) Comparative analysis of 2D NMR spectra of unmodified (green), MovBC-modified (red), and MovXBC-modified (blue) MovA. If present, impurity signals are shown in grey. All observed crosspeaks are labeled and those that drop out post-modification are underlined. (A) HSQC spectra focusing on the Hα region. Compared to unmodified MovA, Cys-Hα is missing from the MovBC-modified product and Thr-Hα is significantly downshifted. Moreover, MovXBC-modified MovA is devoid of Asn-Hα and Lys-Hα. (B) HSQC spectra focusing on the Hβ region. Compared to unmodified MovA, Cys-Hβ is missing from the MovBC-modified product. In addition, MovXBC-modified MovA lacks Asn-Hβ and Lys-Hβ. (C) HMBC spectra highlighting crosspeaks between Gly-Hα and Gly-C and Cys-Cβ. Compared to unmodified MovA, Cys-Cβ shifts upfield in both MovBC- and MovXBC-modified products, while Gly-C remains unchanged. (D) HMBC spectra highlighting crosspeaks between Tyr-Hα and Tyr-C and Ser-C. Compared to unmodified and MovBC-modified MovA, Tyr-C is downshifted in the product, while Ser-C remains unchanged. (E) Relevant NMR correlations used to solve the structure of MovXBC-modified MovA. (F) Reactions of MovX and MovXBC with unlabeled MovA and $^{15}N_2$-Asn-MovA. HR-MS focusing on the $[M+3H]^{3+}$ ion of each peptide. Reactions with $^{15}N_2$-Asn-MovA yielded products 0.9970 Da heavier than the respective MovA products, indicating incorporation of a single ^{15}N label. (G-H) HR-MS/MS analyses of trypsin-cleaved ^{15}N-labeled (G) MovX and (H) MovXBC products after reaction with $^{15}N_2$-Asn-MovA. The observed fragmentation patterns indicate ^{15}N incorporation at the modified *C*-terminus.

that was not observed in the absence of MovX; ascorbate again enhanced product yields. HR-MS/MS analysis indicated an intact oxazolone-thioamide moiety, cleavage of the *C*-terminal Asn-Lys dipeptide, and presence of a *C*-terminal amide (Table S17). Finally, one-pot incubation of synthetic MovA with MovXBC under aerobic conditions yielded product with an overall mass loss of 247.1532 Da and an analogous HR-MS/MS fragmentation pattern as observed for the product of MovX and MovBC-modified MovA (Figure 3E, Table S15 and S19). Relative to the MovBC product, the absorption properties of the MovXBC product were largely unchanged (Figure 3F).

Structural elucidation of the MovXBC product. To definitively elucidate the product of the *mov* BGC, we conducted a large-scale MovX reaction using MovBC-modified MovA as substrate. The trypsin-cleaved MovXBC-modified 7mer peptide was isolated and analyzed by 1D/2D nuclear magnetic resonance (NMR) spectroscopy; trypsin-cleaved MovBC-modified and unmodified 9mer peptides were used for comparison (Table S20, Figures S9–11). Inspection of the $^{1}H–^{13}C$ heteronuclear single quantum coherence (HSQC) spectrum of the MovBC product revealed the disappearance of both Cys-Hα and Cys-Hβ along with a sizeable downfield shift of Thr-Hα from 4.37 ppm to 4.93 ppm (Figure 4A–B). A heteronuclear multiple bond correlation (HMBC) from Gly-Hα to Cys-Cβ, which experienced a significant downshift from 25.7 ppm to 165.6 ppm, provided further evidence for the presence of the oxazolone-thioamide motif (Figure 4C). Equivalent correlations were observed for the MovXBC product, indicating that the modification installed by MovBC remained intact (Figures 4A–C). The HSQC spectrum of the MovXBC product was further devoid of peaks associated with Asn and Lys, indicating cleavage of these *C*-terminal residues (Figure 4A–B). An HMBC correlation from Tyr-Hα to the carbonyl carbon of the same residue, which displayed a downshift from 172.8 ppm to 175.5 ppm relative to unmodified and MovBC-modified peptides, marked the new amidated *C*-terminus (Figure 4D). Collectively, the data are consistent with the structure shown in Figure 4E, and point to a new reaction for the MNIO MovX.

To obtain further evidence for the presence of a *C*-terminal amide, we performed ^{15}N labeling studies. Given that Asn contains two amino groups, we generated a MovA isotopolog containing $^{15}N_2$-Asn at residue 22 by SPPS (Figuyre S7, Figure S12–13) and assessed the fate of the

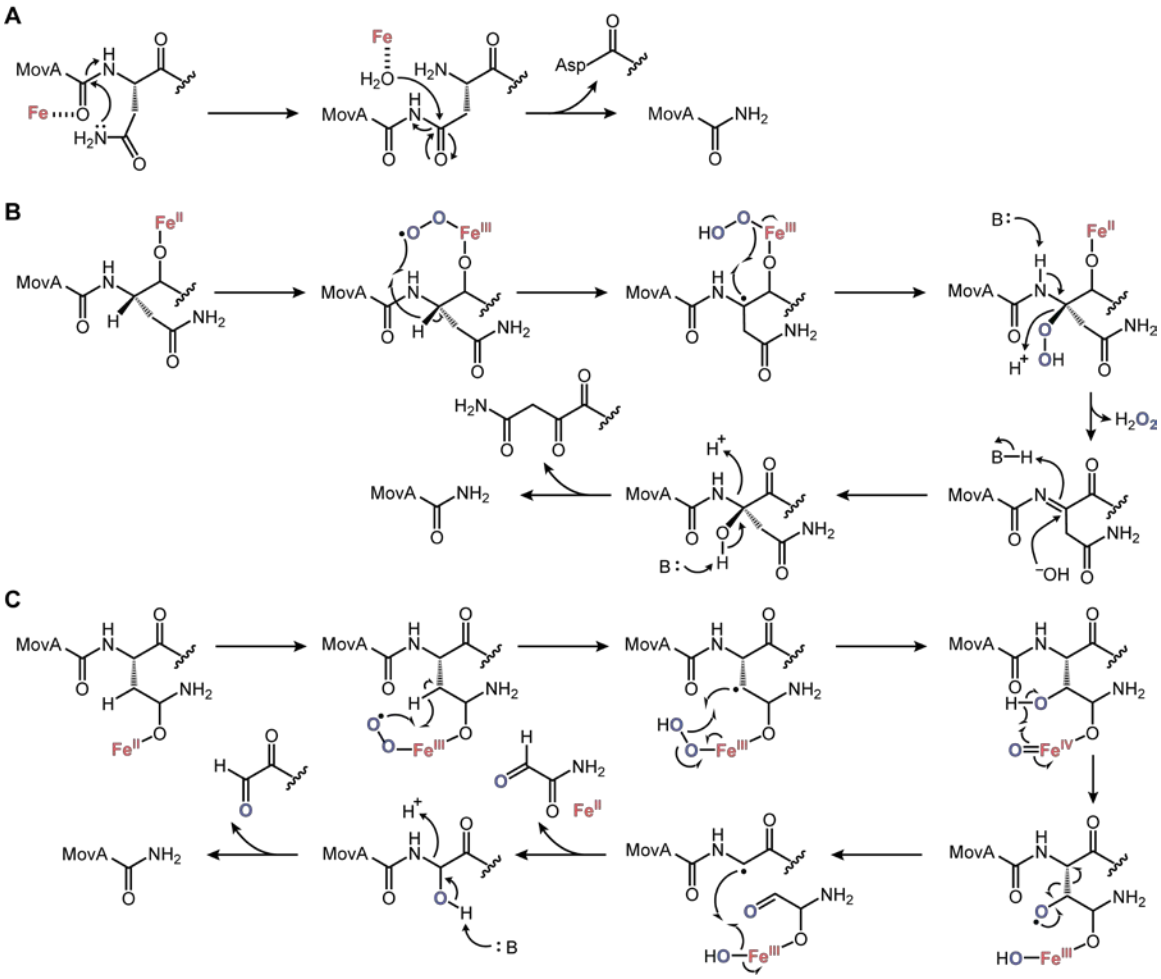

Figure 5. Proposed mechanisms for N–C bond cleavage catalyzed by MbnX. (A) Heterolytic mechanism, in which succinimide formation is followed by Lewis acid-catalyzed hydrolysis to give product. (B) Homolytic mechanism that involves O_2 activation, peroxide rebound, and hydrolysis of an imine intermediate. (C) An alternative homolytic mechanism involving O_2 activation, hydroxylation at Cβ followed by β-scission, and hydroxylation at Cα followed by cleavage of the N–Cα bond. See text for further details.

^{15}N isotopes after reaction with MovX or MovXBC by HR-MS and HR-MS/MS. In both cases, we observed products that were heavier by 0.9970 Da, indicating incorporation of a single ^{15}N isotope (Figure 4F, Table S21) and demonstrating that Asn is the source of the terminal amide-nitrogen. The b-ions generated in the collision-induced dissociation of the ^{15}N-labeled MovX-modified trypsin fragment were either unmodified or not observed, while all observed y-ions displayed a −0.0130 Da shift relative to unmodified 7mer peptide, indicating the presence of a *C*-terminal ^{15}N-amide (Figure 4G, Table S22). Similarly, HR-MS/MS analysis of the ^{15}N-labeled MovXBC-modified fragment located the ^{15}N isotope at the *C*-terminus, thus confirming the structure of the MovX-catalyzed modification (Figure 4H, Table S23).

Toward a Mechanism of MovX. Superposition of an AlphaFold model of MovX onto the crystal structure of MovB from *V. caribbenthicus* BAA-2122 (PDB 7DZ9)[20] reveals all necessary ligands for binding up to three iron atoms (Figure S6B–D). In the MbnB structure, one of these metal ions is coordinated by the Cys residue of MbnA,[20] directing H-atom abstraction from the Cys-Cβ, a feature that unites the three MNIOs studied to date.[19,22,24] Cys ligation to an active-site iron cofactor is unlikely for MovX, as enzymatic activity was retained after substitution of the only Cys in the precursor peptide with Ser or Tyr (Tables S9–11). In line with previous work,[21,28] MovX may require at least two iron atoms for activity: a ferrous iron responsible for dioxygen binding and catalysis, and a ferric iron that facilitates substrate positioning. Furthermore, MovX catalysis proceeded without the addition of external reductant or co-substrates, in support of earlier reports in which MNIOs extract all necessary reducing equivalents from their respective substrates.[19,22,24] However, addition of ascorbate did increase turnover (Figure 3B), likely by reducing one of the Fe(III) ions to the catalytically active Fe(II) species.

We explored three plausible mechanisms for the MovX reaction, the first involving heterolytic Lewis acid catalysis, while the second and third entail canonical oxygen activation and radical chemistry (Figure 5). In the heterolytic pathway, succinimide formation via the Asn22 sidechain, a reaction with precedent in intein splicing, would set up Lewis acid-catalyzed activation of water and subsequent hydrolysis of the succinimide to generate the *C*-amidated product and an Asp-Lys dipeptide (Figure 5A). This mechanism would be oxygen-independent. Alternatively, oxygen binding to Fe(II) could generate an Fe(III)-O_2• species as the oxidant, as previously proposed for the non-heme diiron enzyme myo-inositol oxygenase (MIOX) (Figure 5B).[29,30] H-atom abstraction from the Asn-Cα followed by peroxide rebound, as previously proposed for MIOX, would generate a Cα-hydroperoxo Asn intermediate, which upon elimination of H_2O_2, concomitant with imine formation, and finally hydrolysis would yield product and an Asn-Lys diketone co-product. Finally, we considered H-atom abstraction from Cβ, as proposed for the three MNIOs studied thus far (Figure 5C). In this case, H-atom abstraction would generate an Asn Cβ-based radical that, upon oxygen rebound, would give β-OH-Asn and the Fe(IV)-oxo species. Hydroxyl radical formation, mediated by the highly oxidizing Fe(IV)-oxo species, would facilitate β-scission, as observed for 2-hydroxyethylphosphonate dioxygenase (HEPD)[31] and proposed for TglH,[22] giving rise to a Cα-based radical and 2-oxoacetamide. Another oxygen rebound would set up N–Cα bond cleavage yielding product and *N*-glyoxalyl-L-Lys.

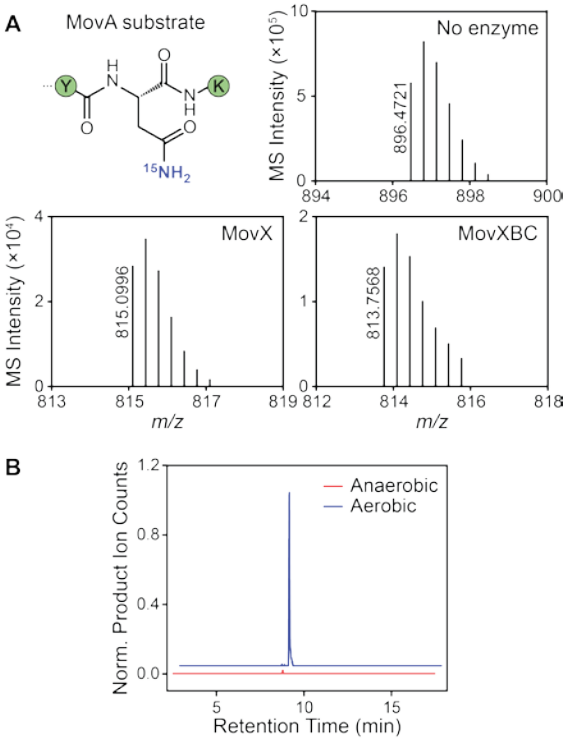

Figure 6. Mechanistic studies with MovX. (A) Reactions of MovX and MovXBC with ^{15}Nβ-Asn-MovA. HR-MS spectra are zoomed in onto the $[M+3H]^{3+}$ peptide ion. The ^{15}N label is not incorporated in the observed products, indicating that the *C*-terminal amide originates from the α-amino group of Asn. (B) Enzymatic activity assays of MovX using MovBC-modified MovA as substrate in the presence or absence of molecular oxygen. Shown are extracted ion chromatograms for the −247.1532-Da product of MovXBC. The MovX reaction proceeds only under aerobic conditions.

As a first step toward differentiating between the heterolytic and homolytic mechanisms, we conducted experiments with a MovA isotopolog containing ^{15}Nβ-Asn at residue 22, which was accessed by SPPS (Figure S7, Figure S14–15). Reaction with MovX or MovXBC, however, only yielded product lacking the ^{15}N isotope (Figure 6A, Table S21). Moreover, no product was observed when the reaction was carried out anaerobically (Figure 6B). Together, these results rule out Mechanism A (Figure 5A) and show that the nitrogen in the product is derived from the α-amino group of Asn (see above). To differentiate between Mechanisms B and C, we attempted to detect the reaction co-product(s). However, repeated attempts using several detection methods, including HPLC-coupled HR-MS with several columns and elution conditions as well as ^{15}N isotope tracing, were unsuccessful, likely due to stability issues. Moreover, efforts to trap the co-product(s) *in situ* using fluorescein-5-thiosemicarbazide,[32] which conjugates

to both ketones and aldehydes, were also unsuccessful. A key feature of Mechanism B is formation of H_2O_2. Assays with a horseradish peroxidase-based H_2O_2 detection system indeed showed enzyme concentration-dependent H_2O_2 formation with similar kinetics as that observed for product (Figure S16). However, it is possible that the second intermediate shown in Mechanism C (Figure 5C), the Fe(III)-hydroperoxo species, uncouples to deliver H_2O_2. The key differentiating feature of Mechanism C is formation of the Fe(IV)=O intermediate. Pre-steady state kinetic and spectroscopic studies will be necessary to differentiate between Mechanisms B and C and provide further insights into the MovX-catalyzed reaction.

Conclusion

The increasing availability of microbial genome sequences and bioinformatic tools has brought about a renaissance in natural product research.[5] Tapping into the biosynthetic potential of underexplored enzyme families using these tools is paramount for expanding our repertoire of enzyme-catalyzed reactions. With this in mind, we recently generated an SSN of MNIO (DUF692) enzymes present in RiPP BGCs.[26] Herein, we have examined a previously uncharacterized MNIO from our network and elucidated a new transformation, thus expanding the reaction scope of this emerging enzyme family and paving the way for future work on other MNIO-RiPP BGCs. It is fair to assume that exciting new reactions will be discovered by exploring MNIO-RiPPs in the future.

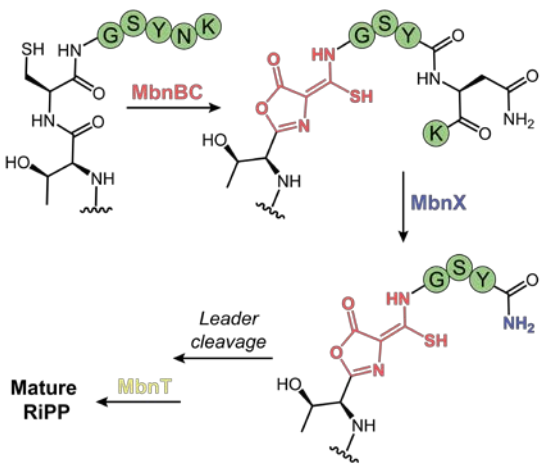

Figure 7. Proposed biosynthesis of the RiPP produced by the *mov* cluster. Upon ribosomal synthesis of the MovA precursor peptide, MovBC catalyzes the formation of the oxazolone-thioamide. MovX then cleaves the N–Cα bond of the penultimate Asn to deliver a *C*-terminally amidated peptide. Following leader peptide cleavage via an unknown mechanism, MovT likely exports the mature RiPP.

All previously studied MNIOs modify Cys residues by oxidative rearrangements that likely commence with H-atom abstraction from the Cys-Cβ.[19,22,24] MovX is the first example of an MNIO that does not modify a Cys residue, but instead catalyzes cleavage of the N–Cα bond of an Asn residue to deliver a *C*-terminally amidated peptide. The MovX reaction resembles that catalyzed by the peptidylglycine α-amidating monooxygenase (PAM), a mammalian bifunctional enzyme involved in the biosynthesis of physiologically important hormones and neurotransmitters, which α-amidates Gly-extended peptides liberating glyoxylate in the process.[33–35] While both PAM and MovX require dioxygen, PAM utilizes a copper- and ascorbate-dependent hydroxylating domain and a zinc-dependent lyase domain for catalysis,[33,35] whereas MovX harbors a singular catalytic domain that presumably binds only iron. PAM hydroxylates the α-carbon of the terminal Gly residue, setting up N–Cα bond cleavage of the resulting hemiaminal.[34] Our proposed pathways involve similar chemistry (Figures 5B–C), though the detailed mechanism of MovX remains to be determined. Aside from providing an additional route for metal-catalyzed amidation, these studies could also uncover the co-product(s), which remained elusive in our studies.

Our findings provide a biosynthetic scheme for the putative mature RiPP from the *mov* BGC. Upon ribosomal synthesis of MovA, MovBC introduces an oxazolone-thioamide motif at Cys18 (Figure 7). Cleavage of the N–Cα bond of the penultimate Asn by MovX then delivers a *C*-terminally amidated peptide. This modification likely protects from proteolytic degradation and increases the hydrophobicity of the peptide by masking the negative charge of the *C*-terminus, which could facilitate transport across cellular membranes and/or interaction with a molecular target.[36] Removal of the leader sequence via an unknown mechanism completes the pathway, followed by export of the mature RiPP via MovT. Despite repeated attempts, we were unable to identify the mature product of the *mov* BGC in culture supernatants of *V. fluvialis*. Supplementing the growth medium with copper, a strategy commonly employed for the isolation of methanobactins,[37] also proved unsuccessful, implying that the *mov* BGC is not responsive to this treatment and perhaps that the mature RiPP lacks copper-chelating properties. Future work will be directed towards identifying the mature RiPP through induction of the *mov* BGC and investigating its bioactivity. The toxic nature of the modified peptide in *E. coli* offers some clues regarding its potential function.

ASSOCIATED CONTENT

Detailed Materials and Methods, tabulated HR-MS and HR-MS/MS data for all products reported, and 1D/2D NMR spectra. This material is available free of charge via the Internet at http://pubs.acs.org.

AUTHOR INFORMATION

Corresponding Author

*Mohammad R. Seyedsayamdost – Departments of Chemistry and Molecular Biology, Princeton University, Princeton, NJ 08544, United States; Email: mrseyed@princeton.edu

Funding Sources

We thank the Edward C. Taylor 3rd Year Fellowship in Chemistry (V.T.C.), the Eli Lilly Edward C. Taylor Fellowship in Chemistry (K.A.C.), and the National Science Foundation (NSF CAREER Award 1847932 to M.R.S.) as well as the National

Institutes of Health (grant GM129496 ad grant GM140034 to M.R.S.) for financial support.

Notes

The authors declare no competing financial interests.

ACKNOWLEDGMENT

We thank Istvan Pelczer for technical support with NMR spectra as well as Dr. Jack G. Ganley and Calvin Spolar for helpful conversations.

REFERENCES

(1) Arnison, P. G.; Bibb, M. J.; Bierbaum, G.; Bowers, A. A.; Bugni, T. S.; Bulaj, G.; Camarero, J. A.; Campopiano, D. J.; Challis, G. L.; Clardy, J.; Cotter, P. D.; Craik, D. J.; Dawson, M.; Dittmann, E.; Donadio, S.; Dorrestein, P. C.; Entian, K.-D.; Fischbach, M. A.; Garavelli, J. S.; Göransson, U.; Gruber, C. W.; Haft, D. H.; Hemscheidt, T. K.; Hertweck, C.; Hill, C.; Horswill, A. R.; Jaspars, M.; Kelly, W. L.; Klinman, J. P.; Kuipers, O. P.; Link, A. J.; Liu, W.; Marahiel, M. A.; Mitchell, D. A.; Moll, G. N.; Moore, B. S.; Müller, R.; Nair, S. K.; Nes, I. F.; Norris, G. E.; Olivera, B. M.; Onaka, H.; Patchett, M. L.; Piel, J.; Reaney, M. J. T.; Rebuffat, S.; Ross, R. P.; Sahl, H.-G.; Schmidt, E. W.; Selsted, M. E.; Severinov, K.; Shen, B.; Sivonen, K.; Smith, L.; Stein, T.; Süssmuth, R. D.; Tagg, J. R.; Tang, G.-L.; Truman, A. W.; Vederas, J. C.; Walsh, C. T.; Walton, J. D.; Wenzel, S. C.; Willey, J. M.; Donk, W. A. van der. Ribosomally Synthesized and Post-Translationally Modified Peptide Natural Products: Overview and Recommendations for a Universal Nomenclature. *Nat. Prod. Rep.* **2012**, *30*, 108–160.

(2) Montalbán-López, M.; Scott, T. A.; Ramesh, S.; Rahman, I. R.; van Heel, A. J.; Viel, J. H.; Bandarian, V.; Dittmann, E.; Genilloud, O.; Goto, Y.; Grande Burgos, M. J.; Hill, C.; Kim, S.; Koehnke, J.; Latham, J. A.; Link, A. J.; Martínez, B.; Nair, S. K.; Nicolet, Y.; Rebuffat, S.; Sahl, H.-G.; Sareen, D.; Schmidt, E. W.; Schmitt, L.; Severinov, K.; Süssmuth, R. D.; Truman, A. W.; Wang, H.; Weng, J.-K.; van Wezel, G. P.; Zhang, Q.; Zhong, J.; Piel, J.; Mitchell, D. A.; Kuipers, O. P.; van der Donk, W. A. New Developments in RiPP Discovery, Enzymology and Engineering. *Nat. Prod. Rep.* **2021**, *38*, 130–239.

(3) McIntosh, J. A.; Donia, M. S.; Schmidt, E. W. Ribosomal Peptide Natural Products: Bridging the Ribosomal and Nonribosomal Worlds. *Nat. Prod. Rep.* **2009**, *26*, 537–559.

(4) Oman, T. J.; van der Donk, W. A. Follow the Leader: The Use of Leader Peptides to Guide Natural Product Biosynthesis. *Nat. Chem. Biol.* **2010**, *6*, 9–18.

(5) Bachmann, B. O.; Van Lanen, S. G.; Baltz, R. H. Microbial Genome Mining for Accelerated Natural Products Discovery: Is a Renaissance in the Making? *J. Ind. Microbiol. Biotechnol.* **2014**, *41*, 175–184.

(6) Cimermancic, P.; Medema, M. H.; Claesen, J.; Kurita, K.; Wieland Brown, L. C.; Mavrommatis, K.; Pati, A.; Godfrey, P. A.; Koehrsen, M.; Clardy, J.; Birren, B. W.; Takano, E.; Sali, A.; Linington, R. G.; Fischbach, M. A. Insights into Secondary Metabolism from a Global Analysis of Prokaryotic Biosynthetic Gene Clusters. *Cell* **2014**, *158*, 412–421.

(7) Ziemert, N.; Alanjary, M.; Weber, T. The Evolution of Genome Mining in Microbes – a Review. *Nat. Prod. Rep.* **2016**, *33*, 988–1005.

(8) Katz, L.; Baltz, R. H. Natural Product Discovery: Past, Present, and Future. *J. Ind. Microbiol. Biotechnol.* **2016**, *43*, 155–176.

(9) Scott, T. A.; Piel, J. The Hidden Enzymology of Bacterial Natural Product Biosynthesis. *Nat. Rev. Chem.* **2019**, *3*, 404–425.

(10) Flühe, L.; Knappe, T. A.; Gattner, M. J.; Schäfer, A.; Burghaus, O.; Linne, U.; Marahiel, M. A. The Radical SAM Enzyme AlbA Catalyzes Thioether Bond Formation in Subtilosin A. *Nat. Chem. Biol.* **2012**, *8*, 350–357.

(11) Schramma, K. R.; Bushin, L. B.; Seyedsayamdost, M. R. Structure and Biosynthesis of a Macrocyclic Peptide Containing an Unprecedented Lysine-to-Tryptophan Crosslink. *Nat. Chem.* **2015**, *7*, 431–437.

(12) Clark, K. A.; Bushin, L. B.; Seyedsayamdost, M. R. RaS-RiPPs in Streptococci and the Human Microbiome. *ACS Bio. Med. Chem. Au* **2022**, *2*, 328–339.

(13) Mahanta, N.; Hudson, G. A.; Mitchell, D. A. Radical S-Adenosylmethionine Enzymes Involved in RiPP Biosynthesis. *Biochemistry* **2017**, *56*, 5229–5244.

(14) Latham, J. A.; Barr, I.; Klinman, J. P. At the Confluence of Ribosomally Synthesized Peptide Modification and Radical S-Adenosylmethionine (SAM) Enzymology. *J. Biol. Chem.* **2017**, *292*, 16397–16405.

(15) Yokoyama, K.; Lilla, E. A. C–C Bond Forming Radical SAM Enzymes Involved in the Construction of Carbon Skeletons of Cofactors and Natural Products. *Nat. Prod. Rep.* **2018**, *35*, 660–694.

(16) Wyche, T. P.; Ruzzini, A. C.; Schwab, L.; Currie, C. R.; Clardy, J. Tryptorubin A: A Polycyclic Peptide from a Fungus-Derived Streptomycete. *J. Am. Chem. Soc.* **2017**, *139*, 12899–12902.

(17) Nam, H.; An, J. S.; Lee, J.; Yun, Y.; Lee, H.; Park, H.; Jung, Y.; Oh, K.-B.; Oh, D.-C.; Kim, S. Exploring the Diverse Landscape of Biaryl-Containing Peptides Generated by Cytochrome P450 Macrocyclases. *J. Am. Chem. Soc.* **2023**, *145*, 22047–22057.

(18) Chigumba, D. N.; Mydy, L. S.; de Waal, F.; Li, W.; Shafiq, K.; Wotring, J. W.; Mohamed, O. G.; Mladenovic, T.; Tripathi, A.; Sexton, J. Z.; Kautsar, S.; Medema, M. H.; Kersten, R. D. Discovery and Biosynthesis of Cyclic Plant Peptides via Autocatalytic Cyclases. *Nat. Chem. Biol.* **2022**, *18*, 18–28.

(19) Kenney, G. E.; Dassama, L. M. K.; Pandelia, M.-E.; Gizzi, A. S.; Martinie, R. J.; Gao, P.; DeHart, C. J.; Schachner, L. F.; Skinner, O. S.; Ro, S. Y.; Zhu, X.; Sadek, M.; Thomas, P. M.; Almo, S. C.; Bollinger, J. M.; Krebs, C.; Kelleher, N. L.; Rosenzweig, A. C. The Biosynthesis of Methanobactin. *Science* **2018**, *359*, 1411–1416.

(20) Dou, C.; Long, Z.; Li, S.; Zhou, D.; Jin, Y.; Zhang, L.; Zhang, X.; Zheng, Y.; Li, L.; Zhu, X.; Liu, Z.; He, S.; Yan, W.; Yang, L.; Xiong, J.; Fu, X.; Qi, S.; Ren, H.; Chen, S.; Dai, L.; Wang, B.; Cheng, W. Crystal Structure and Catalytic Mechanism of the MbnBC Holoenzyme Required for Methanobactin Biosynthesis. *Cell Res.* **2022**, *32*, 302–314.

(21) Park, Y. J.; Jodts, R. J.; Slater, J. W.; Reyes, R. M.; Winton, V. J.; Montaser, R. A.; Thomas, P. M.; Dowdle, W. B.; Ruiz, A.; Kelleher, N. L.; Bollinger, J. M.; Krebs, C.; Hoffman, B. M.; Rosenzweig, A. C. A Mixed-Valent Fe(II)Fe(III) Species Converts Cysteine to an Oxazolone/Thioamide Pair in Methanobactin Biosynthesis. *Proc. Natl. Acad. Sci. USA* **2022**, *119*, e2123566119.

(22) Ting, C. P.; Funk, M. A.; Halaby, S. L.; Zhang, Z.; Gonen, T.; van der Donk, W. A. Use of a Scaffold Peptide in the Biosynthesis of Amino Acid-Derived Natural Products. *Science* **2019**, *365*, 280–284.

(23) McLaughlin, M. I.; Yu, Y.; van der Donk, W. A. Substrate Recognition by the Peptidyl-(S)-2-Mercaptoglycine Synthase TglHI during 3-Thiaglutamate Biosynthesis. *ACS Chem. Biol.* **2022**, *17*, 930–940.

(24) Ayikpoe, R. S.; Zhu, L.; Chen, J. Y.; Ting, C. P.; van der Donk, W. A. Macrocyclization and Backbone Rearrangement During RiPP Biosynthesis by a SAM-Dependent Domain-of-Unknown-Function 692. *ACS Cent. Sci.* **2023**, *9*, 1008–1018.

(25) Gerlt, J. A. Genomic Enzymology: Web Tools for Leveraging Protein Family Sequence-Function Space and Genome Context to Discover Novel Functions. *Biochemistry* **2017**, *56*, 4293–4308.

(26) Clark, K. A.; Seyedsayamdost, M. R. Bioinformatic Atlas of Radical SAM Enzyme-Modified RiPP Natural Products Reveals an Isoleucine–Tryptophan Crosslink. *J. Am. Chem. Soc.* **2022**, *144*, 17876–17888.

(27) Burkhart, B. J.; Hudson, G. A.; Dunbar, K. L.; Mitchell, D. A. A Prevalent Peptide-Binding Domain Guides Ribosomal Natural Product Biosynthesis. *Nat. Chem. Biol.* **2015**, *11*, 564–570.
(28) Wörsdörfer, B.; Lingaraju, M.; Yennawar, N. H.; Boal, A. K.; Krebs, C.; Bollinger, J. M.; Pandelia, M.-E. Organophosphonate-Degrading PhnZ Reveals an Emerging Family of HD Domain Mixed-Valent Diiron Oxygenases. *Proc. Natl. Acad. Sci. USA* **2013**, *110*, 18874–18879.
(29) Brown, P. M.; Caradoc-Davies, T. T.; Dickson, J. M. J.; Cooper, G. J. S.; Loomes, K. M.; Baker, E. N. Crystal Structure of a Substrate Complex of Myo-Inositol Oxygenase, a Di-Iron Oxygenase with a Key Role in Inositol Metabolism. *Proc. Natl. Acad. Sci. USA* **2006**, *103*, 15032–15037.
(30) Xing, G.; Diao, Y.; Hoffart, L. M.; Barr, E. W.; Prabhu, K. S.; Arner, R. J.; Reddy, C. C.; Krebs, C.; Bollinger, J. M. Evidence for C–H Cleavage by an Iron–Superoxide Complex in the Glycol Cleavage Reaction Catalyzed by Myo-Inositol Oxygenase. *Proc. Natl. Acad. Sci. USA* **2006**, *103*, 6130–6135.
(31) Peck, S. C.; Wang, C.; Dassama, L. M. K.; Zhang, B.; Guo, Y.; Rajakovich, L. J.; Bollinger, J. M. Jr.; Krebs, C.; van der Donk, W. A. O–H Activation by an Unexpected Ferryl Intermediate during Catalysis by 2-Hydroxyethylphosphonate Dioxygenase. *J. Am. Chem. Soc.* **2017**, *139*, 2045–2052.
(32) Morinaka, B. I.; Lakis, E.; Verest, M.; Helf, M. J.; Scalvenzi, T.; Vagstad, A. L.; Sims, J.; Sunagawa, S.; Gugger, M.; Piel, J. Natural Noncanonical Protein Splicing Yields Products with Diverse β-Amino Acid Residues. *Science* **2018**, *359*, 779–782.
(33) Bradbury, A. F.; Finnie, M. D. A.; Smyth, D. G. Mechanism of C-Terminal Amide Formation by Pituitary Enzymes. *Nature* **1982**, *298*, 686–688.
(34) Young, S. D.; Tamburini, P. P. Enzymatic Peptidyl .Alpha.-Amidation Proceeds through Formation of an .Alpha.-Hydroxyglycine Intermediate. *J. Am. Chem. Soc.* **1989**, *111*, 1933–1934.
(35) Eipper, B. A.; Milgram, S. L.; Husten, E. J.; Yun, H. Y.; Mains, R. E. Peptidylglycine Alpha-Amidating Monooxygenase: A Multifunctional Protein with Catalytic, Processing, and Routing Domains. *Protein Sci.* **1993**, *2*, 489–497.
(36) Merkler, D. J. C-Terminal Amidated Peptides: Production by the in Vitro Enzymatic Amidation of Glycine-Extended Peptides and the Importance of the Amide to Bioactivity. *Enzyme Microb. Technol.* **1994**, *16*, 450–456.
(37) Bandow, N. L.; Gallagher, W. H.; Behling, L.; Choi, D. W.; Semrau, J. D.; Hartsel, S. C.; Gilles, V. S.; DiSpirito, A. A. Chapter Seventeen - Isolation of Methanobactin from the Spent Media of Methane-Oxidizing Bacteria. In *Methods in Enzymology*; Rosenzweig, A. C., Ragsdale, S. W., Eds.; Methods in Methane Metabolism, Part B: Methanotrophy; Academic Press, 2011; Vol. 495, pp 259–269.

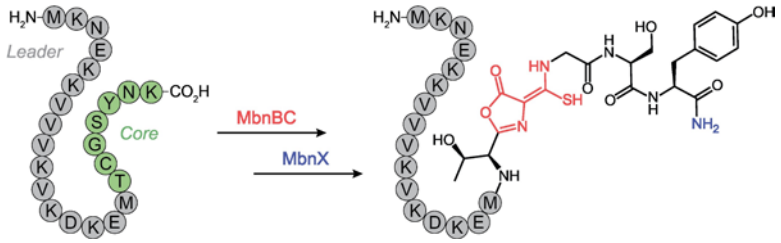

Supplementary Information for

N–Cα Bond Cleavage Catalyzed by a Multinuclear Iron Oxygenase from a Divergent Methanobactin-like RiPP Gene Cluster

Vasiliki T. Chioti,[†] Kenzie A. Clark,[†] and Mohammad R. Seyedsayamdost[†,‡,*]

[†]Department of Chemistry, Princeton University, Princeton, NJ 08544, United States

[‡]Department of Molecular Biology, Princeton University, Princeton, NJ 08544, United States

*Correspondence: mrseyed@princeton.edu

Materials and strains. All materials were obtained from Sigma-Aldrich or Fisher Scientific unless otherwise specified. Competent 5α F'Iq *Escherichia coli*, restriction enzymes, Gibson assembly master mix, trypsin-ultra mass spectrometry grade, shrimp alkaline phosphatase (rSAP), and the corresponding buffers were purchased from New England Biolabs (NEB). DNA purification and gel extraction kits were purchased from Qiagen. Codon-optimized *movA* and *movC* were obtained as linear gene fragments, while *movX*, *movBC*, and *movXBC* were purchased in custom vectors from Twist Bioscience. The *C*-terminal 9mer trypsin fragment of MovA was purchased from GenScript. ^{15}N-labeled amino acids were purchased from Cambridge Isotope Labs (CIL). *Vibrio fluvialis* 33809 was obtained from the American Type Culture Collection (ATCC).

General procedures. High-performance liquid chromatography (HPLC)-coupled high resolution mass spectrometry (HR-MS) and HR-MS/MS were performed on an Agilent 6546 Quadrupole Time-of-flight (Q-Tof) Accurate Mass system, consisting of an automated liquid sampler, a 1260 Infinity Series II HPLC system, a diode array detector, a JetStream electrospray ionization source, and a 6546 Series Q-Tof. HPLC purifications were carried out on Agilent 1260 Infinity Series HPLC systems equipped with a temperature-controlled column compartment, a diode array detector, an automated fraction collector and an automated liquid sampler. Nuclear magnetic resonance (NMR) spectra were collected at the Princeton Chemistry NMR Core Facilities. MovA substrate and product peptide samples were dissolved in D_2O and transferred individually to 2.5-mm diameter tubes. Spectra were collected in the triple resonance cryoprobe of either a Bruker Avance III 800-MHz NMR spectrometer or a Bruker Avance III 500-MHz NMR spectrometer, which were operated using the Bruker Topsin software. 1D/2D NMR data were analyzed with MestReNova, and figures were generated in Adobe Illustrator.

Construction of pRSFDuet-1_6HMBP vectors for *in vivo* activity assays. Amino acid sequences for each gene in the *mov* gene cluster from *V. fluvialis* 33809 were retrieved from the Integrated Microbial Genomes database (locus tags: Ga0174860_121865 for *movX*, Ga0174860_121864 for *movB*, and Ga0174860_121863 for *movC*). Vectors pRSFDuet-1_6HMBP_*movX*, pRSFDuet-1_6HMBP_*movBC*, and pRSFDuet-1_6HMBP _*movXBC*, in which codon-optimized genes encoding MovX, MovB and MovC are arranged in the second multiple cloning site of pRSFDuet-1_6HMBP, were obtained by gene synthesis (Twist Bioscience). To ensure comparable levels of expression for each gene, ribosomal binding sites (RBSs) were designed using the DeNovoDNA RBS calculator and inserted in between coding sequences.[1] The obtained vectors as well as pRSFDuet-1_6HMBP were digested with BamHI/SacI and treated with rSAP before gel extraction using the QIAquick Gel Extraction Kit (Qiagen). A codon-optimized gene fragment for MovA with 5'- and 3'-terminal extensions containing the necessary overlaps for Gibson assembly was purchased from Twist Bioscience. HiFi assembly reactions were performed to insert the MovA fragment into BamHI/SacI-digested pRSFDuet-1_6HMBP, pRSFDuet-1_6HMBP_ *movX*, pRSFDuet-1_6HMBP_*movBC*, and pRSFDuet-1_6HMBP_ *movXBC*, thereby allowing fusion of *movA* to the 3'-end of the 6HMBP coding sequence. Reactions were incubated for 1 hour at 50°C and then transformed into chemically competent *E. coli* DH5α cells. Due to

toxicity, 5α F'Iq competent *E. coli*, rather than DH5α cells, was transformed with pRSFDuet-1_6HMBP*movA_movXBC*. The transformants were selected on LB agar plates containing kanamycin (50 μg/mL). Assembled plasmids were isolated from single-colony cultures using the QIAprep Spin Miniprep Kit (Qiagen) and confirmed by Sanger sequencing. Despite repeated attempts, both DH5α and 5α F'Iq *E. coli* did not uptake the pRSFDuet-1_6HMBP*movA_movXBC* plasmid, presumably due to toxicity associated with the gene products. All observed colonies instead contained mutations in the *movA* sequence, which are listed in Table S8.

Construction of pET-28a(+) and pET-15b vectors for *in vitro* activity assays. Vectors pET-28a(+)_*movX* and pET-28b(+)_*movBC*, in which codon-optimized genes for MovX, MovB and MovC are arranged in the multiple cloning site of pET-28a(+), were purchased from Twist Bioscience. In the case of pET-28b(+)_*movBC*, RBSs were designed using the DeNovoDNA RBS calculator to ensure comparable levels of expression for each gene.[1] Aliquots of each plasmid (2 μL at 100 μM) were used to transform chemically competent *E. coli* DH5α cells. The transformants were selected on LB agar plates containing kanamycin (50 μg/mL). Plasmids were isolated from single-colony cultures using the QIAprep Spin Miniprep Kit (Qiagen) and confirmed by Sanger sequencing. Vector pET-15b was digested with NdeI/BamHI and treated with rSAP before gel extraction using the QIAquick Gel Extraction Kit (Qiagen). A codon-optimized gene fragment for MovC with 5'- and 3'-terminal extensions containing the necessary overlaps for Gibson assembly was purchased from Twist Bioscience. A HiFi assembly reaction was performed to insert the MovC fragment into NdeI/BamHI-digested pET-15b to generate pET-15b_*movC*. Reactions were incubated for 1 hour at 50°C and then transformed into chemically competent *E. coli* DH5α cells. The transformants were selected on an LB agar plate containing ampicillin (100 μg/mL). The assembled plasmid was isolated from a single-colony culture using the QIAprep Spin Miniprep Kit (Qiagen) and confirmed by Sanger sequencing.

Generation of *E. coli* BL21(DE3) strains. All pRSFDuet-1_6HMBP-based plasmids as well as pET-15b_*movC* were transformed into chemically competent *E. coli* BL21(DE3) cells for expression. The transformants were selected on LB agar plates containing kanamycin (50 μg/mL) for pRSFDuet-1_6HMBP-based plasmids or ampicillin (100 μg/mL) for pET-15b_*movC*. Plasmids pET-28a(+)_*movX* and pET-28a(+)_*movBC* were co-transformed with pGro7, which encodes the groES/EL chaperone for protein folding,[2] into chemically competent *E. coli* BL21(DE3) cells. The transformants were selected on LB agar plates containing kanamycin (50 μg/mL) and chloramphenicol (25 μg/mL).

Analytical-scale co-expression of MovX and MovBC with 6HMBP-MovA. A 14-mL sterile culture tube containing 5 mL Terrific Broth (TB) supplemented with kanamycin (50 μg/mL) was inoculated with a single colony of *E. coli* BL21(DE3) carrying either pRSFDuet-1_6HMBP*movA*, pRSFDuet-1_6HMBP*movA_movX*, pRSFDuet-1_6HMBP*movA_movBC*, or mutant pRSFDuet-1_6HMBP*movA_movXBC* (see Table S8 for more details). The 5-mL culture was grown at 37°C with shaking (200 rpm) for 12 hours, at which point 500 μL (1% v/v) were used to inoculate 50 mL TB supplemented with kanamycin (50 μg/mL) in an Erlenmeyer flask (125 mL). The culture was grown at 37°C with shaking (200 rpm) to an OD_{600} of 0.6, cooled in an ice bath, and supplemented

with ferrous ammonium sulfate (160 μM) before induction with isopropyl β-*D*-1-thiogalactopyranoside (IPTG, 1 mM). Following incubation at 18°C with shaking (200 rpm) for 18 h, cells were harvested by centrifugation (8,000 × g, 20 min, 4°C).

Analytical-scale purification and protease digest of 6HMBP-MovA. The 6HMBP-MovA fusion proteins were purified from cell paste in accordance to previously published protocols.[3] Cell paste was resuspended in lysis buffer (0.5 mL/0.1 g cell paste), which consisted of 50 mM sodium phosphate, 300 mM NaCl, and 10 mM imidazole (pH 8). The suspension was supplemented with BugBuster 10x protein extraction reagent (10% v/v), Benzonase nuclease (2.5U, 0.1 μL/mL), phenylmethanesulfonyl fluoride (PMSF, 0.25 mM), and protease inhibitor cocktail (10 μL/mL), and then gently rocked on ice for 30 min. Cell debris was pelleted via centrifugation (18,000 × g, 1 h, 4°C), and the clarified lysate was loaded onto a HisPur Ni-NTA spin column (0.2 mL resin bed volume, Thermo-Fisher) equilibrated with 5 column volumes (CV) of lysis buffer. The column was washed with 5 CV of lysis buffer and 4 CV of wash buffer, which consisted of 50 mM sodium phosphate, 300 mM NaCl, and 20 mM imidazole (pH 8). Finally, the protein was eluted with 2 CV of elution buffer, which consisted of 50 mM sodium phosphate, 300 mM NaCl, and 500 mM imidazole (pH 8). Purified protein was subsequently desalted on a PD-10 desalting column (GE Healthcare) equilibrated with cleavage buffer, which consisted of 50 mM Tris-HCl and 150 mM NaCl (pH 8). Protein elution was monitored using the Bradford assay. To facilitate HR-MS analysis, 6HMBP tags were removed from isolated fusion proteins by incubating with HRV-3C protease (10 μL/mL) for 16 h at 4°C. Reactions were quenched by incubation at 95°C for 2 minutes and centrifuged (18,000 × g, 5 min) to remove precipitate. Peptides were then digested with trypsin-ultra mass spectrometry grade (100:1 sample to trypsin) following manufacturer procedures. Digestion reactions were incubated for 7 h at 37°C. Samples were then analyzed by HPLC-coupled HR-MS using an analytical Phenomenex Jupiter C18 column (300 Å, 5 μm, 4.6 mm × 100 mm) operating at 0.6 mL/min. Elution was performed with an isocratic step of 5% acetonitrile in water (+ 0.1% formic acid) for 5 min, followed by gradient steps of 5-35% and 35-100% acetonitrile in water (+ 0.1% formic acid) over 20 min and 5 min, respectively.

Large-scale co-expression of MovBC with 6HMBP-MovA and purification of 6HMBP-MovA. *E. coli* BL21(DE3) carrying pRSFDuet-1_6HMBP*movA_movBC* was grown at 37°C with shaking (200 rpm) in Erlenmeyer flasks (2 × 250 mL), as described above. After 12 h, 16 mL (1% v/v) were used to inoculate 1.6 L TB supplemented with kanamycin (50 μg/mL) in Erlenmeyer flasks (4 × 4 L). The cultures were grown at 37°C with shaking (200 rpm) to an OD_{600} of 0.6, cooled in an ice bath, and supplemented with ferrous ammonium sulfate (160 μM) before induction with IPTG (1 mM). Following incubation at 18°C with shaking (200 rpm) for 18 h, cells were harvested by centrifugation (8,000 × g, 20 min, 4°C) and stored at -80°C. Typically, a yield of 8 g of cells per liter culture was obtained.

Purification of 6HMBP-MovA was carried out aerobically in a cold room. Cell paste was resuspended in lysis buffer (5 mL/g cell paste), which consisted of 50 mM sodium phosphate, 300 mM NaCl, and 10 mM imidazole (pH 8). The suspension was supplemented with protease inhibitor cocktail (0.2% v/v), PMSF (0.25 mM), lysozyme (1 mg/mL), and DNase I (10 U/mL), and

then stirred for 30 minutes on ice. Once the suspension homogenized, it was sonicated for 4 min in 15 s on/15 s off cycles at a 30% power rating. The cells were allowed to rest for 5 min on ice, and the cycle was repeated. Cell debris was pelleted via centrifugation (32,000 × g, 1 h, 4°C), and the clarified lysate was supplemented with PMSF (0.25 mM) and loaded onto a HisPur Ni-NTA column (5 mL resin bed volume, Thermo-Fisher) equilibrated with 10 CV of lysis buffer. The column was washed with 10 CV of lysis buffer and 4 CV of wash buffer, which consisted of 50 mM sodium phosphate, 300 mM NaCl, and 20 mM imidazole (pH 8). Finally, the protein was eluted with 2 CV of elution buffer, which consisted of 50 mM sodium phosphate, 300 mM NaCl, and 500 mM imidazole (pH 8). Purified protein was subsequently desalted on a Sephadex G-25 column (~50 mL, d = 1.25 cm, l = 25 cm) that had been equilibrated with cleavage buffer, which consisted of 50 mM Tris-HCl and 150 mM NaCl (pH 8). Fractions containing protein, based on the Bradford assay, were pooled, flash frozen in liquid N_2, and stored at -80°C. Protein concentration was determined spectrophotometrically using a calculated extinction coefficient of 67,840 M^{-1} cm^{-1} (at 280 nm). A yield of 9.6 mg 6HMBP-MovA per gram of cell paste was typical.

Large-scale co-expression of MovX with 6HMBP-MovA and purification of 6HMBP-MovA. MovX-modified 6HMBP-MovA was obtained through large-scale co-expression of MovX and 6HMBP-MovA following a procedure analogous to the one detailed above. Typically, a yield of 8.2 g of cells per liter culture and 5.6 mg 6HMBP-MovA per gram of cell paste were obtained.

Protease cleavage and purification of MovBC- and MovX-modified MovA. Enzyme-modified 6HMBP-MovA was incubated with HRV-3C protease (10 µL/mL) for 16 h at 4°C to remove the 6HMBP tag. The reaction was quenched by incubation at 95°C for 2 minutes and centrifuged (18,000 × g, 5 min) to remove precipitate. MovBC-modified, hydrolyzed MovBC-modified, and MovX-modified peptides were isolated from their reaction mixtures by HPLC using a semi-preparative Phenomenex Jupiter C18 column (300 Å, 5 µm, 250 × 10 cm) operating at 2.75 mL/min. Elution was performed with an isocratic step of 5% acetonitrile in water (+ 0.1% formic acid) for 3 min, followed by a gradient step of 5-20% acetonitrile in water (+ 0.1% formic acid) over 22 min. Peptide concentration was determined spectrophotometrically using a calculated extinction coefficient of 1,490 M^{-1} cm^{-1} (at 280 nm) for use in enzymatic assays.

To analyze the MovBC product by NMR, the procedure above was repeated with additional steps. Following 6HMBP tag removal, the MovBC-modified peptide was digested with trypsin-ultra mass spectrometry grade (100:1 sample to trypsin) following manufacturer instructions. Digestion reactions were incubated at 37°C for 10 h. The *C*-terminal 9mer trypsin fragment was isolated from the reaction mixture by HPLC using a semi-preparative Phenomenex Jupiter C18 column (300 Å, 5 µm, 250 × 10 cm) operating at 2.75 mL/min. Elution was performed with an isocratic step of 5% acetonitrile in water (+ 0.1% formic acid) for 5 min, followed by gradient steps of 5-22% and 22-100% acetonitrile in water (+ 0.1% formic acid) over 25 min and 5 min, respectively.

Expression of MovX and MovB. MovX and MovB were expressed according to a previously published procedure with some modifications.[4,5] Briefly, a 14-mL sterile culture tube containing 5 mL TB supplemented with chloramphenicol (25 µg/mL) and kanamycin (50 µg/mL) was inoculated

with a single colony of *E. coli* BL21(DE3) carrying pGro7 and either pET-28a(+)_*movX* or pET-28a(+)_*movBC*, for expression of MovX and MovB, respectively. The 5-mL cultures were grown at 37°C with shaking (200 rpm) for 12 hours, at which point 500 µL (1% v/v) were used to inoculate 50 mL TB supplemented with chloramphenicol (25 µg/mL) and kanamycin (50 µg/mL) in Erlenmeyer flasks (2 × 250 mL). The 50-mL cultures were grown at 37°C with shaking (200 rpm) for 12 h, at which point 16 mL (1% v/v) were used to inoculate 1.6 L TB supplemented with chloramphenicol (25 µg/mL), kanamycin (50 µg/mL), and L-arabinose (2 mg/mL) in Erlenmeyer flasks (4 × 4 L). The cultures were grown at 37°C with shaking (200 rpm) to an OD_{600} of 0.6, cooled in an ice bath, and supplemented with ferrous ammonium sulfate (160 µM) before induction with IPTG (0.2 mM). Following incubation at 18°C with shaking (200 rpm) for 18 h, cells were harvested by centrifugation (8,000 × g, 20 min, 4°C) and stored at -80°C. Typically, a yield of 5–6 g of cells per liter culture was obtained.

Expression of MovC. A 14-mL sterile culture tube containing 5 mL TB supplemented with ampicillin (100 µg/mL) was inoculated with a single colony of *E. coli* BL21(DE3) carrying pET-15b_*movC*. The 5-mL culture was grown at 37°C with shaking (200 rpm) for 12 hours, at which point 500 µL (1% v/v) were used to inoculate 50 mL TB supplemented with ampicillin (100 µg/mL) in Erlenmeyer flasks (2 × 250 mL). The 50-mL cultures were grown at 37°C with shaking (200 rpm) for 12 h, at which point 16 mL (1% v/v) were used to inoculate 1.6 L TB supplemented with ampicillin (100 µg/mL) in Erlenmeyer flasks (6 × 4 L). The cultures were grown at 37°C with shaking (200 rpm) to an OD_{600} of 0.6, cooled in an ice bath, and supplemented with IPTG (0.2 mM) for induction. Following incubation at 18°C with shaking (200 rpm) for 18 h, cells were harvested by centrifugation (8,000 × g, 20 min, 4°C) and stored at -80°C. Typically, a yield of ~8 g of cells per liter culture was obtained.

Purification of MovX, MovB, and MovC. Purification of MovX and MovB was carried out anaerobically in a glovebox (MBraun) using previously published procedures with few modifications.[4,5] Purification of MovC was carried out aerobically in a cold room. Cell paste was resuspended in lysis buffer (5 mL/g cell paste), which consisted of 50 mM HEPES, 300 mM KCl, 2 mM imidazole, 10 mM β-mercaptoethanol, and 10% glycerol (pH 7.5). The suspension was supplemented with PMSF (0.25 mM), lysozyme (1 mg/mL), DNase I (10 U/mL) and either protease inhibitor cocktail (0.2% v/v) for MovC or cOmplete EDTA-free protease inhibitor tablets (1 tablet/50 mL cell suspension, Roche) for MovX and MovB, and was stirred for 30 minutes on ice. Once the suspension homogenized, it was sonicated for 4 min in 15 s on/15 s off cycles at a 30% power rating. The cells were allowed to rest for 5 min on ice, and the cycle was repeated. Cell debris was then pelleted via centrifugation (32,000 × g, 1 h, 4°C), and the clarified lysate was supplemented with PMSF (0.25 mM) and loaded onto a HisPur cobalt column (5 mL resin bed volume, Thermo-Fisher) equilibrated with 10 CV of lysis buffer. The column was washed with 10 CV of lysis buffer and 4 CV of wash buffer, which consisted of 50 mM HEPES, 300 mM KCl, 30 mM imidazole, 10 mM β-mercaptoethanol, and 10% glycerol (pH 7.5). Finally, the protein was eluted with 2 CV of elution buffer, which consisted of 50 mM HEPES, 300 mM KCl, 500 mM imidazole, 10 mM β-mercaptoethanol, and 10% glycerol (pH 7.5). Purified protein was

subsequently desalted on a Sephadex G-25 column (~50 mL, d = 1.25 cm, l = 25 cm) equilibrated with storage buffer, which consisted of 50 mM HEPES, 150 mM KCl, 5 mM dithiothreitol (DTT), and 10% glycerol (pH 7.5). Fractions containing protein, based on the Bradford assay, were pooled, aliquoted, flash frozen in liquid N_2, and stored at -80°C. Protein concentrations were determined spectrophotometrically using calculated extinction coefficients (at 280 nm) of 55,370 M^{-1} cm^{-1} for MovX, 36,440 M^{-1} cm^{-1} for MovB, and 33,920 M^{-1} cm^{-1} for MovC. Yields of 1.7 mg MovX, 2.4 mg MovB, and 0.3 mg MovC per gram of cell paste were typical. For MovX and MovB, iron was quantified using a colorimetric assay with Ferene iron reagent according to previously published procedures.[6]

Synthesis of *N*β-trityl-L-asparagine (^{15}Nβ). According to a procedure adapted from Elgaher et al.,[7] a 25-mL round-bottomed flask equipped with a stir bar was charged with ^{15}Nβ-labeled L-asparagine (250 mg, 1.89 mmol), triphenylcarbinol (984 mg, 3.78 mmol, 2 equiv.), glacial acetic acid (5.68 mL), acetic anhydride (386 mg, 3.78 mmol, 2 equiv.), and sulfuric acid (213 mg, 2.18 mmol, 1.15 equiv.). The suspension was stirred at 60°C for 3 h, and then allowed to cool to room temperature. The solution was then slowly poured on ice-cold water (12 mL) while stirring. After adjusting the pH to 6 using 2 M NaOH, the mixture was stirred on ice for 1 h. The precipitate was filtered, washed with ice-cold water (2 × 10 mL), 1:1 toluene/diethyl ether (2 × 10 mL), and petroleum ether (10 mL), and then dried to provide a white solid (320 mg, 0.85 mmol, yield 45%). ^{1}H NMR (500 MHz, DMSO-d_6) δ 10.04 (d, *J* = 89.3 Hz, 1H), 7.30 – 7.23 (m, 6H), 7.22 – 7.17 (m, 9H), 3.40 (t, *J* = 5.8 Hz, 1H), 2.91 (dd, *J* = 16.0, 6.8 Hz, 1H), 2.37 (dt, *J* = 16.1, 5.3 Hz, 1H). ^{13}C NMR (126 MHz, DMSO-d_6) δ 169.7 (d, *J* = 12.7 Hz), 169.5 (s), 145.0 (s), 128.6 (s), 127.5 (s), 126.3 (s), 69.4 (d, *J* = 9.9 Hz), 50.2 (s), 38.2 (d, *J* = 7.7 Hz).

Synthesis of *N*β-trityl-L-asparagine ($^{15}N_2$). *N*β-trityl-L-asparagine ($^{15}N_2$) was prepared by the same procedure detailed for the synthesis of *N*β-trityl-L-asparagine (^{15}Nβ)**.** A white solid was obtained (302 mg, 0.80 mmol, yield 43%). ^{1}H NMR (500 MHz, DMSO-d_6) δ 10.09 (d, *J* = 89.3 Hz, 1H), 7.28 – 7.24 (m, 6H), 7.22 – 7.17 (m, 9H), 2.88 (ddd, *J* = 16.0, 6.8, 2.2 Hz, 1H), 7.38 – 7.31 (m, 1H). ^{13}C NMR (126 MHz, DMSO-d_6) δ 169.8 (d, *J* = 12.0 Hz), 145.0 (s), 128.6 (s), 127.5 (s), 126.3 (s), 69.4 (d, *J* = 9.6 Hz), 50.3 (d, *J* = 5.4 Hz), 38.5 (d, *J* = 8.1 Hz).

Synthesis of *N*α-Fmoc-*N*β-trityl-L-asparagine (^{15}Nβ). A 25-mL round-bottomed flask equipped with a stir bar was charged with *N*β-trityl-L-asparagine (^{15}Nβ) (300 mg, 0.80 mmol), sodium carbonate (127 mg, 1.20 mmol, 1.5 equiv.), and water (4.3 mL). The suspension was cooled to 0°C and Fmoc-succinimide (270 mg, 0.80 mmol, 1 equiv.) in acetonitrile (4.3 mL) was added dropwise. After stirring overnight at room temperature, the solution was diluted with water (9 mL), transferred to a separatory funnel, and washed with diethyl ether (2 × 20 mL). The aqueous layers were combined, acidified to pH 2 using 2 M HCl, and extracted with ethyl acetate (3 × 20 mL). The organic layers were combined, washed with brine (20 mL), dried over sodium sulfate, filtered, and concentrated *in vacuo* to provide a white solid (427 mg, 0.72 mmol, yield 89%). ^{1}H NMR (500 MHz, DMSO-d_6) δ 12.63 (s, 1H), 8.62 (d, *J* = 90.5 Hz, 1H), 7.90 (d, *J* = 7.5 Hz, 2H), 7.73 (d, *J* = 7.5 Hz, 2H), 7.62 (d, *J* = 8.4 Hz, 1H), 7.42 (q, *J* = 7.1 Hz, 2H), 7.30 (ddd, *J* = 16.1, 8.0, 6.9 Hz, 2H), 7.23 – 7.15 (m, 15H), 4.36 (dd, *J* = 10.3, 6.9 Hz, 1H), 4.32 – 4.20 (m,

3H), 2.67 (d, *J* = 7.1 Hz, 2H). ^{13}C NMR (126 MHz, DMSO-d_6) δ 173.4 (s), 168.8 (d, *J* = 12.9 Hz), 155.9 (s), 144.8 (s), 143.8 (s), 140.8 (s), 128.6 (s), 127.7 (s), 127.5 (s), 127.2 (s), 126.4 (s), 120.2 (s), 69.5 (d, *J* = 9.8 Hz), 65.8 (s), 51.1 (s), 46.7 (s), 38.1 (d, *J* = 8.6 Hz).

Synthesis of *N*α-Fmoc-*N*β-trityl-L-asparagine ($^{15}N_2$). *N*α-Fmoc-*N*β-trityl-L-asparagine ($^{15}N_2$) was prepared by the same procedure detailed for the synthesis of *N*α-Fmoc-*N*β-trityl-L-asparagine (^{15}Nβ). A white solid was obtained (310 mg, 0.52 mmol, yield 65%). ^{1}H NMR (500 MHz, DMSO-d_6) δ 12.72 (s, 1H), 8.65 (d, *J* = 90.6 Hz, 1H), 7.91 (d, *J* = 7.6 Hz, 2H), 7.73 (d, *J* = 7.6 Hz, 2H), 7.71 – 7.58 (m, 1H), 7.42 (q, *J* = 7.1 Hz, 2H), 7.31 (dt, *J* = 15.0, 7.5 Hz, 2H), 7.28 – 7.10 (m, 15H), 4.36 (dd, *J* = 10.4, 6.9 Hz, 1H), 4.31 – 4.21 (m, 3H), 2.67 (dd, *J* = 7.5, 2.9 Hz, 2H). ^{13}C NMR (126 MHz, DMSO-d_6) δ 173.3 (s), 168.8 (d, *J* = 13.6 Hz), 155.8 (d, *J* = 26.7 Hz), 144.7 (s), 143.8 (s), 140.8 (s), 128.6 (s), 127.7 (s), 127.5 (s), 127.2 (s), 126.4 (s), 120.2 (s), 69.4 (d, *J* = 9.5 Hz), 65.8 (s), 51.1 (d, *J* = 13.1 Hz), 46.7 (s), 38.1 (d, *J* = 9.2 Hz).

Solid phase peptide synthesis of MovA substrates. MovA, ^{15}Nβ-Asn-MovA and $^{15}N_2$-Asn-MovA substrates were synthesized via Fmoc-based solid phase chemistry using a Liberty Blue automated microwave peptide synthesizer equipped with a Discover microwave module (CEM). Preloaded Fmoc-Lys(Boc)-Wang resin LL (0.3 mmol/g loading capacity) and standard Fmoc- and side chain-protected amino acids, unless otherwise specified, were used for 0.05 mmol scale syntheses. For the synthesis of ^{15}Nβ-Asn-MovA and $^{15}N_2$-Asn-MovA, ^{15}Nβ- and $^{15}N_2$-labeled *N*α-Fmoc-*N*β-trityl-L-asparagine analogues were respectively incorporated at residue 22. Briefly, the resin was swelled in dimethylformamide (DMF, 10 mL) for 3 minutes. Fmoc deprotection reactions were performed using 10% piperazine (w/v) in a 10:90 solution of ethanol/*N*-methylpyrrolidinone (NMP) containing 0.1 M 1-hydroxybenzotriazole (HOBt). Coupling reactions were performed using 0.5 M *N*,*N*′-diisopropylcarbodiimide (DIC) activator in DMF and activator base solution of 1.0 M Oxyma and 0.1 M N,N′-diisopropylethylamine (DIPEA) in DMF. Coupling reactions proceeded for 4 minutes at 90 °C with 5 equiv. of each amino acid. Lys_5, Lys_6, Val_7, Val_8, Val_9, Lys_{10}, Val_{11}, Met_{16}, Thr_{17}, Cys_{18} were coupled twice. Upon completion of the synthesis, the resin was transferred to an Econo-Pac column (BioRad), washed with DMF, followed by dichloromethane (DCM), and then dried fully under vacuum. For peptide cleavage and global deprotection, the resin was incubated in cleavage cocktail (7 mL), consisting of 92.5% trifluoroacetic acid (TFA), 2.5% water, 2.5% triisopropylsilane (TIS), and 2.5% 2,2′-(ethylenedioxy)diethanethiol (DOPT), for 5 hours at room temperature. The solution was drained from the reaction tube and the resin was rinsed several times with TFA. The filtrate and rinses were combined, concentrated by evaporation of TFA under a stream of N_2, and precipitated by addition of chilled diethyl ether. The suspension was incubated at -20°C for 20 minutes, before pelleting the peptide by centrifugation (4,000 g, 20 min, 4°C). After decanting the ether, the crude peptide was air-dried at room temperature.

Purification of MovA substrates. Crude peptides were dissolved in a minimal amount of acetic acid, diluted with water, and filtered. Repeated injections were carried out onto a semi-preparative Phenomenex Jupiter C18 column (300 Å, 5 µm, 250 × 10 cm) operating at 2.75 mL/min. Unlabeled and ^{15}N-labeled MovA peptides were eluted with an isocratic step of 5%

acetonitrile in water (+ 0.1% formic acid) for 5 min, followed by a gradient of 5–25% acetonitrile in water (+ 0.1% formic acid) over 22 minutes. Pure peptides were verified by HPLC-coupled HR-MS.

Enzymatic activity assays. Enzymatic assays were performed under aerobic conditions by removing aliquots of MovX and MovB from the glovebox (MBraun). Reactions were carried out in assay buffer, which consisted of 50 mM HEPES, 150 mM KCl, and 5% glycerol (pH 7.5), in 1.5 mL Eppendorf tubes on a 30-µL scale. Synthetic MovA was typically used as a substrate for enzymatic assays. Alternatively, MovBC-modified MovA or hydrolyzed MovBC-modified MovA, generated through co-expression of 6HMBP-MovA and MovBC in *E. coli*, was used as a substrate for MovX assays, while MovX-modified MovA, generated through co-expression of 6HMBP-MovA and MovX in *E. coli*, was used as a substrate for MovBC assays. ^{15}Nβ-Asn-MovA and $^{15}N_2$-Asn-MovA peptides were used for labeling studies. A typical assay contained 250 µM substrate, 20 µM MovB, 20 µM MovC, 20 µM MovX, 1 mM sodium ascorbate, and 2.5 mM DTT. For assays with only MovBC, MovX was not included. Respectively, for assays with only MovX, MovB and MovC were not included. After overnight incubation at room temperature, reactions were heated at 95 °C for 2 minutes. Precipitated protein was removed by centrifugation (18,000 × g, 5 min). Samples were then diluted with an equal volume of acetonitrile (+0.1% formic acid) and directly analyzed by HPLC-coupled HR-MS using an analytical Phenomenex Jupiter C18 column (300 Å, 5 µm, 4.6 mm × 100 mm) operating at 0.6 mL/min. Elution was performed with an isocratic step of 5% acetonitrile in water (+ 0.1% formic acid) for 3 min, followed by gradient steps of 5-30% and 30-100% acetonitrile in water (+ 0.1% formic acid) over 9 min and 3 min, respectively.

Time course assays. Time course assays with MovBC and MovX were performed following the assay conditions described above, with the exception that MovX was added at 5 µM. Synthetic MovA was used as a substrate for the MovBC assay, while MovBC-modified MovA, generated through co-expression of 6HMBP-MovA and MovBC in *E. coli*, was used as a substrate for the MovX assay. Time course assays were performed in duplicate on a 200-µL scale. An aliquot of 20 µL was removed from the reaction mixture at each time point, immediately quenched at 95 °C for 1 minute, and diluted with an equal volume of acetonitrile (+0.1% formic acid). Samples were centrifuged (18,000 × g, 5 min) to remove precipitated protein and analyzed by HPLC-coupled HR-MS using the conditions described above.

Large-scale MovX assay and purification of MovXBC-modified MovA. Following the heterologous co-expression approach described above, MovBC-modified 6HMBP-MovA was isolated. After 6HMBP tag removal and purification on a semi-preparative scale as detailed above, the peptide (12 mg) was dissolved in 3.4 mL assay buffer, which consisted of 50 mM HEPES, 150 mM KCl, and 5% glycerol (pH 7.5), in a 15-mL Falcon tube. The peptide solution was mixed with 50 µM MovX, 1 mM sodium ascorbate, and 2.5 mM DTT for a final assay volume of 10 mL. After overnight incubation at room temperature, reactions were heat-quenched at 95 °C for 2 minutes. Precipitated protein was removed by centrifugation (18,000 × g, 5 min). MovXBC-modified peptide was isolated from the reaction mixture by HPLC using a semi-preparative Phenomenex Jupiter C18 column (300 Å, 5 µm, 250 × 10 cm) operating at 2.75 mL/min. Elution

was performed with an isocratic step of 8% acetonitrile in water (+ 0.1% formic acid) for 3 min, followed by a gradient step of 8-20% acetonitrile in water (+ 0.1% formic acid) over 22 min. Purified peptide was digested with trypsin-ultra mass spectrometry grade (100:1 sample to trypsin) following manufacturer instructions. Digestion reactions were incubated at 37°C for 10 h. The *C*-terminal 7mer trypsin fragment was isolated from the reaction mixture by HPLC using a semi-preparative Phenomenex Jupiter C18 column (300 Å, 5 µm, 250 × 10 cm) operating at 2.75 mL/min. Elution was performed with an isocratic step of 8% acetonitrile in water (+ 0.1% formic acid) for 3 min, followed by a gradient step of 8-18% acetonitrile in water (+ 0.1% formic acid) over 22 min.

DNA and Amino Acid Sequences

MovA

Amino acid sequence

MKNEKKVVVKVKDKEMTCGSYNK

DNA sequence

ATGAAAAACGAAAAGAAAGTAGTAGTTAAAGTTAAAGATAAAGAAATGACTTGCGGTAGCTA
CAACAAGTAATT

DNA sequence (codon optimized for E. coli)

ATGAAAAACGAAAAAAAAGTGGTGGTGAAAGTGAAAGATAAAGAAATGACCTGCGGCAGCT
ATAACAAATAA

MovX

Amino acid sequence

MNFACSYNHHFSTGKLYPSDEVKLIELGFKAYRSLFVENTPPEKVKHTPISLHISRSPITENEIYQ
DRFINEKLIDTQYDNRIISLGFHLCGDRNDNIGKLGFSSHYNHDHGSEDNAIRFLTKVRQVTKKP
VWLENANFYSSSVNEIITNWKSFNRVVKESGSGAIIDLSHLIIDCKNNDINPTSMIGFIDWDSVIEI
HLSGIIEGKDGALHDGHGTQVHPSVWELLRQILKLKLVDKNVFINIEHSDDVWAEKTDLYKSDFD
ILKKLLSEPLSEISKAEYARVYAESYLKKLLNQEVENIKDISDFFNITPSELLNEWMDYVVSVDKR
VALSIDDMDSLIEKNSIHFIQSFTDFVDYKQQ

DNA sequence

ATGAATTTTGCTTGTAGCTATAATCATCACTTTTCCACAGGAAAACTCTATCCTTCAGACGAA
GTTAAACTTATCGAACTTGGTTTCAAGGCTTATCGTAGTTTATTTGTTGAAAATACTCCACCA
GAGAAAGTTAAACACACTCCAATATCACTACATATATCAAGATCACCAATAACCGAAAATGA
GATATACCAAGATCGTTTCATCAATGAAAAACTAATTGATACACAATATGATAATAGAATTAT
CAGCCTTGGTTTTCATTTATGTGGTGATAGAAATGATAATATAGGAAAGCTTGGGTTTTCCT
CGCACTATAATCATGATCATGGCAGTGAAGACAATGCGATTCGTTTTTTGACTAAAGTGCGT
CAAGTGACAAAAAAACCGGTATGGTTGGAAAATGCGAATTTTTACTCCTCTTCAGTAAATGA
AATCATAACGAATTGGAAGAGCTTTAATCGTGTAGTTAAAGAGTCCGGATCTGGTGCTATCA
TCGACCTATCTCATTTAATTATTGACTGTAAGAACAATGATATAAATCCAACTTCCATGATTG
GCTTCATTGATTGGGACTCCGTTATAGAAATCCACTTATCTGGGATTATCGAGGGTAAAGAT
GGAGCTTTGCATGATGGTCACGGCACTCAAGTCCATCCTTCTGTATGGGAATTACTCCGAC
AGATCTTAAAGTTAAAGTTAGTGGATAAAAATGTCTTTATCAATATAGAGCACAGCGATGAT
GTTTGGGCGGAAAAAACAGATCTTTACAAAAGTGATTTCGATATACTTAAAAAACTACTAAG
TGAACCACTGAGTGAAATCAGCAAAGCAGAATATGCTCGAGTGTATGCCGAATCTTATCTA
AAAAAGTTATTAAACCAAGAGGTAGAGAATATCAAAGATATATCCGATTTCTTTAATATTACA
CCCTCAGAGCTTTTGAATGAGTGGATGGATTACGTCGTTAGTGTAGATAAGAGAGTTGCAC
TCTCAATTGACGACATGGATTCACTAATTGAGAAAAATTCAATACACTTTATTCAATCATTTA
CAGATTTCGTAGATTATAAACAACAATGA

DNA sequence (codon optimized for E. coli)

ATGAACTTTGCGTGCAGCTATAACCATCATTTTAGCACCGGCAAACTGTATCCGAGCGATG
AAGTGAAACTGATTGAACTTGGCTTCAAGGCGTATCGCAGCCTGTTTGTGGAAAACACCCC
GCCGGAAAAAGTGAAACATACCCCGATTAGCCTGCATATTAGCCGCAGCCCGATTACCGA
AAACGAAATTTATCAAGATCGCTTTATTAACGAAAAACTGATTGATACGCAGTATGATAACC
GCATTATTAGCCTGGGCTTTCATCTGTGCGGCGATCGCAACGATAACATTGGCAAACTGGG

CTTTAGTAGCCATTATAACCATGATCATGGCAGCGAAGATAACGCGATTCGCTTTCTGACC
AAAGTGCGCCAAGTGACCAAAAAACCGGTGTGGCTGGAAAACGCGAACTTTTATAGCAGC
AGCGTGAACGAAATTATTACCAACTGGAAAAGCTTTAACCGCGTGGTGAAAGAAAGCGGCA
GCGGCGCGATTATTGATCTGAGCCATCTGATTATTGATTGCAAAAACAACGATATTAACCC
GACGAGCATGATTGGCTTTATTGATTGGGATAGCGTGATTGAAATTCATCTGAGCGGCATT
ATTGAAGGCAAAGATGGCGCGCTGCATGATGGCCATGGCACCCAAGTGCATCCGAGCGTG
TGGGAACTGCTGCGTCAGATTCTGAAACTGAAACTGGTGGATAAAAACGTGTTTATTAACAT
TGAACATAGCGATGATGTGTGGGCGGAAAAAACCGATCTGTATAAAAGCGATTTTGATATTT
TAAAGAAACTTTTGAGCGAGCCGCTGAGCGAAATTAGCAAAGCGGAATATGCGCGCGTGT
ATGCGGAAAGCTATCTGAAAAAACTTCTTAACCAAGAAGTGGAAAACATTAAAGATATTAGC
GATTTTTTTAACATTACCCCGAGCGAACTGCTGAACGAATGGATGGATTATGTGGTGAGCG
TGGATAAACGCGTGGCGCTGAGCATTGATGATATGGATAGCCTGATTGAAAAAAACAGCAT
TCATTTTATTCAGAGCTTTACCGATTTTGTGGATTATAAACAGCAGTAA

MovB

Amino acid sequence

MKVGINWSGQRELTCIKELFENRDIEFVELLIDNFLTTDVNSIKEILKGRPCAFHIMNSQFLHRDE
LELKNMAQIINTLIADLKPIYISDHIGKFYHNEQALPQMLEVNYVKDTEWVLEKLTYWSSLLHGQL
LLENYPSIIPQSTTQVSFFKEILSKTQCGLLFDLSNAFIAEKNTGQKKEAWHELTKECQHFHIAGF
EDGPEGEFLVDTHNQCINELVLDYLVQFAREHDIQTISVERDDNFNAREWMRDVDNVRGCQIH
G

DNA sequence

ATGAAAGTAGGCATTAACTGGTCAGGACAAAGAGAACTGACTTGTATAAAAGAATTATTCGA
GAATAGAGATATAGAGTTTGTTGAGTTATTAATAGATAACTTTTTAACGACAGATGTTAACTC
AATCAAAGAGATCCTTAAAGGGCGTCCCTGTGCGTTTCATATCATGAACTCTCAGTTTCTTC
ACAGAGATGAACTTGAGTTAAAAAACATGGCACAAATAATAAATACCTTAATAGCAGACCTA
AAACCTATATATATATCTGATCATATCGGTAAGTTCTATCATAACGAGCAAGCACTGCCCCA
AATGCTAGAGGTTAACTACGTAAAAGATACTGAGTGGGTCCTAGAAAAACTAACATACTGG
TCTAGTCTTTTACATGGTCAATTATTATTAGAAAACTATCCATCGATAATACCGCAATCCACA
ACGCAGGTGAGCTTTTTCAAAGAAATCCTGTCTAAAACTCAATGTGGTCTTCTTTTTGATCT
TTCTAACGCATTTATAGCTGAAAAAAATACAGGTCAAAAAAAAGAGGCTTGGCATGAGTTAA
CCAAAGAATGCCAACACTTTCATATCGCAGGTTTTGAAGATGGGCCGGAGGGTGAGTTTTT
AGTAGATACACATAATCAATGTATTAACGAGTTAGTACTCGACTACCTTGTGCAATTCGCGC
GAGAGCATGACATCCAGACTATCTCAGTTGAAAGAGATGACAACTTCAACGCTCGTGAATG
GATGAGAGACGTCGATAATGTTAGAGGTTGTCAAATTCATGGATAA

DNA sequence (codon optimized for E. coli with linker including artificial RBS underlined)

GGGAGATTAATTTCTTAAGGATTATTATATGAAAGTGGGCATTAACTGGAGCGGTCAGCGC
GAACTGACCTGCATTAAAGAACTGTTTGAAAACCGCGATATTGAATTTGTGGAACTGCTGAT
TGATAACTTTCTGACCACCGATGTGAACAGCATCAAGGAAATATTGAAAGGTCGCCCGTGC
GCGTTTCATATTATGAACAGTCAGTTTCTGCATCGCGATGAACTGGAACTGAAAAACATGG
CGCAGATTATTAACACCCTGATTGCGGATCTGAAACCGATTTATATTAGCGATCATATTGGC
AAATTTTATCATAACGAACAAGCGCTGCCGCAGATGCTGGAAGTGAACTATGTGAAAGATA
CCGAATGGGTGCTGGAAAAACTGACCTATTGGAGCAGCCTGCTGCATGGTCAGCTGCTGC
TGGAAAACTATCCGAGCATTATTCCGCAGAGCACCACCCAAGTGAGCTTTTTTAAAGAAATA
CTTAGTAAGACGCAGTGCGGCCTGCTGTTTGATCTGAGCAACGCGTTTATTGCGGAAAAAA
ACACCGGTCAGAAAAAAGAAGCGTGGCATGAACTGACCAAAGAATGTCAGCATTTTCATAT

TGCGGGCTTTGAAGATGGCCCGGAAGGCGAATTTCTGGTGGATACCCATAATCAGTGCAT
TAACGAACTGGTGCTGGATTATCTGGTGCAGTTTGCGCGCGAACATGATATTCAGACCATT
AGCGTGGAACGCGATGATAACTTTAACGCGCGCGAATGGATGCGCGATGTGGATAACGTG
CGCGGCTGTCAGATTCATGGCTAA

MovC

Amino acid sequence

MLEVVKFMDNILNSVVAPFFSEHLNHKEALYSSLIIDASSNQILSGCPSLKENKVLCSDHLYAGF
VNWCYVNHKKMDWRLSLSFYDYLIDSNELVTEEAHKELIFLACSQWTYNDKSANQTFVLCHTS
LPSCVFGSNKSLRAENFREVFYFETNQLDAFLRTSQRQQAFMYWILENDNDFPTSLGTLI

DNA sequence

ATGTTAGAGGTTGTCAAATTCATGGATAACATCTTAAATTCTGTCGTTGCCCCCTTCTTTAG
CGAGCATCTTAACCACAAAGAAGCTTTGTATAGCTCTCTCATCATCGATGCATCATCCAACC
AAATCTTAAGCGGGTGTCCGAGTTTAAAGGAAAATAAAGTATTATGCTCAGATCACTTGTAT
GCTGGATTCGTTAATTGGTGCTACGTAAATCACAAAAAGATGGACTGGAGACTCTCGCTCT
CGTTCTACGATTATCTAATTGATTCAAATGAACTTGTCACTGAGGAAGCGCATAAGGAGCTG
ATTTTCTTAGCTTGCTCTCAGTGGACATACAATGACAAGAGCGCCAATCAAACCTTCGTGTT
GTGTCACACCTCATTACCTTCATGTGTATTTGGCAGTAATAAGTCTCTACGAGCCGAAAACT
TTCGTGAAGTCTTTTACTTCGAAACCAATCAACTTGACGCGTTTCTAAGAACCAGTCAACGT
CAACAGGCTTTTATGTACTGGATACTTGAAAATGATAACGACTTCCCTACGTCACTAGGAAC
TTTAATATGA

DNA sequence (codon optimized for E. coli with linker including artificial RBS underlined)

GATACAAATTAACGAATATACCTGGGGAGAGGAGGAGATGCTGGAAGTGGTGAAATTTATG
GATAACATTCTGAACAGCGTGGTGGCGCCGTTTTTTAGCGAACATCTGAACCATAAAGAAG
CGCTGTATAGCAGCCTGATTATTGATGCGAGCAGCAATCAGATTCTGAGCGGCTGCCCGA
GCCTGAAAGAAAACAAAGTGCTGTGCAGCGATCATCTGTATGCGGGCTTTGTGAACTGGT
GCTATGTGAACCATAAAAAAATGGATTGGCGCCTGAGCCTGAGCTTTTATGATTATCTGATT
GATAGCAACGAACTGGTGACCGAAGAAGCGCATAAAGAACTGATTTTTCTGGCGTGCAGTC
AGTGGACCTATAACGATAAAAGCGCGAATCAGACCTTTGTGCTGTGCCATACGAGCCTGCC
GAGCTGCGTGTTTGGCAGCAACAAAAGCCTGCGCGCGGAAAACTTTCGCGAAGTGTTTTA
TTTTGAAACCAATCAGCTGGATGCGTTTCTGCGCACGAGTCAGCGTCAGCAAGCGTTTATG
TATTGGATTCTGGAAAACGATAACGATTTTCCGACGAGCCTGGGCACCCTGATTTAA

Table S1. Plasmids and strains used in this study.

Plasmids	Purpose	Source
pET-15b	Amp^R, Expression vector	Addgene
pGro7	Chl^R, Expression of GroES/EL	Takara Bio
pET-28a(+)_*movX*	Kan^R, Expression of MovX	This study
pET-28a(+)_*movBC*	Kan^R, Expression of MovB	This study
pET-15b_*movC*	Kan^R, Expression of MovC	This study
pRSFDuet-1_6HMBP	Kan^R, Co-expression vector	Mo Lab
pRSFDuet-1_ 6HMBP*movA*	Kan^R, Expression of 6HMBP-MovA	This study
pRSFDuet-1_ 6HMBP*movA*_*movX*	Kan^R, Expression of 6HMBP-MovA modified by MovX	This study
pRSFDuet-1_ 6HMBP*movA*_*movBC*	Kan^R, Expression of 6HMBP-MovA modified by MovBC	This study
pRSFDuet-1_ 6HMBP*movA*(53G>C) _*movXBC*	Kan^R, Expression of 6HMBP-MovA mutant modified by MovX	This study
pRSFDuet-1_ 6HMBP*movA*(53G>A) _*movXBC*	Kan^R, Expression of 6HMBP-MovA mutant modified by MovX	This study
pRSFDuet-1_ 6HMBP*movA*(59delG) _*movXBC*	Kan^R, Expression of 6HMBP-MovA mutant modified by MovBC	This study
Strains	**Purpose**	**Source**
E. coli DH5α	Host strain for cloning	NEB
E. coli BL21(DE3)	Host strain for expression	NEB
E. coli BL21(DE3) + pET-28a(+)_*movX* + pGro7	Expression of MovX	This study
E. coli BL21(DE3) + pET-28a(+)_*movBC* + pGro7	Expression of MovB	This study
E. coli BL21(DE3) + pET-15b_*movC*	Expression of MovC	This study
E. coli BL21(DE3) + pRSFDuet-1_ 6HMBP*movA*	Expression of 6HMBP-MovA	This study
E. coli BL21(DE3) + pRSFDuet-1_ 6HMBP*movA*_*movX*	Expression of 6HMBP-MovA modified by MovX	This study
E. coli BL21(DE3) + pRSFDuet-1_ 6HMBP*movA*_*movBC*	Expression of 6HMBP-MovA modified by MovBC	This study
E. coli BL21(DE3) + pRSFDuet-1_ 6HMBP*movA*(53G>C)_*movXBC*	Expression of 6HMBP-MovA mutant modified by MovX	This study
E. coli BL21(DE3) + pRSFDuet-1_ 6HMBP*movA*(53G>A) _*movXBC*	Expression of 6HMBP-MovA mutant modified by MovX	This study
E. coli BL21(DE3) + pRSFDuet-1_ 6HMBP*movA*(59delG) _*movXBC*	Expression of 6HMBP-MovA mutant modified by MovBC	This study
V. fluvialis 33809	Search for mature natural product	ATCC

Table S2. Prevalence of MovX in microbial genomes. Strains and protein accession numbers are provided. Entries are in order of highest sequence similarity (%ID) to the MovX sequence from *V. fluvialis* 33809. Precursor sequences were identified through manual search of the genome region upstream of each homolog.

Strain	Accession	%ID	Precursor
Vibrio chagasii 30_O_60	CAH6879610.1	82.0	MNSEKKVVVKVKD KEMTCGSYNK
Vibrio chagasii 9_O_224	CAH7247531.1	81.7	MNSEKKVVVKVKD KEMTCGSYNK
Vibrio caribbeanicus Mu-116 Seq13	WP_268676783.1	64.7	MKNDKKVVVKVKN KEMTCGAFNQ
Vibrio caribbeanicus BAA-2122	EFP96643.1	57.8	MKNDKKVVVKVKD KEMTCGAFNK
Vibrio cholerae VC53	WP_071186992.1	57.5	MKNVKKVVVKVKD KEQTCGSYNK
Vibrio cholerae OYP4E08	WP_033933206.1	57.2	MKNVKKVVVKVKD KEQTCGSYNK
Xenorhabdus lircayensis VLS	WP_198690504.1	51.3	MKYEKCKKIVVKVK DKDKEITCGNYNK
Xenorhabdus beddingii DSM 4764	WP_086111277.1	49.4	MKNTIKVVVKVKDK ESTCASYNK
Achromobacter spanius UQ283	WP_164741260.1	46.2	MKSKKIVVKVNDK DATCGSYNK
Photorhabdus laumondii subsp. *laumondii* HP88	WP_058589819.1	40.5	MQKKTSVEIEVEVE DKEMTCGSYNK
Photorhabdus laumondii subsp. *laumondii* TT01	WP_011144912.1	40.5	MQKKTSVEIEVEVE DKEMTCGSYNK
Photorhabdus hindustanensis H1	WP_105396401.1	40.3	MQKKTSVEVEVED KEMTCGSYNK
Photorhabdus noenieputensis DSM 25462	WP_214088745.1	40.2	MQKKTSVEIEVEVE DKEMTCGSYNK
Chitinimonas sp. BJB300	WP_186293357.1	40.1	MNEKTITVEETNLIE ELQETELLEVNGG NRKLPQEIIRFIDDA TCGSYNL
Photorhabdus khanii subsp. *guanajuatensis* MEX20-17	WP_132355546.1	39.4	MQKKISVEVEVED KEMTCGSYNK
Sodalis ligni 159R	WP_165934114.1	39.4	MQNQMPVENEVE DEVEVIVEDKERTC GAYNL
Photorhabdus sp. S10-54	WP_205074150.1	38.7	MQKKTSVEVEDKE MTCGSYNK
Photorhabdus kleinii DSM 23513	WP_262980519.1	38.1	MQKKTSVEVEVED KEMTCGSYNK
Bacterium NHP-B	TGW14584.1	35.5	MTELNLEPVNTKD TQGIEELFLKDDEG GETCGDYTL

Bdellovibrio bacteriovorus R0	WP_157684773.1	34.4	MRMKVSDESVQRI GHGMTCGDYNL
Acinetobacter pittii WU_MDCI_Ap64	WP_262440532.1	33.7	MEFINVEEIQIIVSA VTCGDYNGIDIHKM
Acinetobacter baumannii 901B6-12EESBL	WP_162281436.1	33.6	MEFINVEEIQIIVSA VTCGDYNGIDIHKM
Streptomyces sp. SM10	WP_181011449.1	32.7	MIDIEEIEVVAEALT CGDYIR
Streptomyces zhihengii YIM T102	WP_205376219.1	32.7	MIDIEEIEVVAEALT CGDYIR
Kitasatospora viridis DSM 44826	WP_170304897.1	31.4	MIDIQDIEVMAEALT CGSYNKG
Streptomyces katrae ISP-5550	WP_045949669.1	30.3	MIDIQDIEVMAEALT CGSYNKG
Streptomyces virginiae NBC_00276	WP_266384123.1	29.8	MIDIQDIEVMAEALT CGSYNKG
Streptomyces sp. NRRL F-4428	WP_030028438.1	29.5	MIDIQDIEVVAEALT CGSYNRV
Streptomyces sp. TN58	WP_075971007.1	26.6	MIDIQDIEVVAEALT CGSYNRV

Table S3. HR-MS data for trypsin-cleaved MovA peptides following heterologous co-expression with either no enzyme, MovBC, or MovX.

Expression	Ion	Calc *m/z*	Obs *m/z*	Δppm
6HMBP-MovA	$[M+1H]^{1+}$	1032.4125	1032.4136	1.0
	$[M+2H]^{2+}$	516.7099	516.7127	5.4
6HMBP-MovA + MovBC	$[M+1H]^{1+}$	1028.3812	1028.3822	0.9
	$[M+2H]^{2+}$	514.6943	514.6940	0.5
6HMBP-MovA + MovX	$[M+1H]^{1+}$	789.2906	789.2915	1.1
	$[M+2H]^{2+}$	395.1489	395.1496	1.8

Table S4. HR-MS/MS data for trypsin-cleaved MovA.

Ion	Calc *m/z*	Obs *m/z*	Δppm	Sequence
b_1^{+1}	130.0499	130.0504	3.8	E
b_2^{+1}	261.0904	261.0912	3.1	EM
b_3^{+1}	362.1381	362.1389	2.3	EMT
b_4^{+1}	465.1473	465.1467	1.2	EMTC
b_5^{+1}	522.1687	522.1690	0.5	EMTCG
b_6^{+1}	609.2008	609.2001	1.1	EMTCGS
b_7^{+1}	772.2641	772.2628	1.7	EMTCGSY
b_8^{+1}	886.3070	886.3082	1.3	EMTCGSYN
b_9^{+1}	1014.4020	1014.4039	1.9	EMTCGSYNK
y_1^{+1}	147.1129	147.1133	3.1	K
y_2^{+1}	261.1558	261.1566	3.1	NK
y_3^{+1}	424.2191	424.2201	2.4	YNK
y_4^{+1}	511.2511	511.2524	2.5	SYNK
y_5^{+1}	568.2726	568.2743	3.0	GSYNK
y_6^{+1}	671.2818	671.2837	2.9	CGSYNK
y_7^{+1}	772.3295	772.3315	2.6	TCGSYNK
y_8^{+1}	903.3699	903.3713	1.5	MTCGSYNK
y_9^{+1}	1032.4125	1032.4147	2.1	EMTCGSYNK

Table S5. HR-MS/MS data for trypsin-cleaved, MovBC-modified MovA. The observed species is 4.0313 Da lighter than the substrate.

Ion	Calc *m/z*	Obs *m/z*	Δppm	Sequence
b_1^{+1}	130.0499	130.0503	3.0	E
b_2^{+1}	261.0904	261.0907	1.1	EM
b_3^{+1}	362.1381	Not Obs.	n/a	EMT
b_4^{+1}	461.1160	461.1191	6.8	EMTC
b_5^{+1}	518.1374	518.1335	7.6	EMTCG
b_6^{+1}	605.1695	605.1698	0.6	EMTCGS
b_7^{+1}	768.2328	768.2333	0.7	EMTCGSY
b_8^{+1}	882.2757	882.2789	3.6	EMTCGSYN
b_9^{+1}	1010.3707	1010.3718	1.1	EMTCGSYNK
y_1^{+1}	147.1129	147.1131	1.7	K
y_2^{+1}	261.1558	261.1565	2.8	NK
y_3^{+1}	424.2191	424.2200	2.1	YNK
y_4^{+1}	511.2511	511.2521	1.9	SYNK
y_5^{+1}	568.2726	568.2732	1.1	GSYNK
y_6^{+1}	667.2505	Not Obs.	n/a	CGSYNK
y_7^{+1}	768.2982	768.2993	1.5	TCGSYNK
y_8^{+1}	899.3386	899.3399	1.4	MTCGSYNK
y_9^{+1}	1028.3812	1028.3826	1.3	EMTCGSYNK

Table S6. HR-MS/MS data for trypsin-cleaved, MovBC-modified MovA that has undergone hydrolysis and decarboxylation. The observed species is 30.0105 Da lighter than the substrate.

Ion	Calc *m/z*	Obs *m/z*	Δppm	Sequence
b_1^{+1}	130.0499	Not Obs.	n/a	E
b_2^{+1}	261.0904	261.0908	1.5	EM
b_3^{+1}	362.1381	362.1362	5.2	EMT
b_4^{+1}	435.1368	Not Obs.	n/a	EMTC
b_5^{+1}	492.1582	492.1574	1.7	EMTCG
b_6^{+1}	579.1903	579.1950	8.2	EMTCGS
b_7^{+1}	742.2536	742.2506	4.0	EMTCGSY
b_8^{+1}	856.2965	856.2968	0.3	EMTCGSYN
b_9^{+1}	984.3915	984.3822	9.4	EMTCGSYNK
y_1^{+1}	147.1129	Not Obs.	n/a	K
y_2^{+1}	261.1558	261.1557	0.3	NK
y_3^{+1}	424.2191	424.2195	0.9	YNK
y_4^{+1}	511.2511	511.2538	5.2	SYNK
y_5^{+1}	568.2726	568.2727	0.2	GSYNK
y_6^{+1}	641.2713	641.2703	1.5	CGSYNK
y_7^{+1}	742.3190	742.3241	6.9	TCGSYNK
y_8^{+1}	873.3594	873.3569	2.9	MTCGSYNK
y_9^{+1}	1002.4020	1002.4001	1.9	EMTCGSYNK

Table S7. HR-MS/MS data for trypsin-cleaved, MovX-modified MovA. The observed species lacks the two *C*-terminal residues and is 0.9840 Da lighter than the unmodified 7mer peptide.

Ion	Calc *m/z*	Obs *m/z*	Δppm	Sequence
b_1^{+1}	130.0499	Not Obs.	n/a	E
b_2^{+1}	261.0904	261.0918	5.4	EM
b_3^{+1}	362.1381	362.1388	2.0	EMT
b_4^{+1}	465.1473	465.1473	0.1	EMTC
b_5^{+1}	522.1687	522.1666	4.1	EMTCG
b_6^{+1}	609.2008	609.1996	1.9	EMTCGS
b_7^{+1}	772.2641	772.2639	0.2	EMTCGSY
y_1^{+1}	181.0972	181.0960	6.8	Y
y_2^{+1}	268.1293	268.1273	7.3	SY
y_3^{+1}	325.1507	325.1525	5.4	GSY
y_4^{+1}	428.1599	428.1637	8.8	CGSY
y_5^{+1}	529.2076	529.2089	2.5	TCGSY
y_6^{+1}	660.2481	660.2532	7.7	MTCGSY
y_7^{+1}	789.2907	789.2889	2.3	EMTCGSY

Table S8. Observed mutations in the MovA coding sequence during cloning attempts for the heterologous co-expression of MovXBC with 6HMBP-MovA. For each mutant, DNA sequences and open reading frames are shown, with mutation sites underlined and dashes representing translational stops.

	DNA and Amino Acid Sequences
Mutant 1 (53G>C)	ATGAAAAACGAAAAAAAAGTGGTGGTGAAAGTGAAAGATAAAGAAATGA CCTCCGGCAGCTATAACAAATAA MKNEKKVVVKVKDKEMTSGSYNK-
Mutant 2 (53G>A)	ATGAAAAACGAAAAAAAAGTGGTGGTGAAAGTGAAAGATAAAGAAATGA CCTACGGCAGCTATAACAAATAA MKNEKKVVVKVKDKEMTYGSYNK-
Mutant 3 (59delG)	ATGAAAAACGAAAAAAAAGTGGTGGTGAAAGTGAAAGATAAAGAAATGA CCTGCGGCA_CTATAACAAATAAGAGCTCGGCGCGCCTGCAGGTCGAC AAGCTTGCGGCCGCATAA MKNEKKVVVKVKDKEMTCGTITNKSSARLQVDKLAAA-
Mutant 4 (23delT)	ATGAAAAACGAAAAAAAAGTGG_GGTGAAAGTGAAAGATAAAGAAATGA CCTGCGGCAGCTATAACAAATAA MKNEKKVG-K-KIKK-PAAAITN
Mutant 5 (42_43insA)	ATGAAAAACGAAAAAAAAGTGGTGGTGAAAGTGAAAGATAAAAGAAATG ACCTGCGGCAGCTATAACAAATAA MKNEKKVVVKVKDKRNDLRQL-QI
Mutant 6 (38_39insA)	ATGAAAAACGAAAAAAAAGTGGTGGTGAAAGTGAAAGAATAAAGAAATG ACCTGCGGCAGCTATAACAAATAA MKNEKKVVVKVKE-RNDLRQL-QI
Mutant 7 (43_44insG)	ATGAAAAACGAAAAAAAAGTGGTGGTGAAAGTGAAAGATAAAGGAAATG ACCTGCGGCAGCTATAACAAATAA MKNEKKVVVKVKDKGNDLRQL-QI

Table S9. HR-MS data for trypsin-cleaved mutant MovA peptides following heterologous co-expression with MovXBC.

Mutant	Ion	Calc *m/z*	Obs *m/z*	Δppm
1 (C18S)	$[M+1H]^{1+}$	773.3134	773.3155	2.7
	$[M+2H]^{2+}$	387.1604	387.1604	0.0
2 (C18Y)	$[M+1H]^{1+}$	849.3447	849.3461	1.6
	$[M+2H]^{2+}$	425.1760	425.1760	0.0
3	$[M+1H]^{1+}$	1093.4653	1093.4649	0.4
	$[M+2H]^{2+}$	547.2363	547.2373	1.8

Table S10. HR-MS/MS data for trypsin-cleaved MovA mutant 1 (C18S). The observed species lacks the two *C*-terminal residues and is 0.9840 Da lighter than the unmodified 7mer peptide.

Ion	Calc *m/z*	Obs *m/z*	Δppm	Sequence
b_1^{+1}	130.0499	Not Obs.	n/a	E
b_2^{+1}	261.0904	261.0903	0.4	EM
b_3^{+1}	362.1381	362.1374	1.9	EMT
b_4^{+1}	449.1701	449.1704	0.6	EMTS
b_5^{+1}	506.1916	506.1913	0.5	EMTSG
b_6^{+1}	593.2236	593.2236	0.0	EMTSGS
b_7^{+1}	756.2869	756.2872	0.4	EMTSGSY
y_1^{+1}	181.0972	181.0972	0.0	Y
y_2^{+1}	268.1293	268.1287	2.1	SY
y_3^{+1}	325.1507	325.1507	0.1	GSY
y_4^{+1}	412.1828	412.1828	0.1	SGSY
y_5^{+1}	513.2304	513.2303	0.3	TSGSY
y_6^{+1}	644.2709	644.2699	1.6	MTSGSY
y_7^{+1}	773.3135	773.3138	0.4	EMTSGSY

Table S11. HR-MS/MS data for trypsin-cleaved MovA mutant 2 (C18Y). The observed species lacks the two *C*-terminal residues and is 0.9840 Da lighter than the unmodified 7mer peptide.

Ion	Calc *m/z*	Obs *m/z*	Δppm	Sequence
b_1^{+1}	130.0499	Not Obs.	n/a	E
b_2^{+1}	261.0904	261.0899	1.9	EM
b_3^{+1}	362.1381	362.1371	2.7	EMT
b_4^{+1}	525.2014	525.2009	1.0	EMTY
b_5^{+1}	582.2229	582.2214	2.5	EMTYG
b_6^{+1}	669.2549	669.2545	0.6	EMTYGS
b_7^{+1}	832.3182	832.3189	0.8	EMTYGSY
y_1^{+1}	181.0972	181.0972	0.0	Y
y_2^{+1}	268.1293	268.1288	1.8	SY
y_3^{+1}	325.1507	325.1503	1.4	GSY
y_4^{+1}	488.2141	488.2131	2.0	YGSY
y_5^{+1}	589.2617	589.2612	0.9	TYGSY
y_6^{+1}	720.3022	720.3029	0.9	MTYGSY
y_7^{+1}	849.3448	849.3437	1.3	EMTYGSY

Table S12. HR-MS/MS data for trypsin-cleaved MovA mutant 3. The observed species is 4.0313 Da lighter than the substrate.

Ion	Calc *m/z*	Obs *m/z*	Δppm	Sequence
b_1^{+1}	130.0499	Not Obs.	n/a	E
b_2^{+1}	261.0904	261.0922	6.9	EM
b_3^{+1}	362.1381	Not Obs.	n/a	EMT
b_4^{+1}	461.1160	461.1173	2.9	EMTC
b_5^{+1}	518.1374	518.1352	4.3	EMTCG
b_6^{+1}	619.1851	619.1876	4.0	EMTCGT
b_7^{+1}	732.2692	732.2626	9.0	EMTCGTI
b_8^{+1}	833.3169	833.3159	1.1	EMTCGTIT
b_9^{+1}	947.3598	947.3565	3.5	EMTCGTITN
b_{10}^{+1}	1075.4547	1075.4539	0.8	EMTCGTITNK
y_1^{+1}	147.1129	147.1142	9.2	K
y_2^{+1}	261.1558	261.1555	1.1	NK
y_3^{+1}	362.2035	362.2037	0.7	TNK
y_4^{+1}	475.2875	475.2848	5.7	ITNK
y_5^{+1}	576.3352	576.3336	2.8	TITNK
y_6^{+1}	633.3567	633.3554	2.0	GTITNK
y_7^{+1}	732.3345	Not Obs.	n/a	CGTITNK
y_8^{+1}	833.3822	833.3813	1.1	TCGTITNK
y_9^{+1}	964.4227	964.4291	6.6	MTCGTITNK
y_{10}^{+1}	1093.4653	1093.4644	0.8	EMTCGTITNK

Table S13. Fe quantification for MovB and MovX. Shown are the averages of three independent measurements with the standard deviation (SD) noted in parentheses.

Protein	Fe equivalent (SD)
MovX	1.2 (0.1)
MovB	0.7 (0.1)

Table S14. HR-MS/MS data for MovA peptide.

Ion	Calc *m/z*	Obs *m/z*	Δppm	Sequence
b_1^{+1}	132.0478	132.0491	9.8	M
b_2^{+1}	260.1428	Not Obs.	n/a	MK
b_3^{+1}	374.1857	374.1883	6.9	MKN
b_4^{+1}	503.2283	503.2321	7.5	MKNE
b_5^{+1}	631.3233	631.3245	2.0	MKNEK
b_6^{+1}	759.4182	759.4177	0.7	MKNEKK
b_7^{+1}	858.4866	858.4865	0.2	MKNEKKV
b_8^{+1}	957.5550	957.5539	1.2	MKNEKKVV
b_9^{+1}	1056.6235	1056.6218	1.6	MKNEKKVVV
b_{10}^{+1}	1184.7184	1184.7125	5.0	MKNEKKVVVK
b_{11}^{+1}	1283.7868	1283.7904	2.8	MKNEKKVVVKV
b_{12}^{+1}	1411.8818	1411.8773	3.2	MKNEKKVVVKVK
b_{13}^{+1}	1526.9087	1526.9133	3.0	MKNEKKVVVKVKD
b_{14}^{+1}	1655.0037	1654.9946	5.5	MKNEKKVVVKVKDK
b_{15}^{+1}	1784.0463	1784.0287	9.9	MKNEKKVVVKVKDKE
b_{16}^{+1}	1915.0868	1915.0742	6.6	MKNEKKVVVKVKDKEM
b_{17}^{+1}	2016.1345	2016.1247	4.8	MKNEKKVVVKVKDKEMT
b_{18}^{+1}	2119.1436	2119.1483	2.2	MKNEKKVVVKVKDKEMTC
b_{19}^{+1}	2176.1651	2176.1777	5.8	MKNEKKVVVKVKDKEMTCG
b_{20}^{+1}	2263.1971	2263.1810	7.1	MKNEKKVVVKVKDKEMTCGS
b_{21}^{+1}	2426.2605	2426.2494	4.6	MKNEKKVVVKVKDKEMTCGSY
b_{22}^{+1}	2540.3034	2540.3018	0.6	MKNEKKVVVKVKDKEMTCGSYN
b_{23}^{+1}	2668.3984	Not Obs.	n/a	MKNEKKVVVKVKDKEMTCGSYNK
y_1^{+1}	147.1129	Not Obs.	n/a	K
y_2^{+1}	261.1558	Not Obs.	n/a	NK
y_3^{+1}	424.2191	424.2231	9.4	YNK
y_4^{+1}	511.2511	511.2551	7.8	SYNK
y_5^{+1}	568.2726	568.2759	5.8	GSYNK
y_6^{+1}	671.2818	671.2830	1.8	CGSYNK
y_7^{+1}	772.3295	772.3296	0.2	TCGSYNK
y_8^{+1}	903.3699	903.3684	1.7	MTCGSYNK
y_9^{+1}	1032.4125	1032.4116	0.9	EMTCGSYNK
y_{10}^{+1}	1160.5075	1160.5072	0.3	KEMTCGSYNK
y_{11}^{+1}	1275.5344	1275.5364	1.5	DKEMTCGSYNK
y_{12}^{+1}	1403.6294	1403.6311	1.2	KDKEMTCGSYNK
y_{13}^{+1}	1502.6978	1502.7010	2.1	VKDKEMTCGSYNK
y_{14}^{+1}	1630.7928	1630.7942	0.9	KVKDKEMTCGSYNK
y_{15}^{+1}	1729.8612	1729.8597	0.9	VKVKDKEMTCGSYNK
y_{16}^{+1}	1828.9296	1828.9296	0.0	VVKVKDKEMTCGSYNK
y_{17}^{+1}	1927.9980	1927.9955	1.3	VVVKVKDKEMTCGSYNK
y_{18}^{+1}	2056.0930	2056.0730	9.7	KVVVKVKDKEMTCGSYNK
y_{19}^{+1}	2184.1880	2184.1705	8.0	KKVVVKVKDKEMTCGSYNK
y_{20}^{+1}	2313.2305	2313.2272	1.4	EKKVVVKVKDKEMTCGSYNK
y_{21}^{+1}	2427.2735	2427.2773	1.6	NEKKVVVKVKDKEMTCGSYNK
y_{22}^{+1}	2555.3684	Not Obs.	n/a	KNEKKVVVKVKDKEMTCGSYNK
y_{23}^{+1}	2686.4089	Not Obs.	n/a	MKNEKKVVVKVKDKEMTCGSYNK

Table S15. HR-MS data for *in vitro* enzymatic assays with either synthetic MovA or MovA obtained via heterologous co-expression in *E. coli* (indicated with a star).

Substrate	Enzyme	Ion	Calc *m/z*	Obs *m/z*	Δppm
MovA	No Enzyme	$[M+2H]^{2+}$	1343.7081	1343.7085	0.3
		$[M+3H]^{3+}$	896.1412	896.1418	0.7
		$[M+4H]^{4+}$	672.3577	672.3584	1.0
MovA	MovB (-4 Da)	$[M+2H]^{2+}$	1341.6925	1341.6869	4.2
		$[M+3H]^{3+}$	894.7974	894.7926	5.4
		$[M+4H]^{4+}$	671.3499	671.3483	2.4
MovA	MovC	$[M+2H]^{2+}$	1343.7081	1343.7023	4.3
		$[M+3H]^{3+}$	896.1412	896.1352	6.7
		$[M+4H]^{4+}$	672.3577	672.3556	3.1
MovA	MovBC (-4 Da)	$[M+2H]^{2+}$	1341.6925	1341.6898	2.0
		$[M+3H]^{3+}$	894.7974	894.7987	1.4
		$[M+4H]^{4+}$	671.3499	671.3511	1.8
MovA	MovX (-243 Da)	$[M+3H]^{2+}$	1222.1472	1222.1419	4.3
		$[M+4H]^{3+}$	815.1006	815.0979	3.3
		$[M+5H]^{4+}$	611.5773	611.5777	0.7
MovA	MovXBC (-247 Da)	$[M+3H]^{2+}$	1220.1315	1220.1319	0.3
		$[M+4H]^{3+}$	813.7568	813.7584	2.0
		$[M+5H]^{4+}$	610.5694	610.5731	6.1
MovA*	No Enzyme	$[M+3H]^{3+}$	1087.5541	1087.5522	1.7
		$[M+4H]^{4+}$	815.9174	815.9165	1.1
		$[M+5H]^{5+}$	652.9353	652.9371	2.8
MovX-modified MovA* (-243 Da)	MovBC (-4 Da)	$[M+3H]^{3+}$	1005.1697	1005.1694	0.3
		$[M+4H]^{4+}$	754.1291	754.1299	1.0
		$[M+5H]^{5+}$	603.5047	603.5077	5.0
MovBC-modified MovA* (-4 Da)	MovX (-243 Da)	$[M+3H]^{3+}$	1005.1697	1005.1637	6.0
		$[M+4H]^{4+}$	754.1291	754.1256	4.7
		$[M+5H]^{5+}$	603.5047	603.5043	0.7
Hydrolyzed MovBC-modified MovA* (+14 Da)	MovX (-243 Da)	$[M+3H]^{3+}$	1011.1732	1011.1695	3.7
		$[M+4H]^{4+}$	758.6318	785.6302	2.1
		$[M+5H]^{5+}$	607.1068	607.1083	2.5

Table S16. HR-MS/MS data for MovA peptide following the *in vitro* reaction with MovBC in the presence of ascorbate and DTT. The observed species is 4.0313 Da lighter than the substrate.

Ion	Calc *m/z*	Obs *m/z*	Δppm	Sequence
b_1^{+1}	132.0478	Not Obs.	n/a	M
b_2^{+1}	260.1428	260.1421	2.6	MK
b_3^{+1}	374.1857	374.1840	4.5	MKN
b_4^{+1}	503.2283	503.2241	8.3	MKNE
b_5^{+1}	631.3233	631.3247	2.3	MKNEK
b_6^{+1}	759.4182	759.4196	1.8	MKNEKK
b_7^{+1}	858.4866	858.4868	0.2	MKNEKKV
b_8^{+1}	957.5550	957.5559	0.9	MKNEKKVV
b_9^{+1}	1056.6235	1056.6214	1.9	MKNEKKVVV
b_{10}^{+1}	1184.7184	1184.7212	2.3	MKNEKKVVVK
b_{11}^{+1}	1283.7868	1283.7847	1.7	MKNEKKVVVKV
b_{12}^{+1}	1411.8818	1411.8855	2.6	MKNEKKVVVKVK
b_{13}^{+1}	1526.9087	1526.9169	5.3	MKNEKKVVVKVKD
b_{14}^{+2}	828.0055	828.0073	2.2	MKNEKKVVVKVKDK
b_{15}^{+2}	892.5268	892.5272	0.4	MKNEKKVVVKVKDKE
b_{16}^{+2}	958.0471	958.0417	5.6	MKNEKKVVVKVKDKEM
b_{17}^{+2}	1006.5552	Not Obs.	n/a	MKNEKKVVVKVKDKEMT
b_{18}^{+2}	1058.0598	1058.0700	9.6	MKNEKKVVVKVKDKEMTC
b_{19}^{+2}	1086.5706	1086.5704	0.1	MKNEKKVVVKVKDKEMTCG
b_{20}^{+2}	1130.0866	1130.0830	3.2	MKNEKKVVVKVKDKEMTCGS
b_{21}^{+2}	1211.6182	1211.6085	8.0	MKNEKKVVVKVKDKEMTCGSY
b_{22}^{+2}	1268.6397	1268.6335	4.9	MKNEKKVVVKVKDKEMTCGSYN
b_{23}^{+2}	1332.6872	1332.6991	8.9	MKNEKKVVVKVKDKEMTCGSYNK
y_1^{+1}	147.1129	Not Obs.	n/a	K
y_2^{+1}	261.1558	261.1562	1.6	NK
y_3^{+1}	424.2191	424.2223	7.5	YNK
y_4^{+1}	511.2511	511.2535	4.6	SYNK
y_5^{+1}	568.2726	568.2749	4.0	GSYNK
y_6^{+1}	667.2505	Not Obs.	n/a	CGSYNK
y_7^{+1}	768.2982	768.2933	6.3	TCGSYNK
y_8^{+1}	899.3386	899.3374	1.4	MTCGSYNK
y_9^{+1}	1028.3812	1028.3777	3.4	EMTCGSYNK
y_{10}^{+1}	1156.4762	1156.4721	3.5	KEMTCGSYNK
y_{11}^{+1}	1271.5031	1271.4972	4.7	DKEMTCGSYNK
y_{12}^{+1}	1399.5981	1399.5874	7.7	KDKEMTCGSYNK
y_{13}^{+1}	1498.6665	1498.6592	4.9	VKDKEMTCGSYNK
y_{14}^{+1}	1626.7615	1626.7702	5.4	KVKDKEMTCGSYNK
y_{15}^{+1}	1725.8299	1725.8414	6.7	VKVKDKEMTCGSYNK
y_{16}^{+1}	1824.8983	1824.9164	9.9	VVKVKDKEMTCGSYNK
y_{17}^{+1}	1923.9667	1923.9626	2.1	VVVKVKDKEMTCGSYNK
y_{18}^{+1}	2052.0617	2052.0452	8.0	KVVVKVKDKEMTCGSYNK
y_{19}^{+2}	1090.5820	1090.5745	6.9	KKVVVKVKDKEMTCGSYNK
y_{20}^{+2}	1155.1033	1155.1113	6.9	EKKVVVKVKDKEMTCGSYNK
y_{21}^{+2}	1212.1247	1212.1208	3.3	NEKKVVVKVKDKEMTCGSYNK
y_{22}^{+2}	1276.1722	Not Obs.	n/a	KNEKKVVVKVKDKEMTCGSYNK
y_{23}^{+2}	1341.6925	Not Obs.	n/a	MKNEKKVVVKVKDKEMTCGSYNK

Table S17. HR-MS/MS data for MovBC-modified MovA, obtained via heterologous co-expression of 6HMBP-MovA and MovBC, following the *in vitro* reaction with MovX in the presence of ascorbate and DTT. The observed species lacks the two *C*-terminal residues and is 5.0153 Da lighter than the unmodified 27mer peptide.

Ion	Calc *m/z*	Obs *m/z*	Δppm	Sequence
b_1^{+1}	58.0288	Not Obs.	n/a	G
b_2^{+1}	155.0816	155.0819	2.3	GP
b_3^{+1}	284.1241	284.1240	0.5	GPE
b_4^{+1}	431.1926	431.1932	1.5	GPEF
b_5^{+1}	488.2140	488.2128	2.5	GPEFG
b_6^{+1}	575.2461	575.2513	9.1	GPEFGS
b_7^{+1}	706.2865	706.2904	5.5	GPEFGSM
b_8^{+1}	834.3815	834.3746	8.3	GPEFGSMK
b_9^{+1}	948.4244	948.4230	1.5	GPEFGSMKN
b_{10}^{+1}	1077.4670	1077.4659	1.0	GPEFGSMKNE
b_{11}^{+1}	1205.5620	1205.5629	0.8	GPEFGSMKNEK
b_{12}^{+1}	1333.6569	1333.6555	1.1	GPEFGSMKNEKK
b_{13}^{+1}	1432.7254	1432.7269	1.1	GPEFGSMKNEKKV
b_{14}^{+1}	1531.7938	1531.7981	2.8	GPEFGSMKNEKKVV
b_{15}^{+1}	1630.8622	1630.8539	5.1	GPEFGSMKNEKKVVV
b_{16}^{+1}	1758.9571	1758.9588	0.9	GPEFGSMKNEKKVVVK
b_{17}^{+2}	929.5164	929.5186	2.3	GPEFGSMKNEKKVVVKV
b_{18}^{+2}	993.5639	993.5592	4.8	GPEFGSMKNEKKVVVKVK
b_{19}^{+2}	1051.0774	1051.0738	3.4	GPEFGSMKNEKKVVVKVKD
b_{20}^{+2}	1115.1249	1115.1345	8.6	GPEFGSMKNEKKVVVKVKDK
b_{21}^{+2}	1179.6462	Not Obs.	n/a	GPEFGSMKNEKKVVVKVKDKE
b_{22}^{+2}	1245.1664	1245.1572	7.4	GPEFGSMKNEKKVVVKVKDKEM
b_{23}^{+2}	1295.6903	Not Obs.	n/a	GPEFGSMKNEKKVVVKVKDKEMT
b_{24}^{+2}	1345.1792	Not Obs.	n/a	GPEFGSMKNEKKVVVKVKDKEMTC
b_{25}^{+2}	1373.6899	1373.6951	3.8	GPEFGSMKNEKKVVVKVKDKEMTCG
b_{26}^{+2}	1417.2059	Not Obs.	n/a	GPEFGSMKNEKKVVVKVKDKEMTCGS
b_{27}^{+2}	1498.7376	Not Obs.	n/a	GPEFGSMKNEKKVVVKVKDKEMTCGSY
y_1^{+1}	181.0972	181.0974	1.0	Y
y_2^{+1}	268.1292	268.1295	1.0	SY
y_3^{+1}	325.1507	325.1515	2.4	GSY
y_4^{+1}	424.1286	Not Obs.	n/a	CGSY
y_5^{+1}	525.1763	525.1806	8.2	TCGSY
y_6^{+1}	656.2168	656.2163	0.7	MTCGSY
y_7^{+1}	785.2594	785.2624	3.9	EMTCGSY
y_8^{+1}	913.3543	913.3604	6.7	KEMTCGSY
y_9^{+1}	1028.3813	1028.3811	0.1	DKEMTCGSY
y_{10}^{+1}	1156.4762	1156.4768	0.5	KDKEMTCGSY
y_{11}^{+1}	1255.5446	1255.5468	1.7	VKDKEMTCGSY
y_{12}^{+2}	692.3235	692.3271	5.3	KVKDKEMTCGSY
y_{13}^{+2}	741.8577	741.8627	6.8	VKVKDKEMTCGSY
y_{14}^{+2}	791.3919	791.3910	1.1	VVKVKDKEMTCGSY
y_{15}^{+2}	840.9261	840.9287	3.1	VVVKVKDKEMTCGSY
y_{16}^{+2}	904.9736	904.9754	2.0	KVVVKVKDKEMTCGSY
y_{17}^{+2}	969.0210	969.0234	2.4	KKVVVKVKDKEMTCGSY

y_{18}^{+2}	1033.5423	1033.5387	3.5	EKKVVVKVKDKEMTCGSY
y_{19}^{+2}	1090.5638	1090.5701	5.8	NEKKVVVKVKDKEMTCGSY
y_{20}^{+2}	1154.6113	1154.6090	2.0	KNEKKVVVKVKDKEMTCGSY
y_{21}^{+2}	1220.1315	Not Obs.	n/a	MKNEKKVVVKVKDKEMTCGSY
y_{22}^{+2}	1263.6475	1263.6351	9.8	SMKNEKKVVVKVKDKEMTCGSY
y_{23}^{+2}	1292.1583	1292.153	4.1	GSMKNEKKVVVKVKDKEMTCGSY
y_{24}^{+2}	1365.6925	1365.6901	1.7	FGSMKNEKKVVVKVKDKEMTCGSY
y_{25}^{+2}	1430.2138	Not Obs.	n/a	EFGSMKNEKKVVVKVKDKEMTCGSY
y_{26}^{+2}	1478.7402	Not Obs.	n/a	PEFGSMKNEKKVVVKVKDKEMTCGSY
y_{27}^{+2}	1507.2509	Not Obs.	n/a	GPEFGSMKNEKKVVVKVKDKEMTCGSY

Table S18. HR-MS/MS data for MovA peptide following the *in vitro* reaction with MovX in the presence of ascorbate and DTT. The observed species lacks the two *C*-terminal residues and is 0.9840 Da lighter than the unmodified 21mer peptide.

Ion	Calc *m/z*	Obs *m/z*	Δppm	Sequence
b_1^{+1}	132.0478	Not Obs.	n/a	M
b_2^{+1}	260.1428	Not Obs.	n/a	MK
b_3^{+1}	374.1857	374.1880	6.1	MKN
b_4^{+1}	503.2283	503.2285	0.4	MKNE
b_5^{+1}	631.3233	631.3218	2.3	MKNEK
b_6^{+1}	759.4182	759.4163	2.5	MKNEKK
b_7^{+1}	858.4866	858.4870	0.4	MKNEKKV
b_8^{+1}	957.5550	957.5534	1.7	MKNEKKVV
b_9^{+1}	1056.6235	1056.6192	4.0	MKNEKKVVV
b_{10}^{+1}	1184.7184	1184.7133	4.3	MKNEKKVVVK
b_{11}^{+1}	1283.7868	1283.7906	2.9	MKNEKKVVVKV
b_{12}^{+2}	706.4446	706.4424	3.1	MKNEKKVVVKVK
b_{13}^{+2}	763.9580	763.9586	0.7	MKNEKKVVVKVKD
b_{14}^{+2}	828.0055	828.0065	1.2	MKNEKKVVVKVKDK
b_{15}^{+2}	892.5268	892.5282	1.6	MKNEKKVVVKVKDKE
b_{16}^{+2}	958.0471	958.0435	3.7	MKNEKKVVVKVKDKEM
b_{17}^{+2}	1008.5709	1008.5727	1.8	MKNEKKVVVKVKDKEMT
b_{18}^{+2}	1060.0755	1060.0786	2.9	MKNEKKVVVKVKDKEMTC
b_{19}^{+2}	1088.5862	1088.5835	2.5	MKNEKKVVVKVKDKEMTCG
b_{20}^{+2}	1132.1022	1132.1026	0.3	MKNEKKVVVKVKDKEMTCGS
b_{21}^{+2}	1213.6339	Not Obs.	n/a	MKNEKKVVVKVKDKEMTCGSY
y_1^{+1}	181.0972	Not Obs.	n/a	Y
y_2^{+1}	268.1293	268.1267	9.6	SY
y_3^{+1}	325.1507	325.1535	8.5	GSY
y_4^{+1}	428.1599	428.1601	0.4	CGSY
y_5^{+1}	529.2076	Not Obs.	n/a	TCGSY
y_6^{+1}	660.2481	660.2502	3.2	MTCGSY
y_7^{+1}	789.2907	789.2887	2.5	EMTCGSY
y_8^{+1}	917.3856	917.3851	0.6	KEMTCGSY
y_9^{+1}	1032.4126	1032.4124	0.2	DKEMTCGSY
y_{10}^{+1}	1160.5076	Not Obs.	n/a	KDKEMTCGSY
y_{11}^{+1}	1259.5760	1259.5666	7.4	VKDKEMTCGSY
y_{12}^{+1}	1387.6709	1387.6643	4.8	KVKDKEMTCGSY
y_{13}^{+1}	1486.7393	1486.7487	6.3	VKVKDKEMTCGSY
y_{14}^{+1}	1585.8078	1585.8040	2.4	VVKVKDKEMTCGSY
y_{15}^{+1}	1684.8762	1684.8871	6.5	VVVKVKDKEMTCGSY
y_{16}^{+2}	906.9892	906.9817	8.3	KVVVKVKDKEMTCGSY
y_{17}^{+2}	971.0367	971.0336	3.2	KKVVVKVKDKEMTCGSY
y_{18}^{+2}	1035.5580	1035.5615	3.4	EKKVVVKVKDKEMTCGSY
y_{19}^{+2}	1092.5795	1092.5800	0.5	NEKKVVVKVKDKEMTCGSY
y_{20}^{+2}	1156.6270	1156.6258	1.0	KNEKKVVVKVKDKEMTCGSY
y_{21}^{+2}	1222.1472	Not Obs.	n/a	MKNEKKVVVKVKDKEMTCGSY

Table S19. HR-MS/MS data for MovA peptide following the *in vitro* reaction with MovXBC in the presence of ascorbate and DTT. The observed species lacks the two *C*-terminal residues and is 5.0153 Da lighter than the unmodified 21mer peptide.

Ion	Calc *m/z*	Obs *m/z*	Δppm	Sequence
b_1^{+1}	132.0478	Not Obs.	n/a	M
b_2^{+1}	260.1428	260.1423	1.8	MK
b_3^{+1}	374.1857	374.1863	1.6	MKN
b_4^{+1}	503.2283	503.2272	2.2	MKNE
b_5^{+1}	631.3233	631.3220	2.0	MKNEK
b_6^{+1}	759.4182	759.4175	0.9	MKNEKK
b_7^{+1}	858.4866	858.4827	4.6	MKNEKKV
b_8^{+1}	957.5550	957.5545	0.6	MKNEKKVV
b_9^{+1}	1056.6235	1056.6280	4.3	MKNEKKVVV
b_{10}^{+1}	1184.7184	1184.7149	3.0	MKNEKKVVVK
b_{11}^{+1}	1283.7868	1283.7857	0.9	MKNEKKVVVKV
b_{12}^{+2}	706.4446	706.4417	4.0	MKNEKKVVVKVK
b_{13}^{+2}	763.9580	763.9554	3.4	MKNEKKVVVKVKD
b_{14}^{+2}	828.0055	828.0023	3.9	MKNEKKVVVKVKDK
b_{15}^{+2}	892.5268	892.5268	0.0	MKNEKKVVVKVKDKE
b_{16}^{+2}	958.0471	958.0453	1.8	MKNEKKVVVKVKDKEM
b_{17}^{+2}	1008.5709	Not Obs.	n/a	MKNEKKVVVKVKDKEMT
b_{18}^{+2}	1058.0598	1058.0547	4.8	MKNEKKVVVKVKDKEMTC
b_{19}^{+2}	1086.5706	1086.5712	0.6	MKNEKKVVVKVKDKEMTCG
b_{20}^{+2}	1130.0866	1130.0837	2.5	MKNEKKVVVKVKDKEMTCGS
b_{21}^{+2}	1211.6182	Not Obs.	n/a	MKNEKKVVVKVKDKEMTCGSY
y_1^{+1}	181.0972	181.0970	1.2	Y
y_2^{+1}	268.1292	268.1288	1.6	SY
y_3^{+1}	325.1507	325.1493	4.3	GSY
y_4^{+1}	424.1286	Not Obs.	n/a	CGSY
y_5^{+1}	525.1763	525.1788	4.8	TCGSY
y_6^{+1}	656.2168	656.2142	3.9	MTCGSY
y_7^{+1}	785.2594	Not Obs.	n/a	EMTCGSY
y_8^{+1}	913.3543	913.3484	6.5	KEMTCGSY
y_9^{+1}	1028.3813	1028.3794	1.8	DKEMTCGSY
y_{10}^{+1}	1156.4762	1156.4740	1.9	KDKEMTCGSY
y_{11}^{+1}	1255.5446	1255.5458	0.9	VKDKEMTCGSY
y_{12}^{+1}	1383.6396	1383.6441	3.3	KVKDKEMTCGSY
y_{13}^{+1}	1482.7080	Not Obs.	n/a	VKVKDKEMTCGSY
y_{14}^{+1}	1581.7764	1581.7842	4.9	VVKVKDKEMTCGSY
y_{15}^{+1}	1680.8448	1680.8296	9.1	VVVKVKDKEMTCGSY
y_{16}^{+2}	904.9736	904.9715	2.3	KVVVKVKDKEMTCGSY
y_{17}^{+2}	969.0210	969.0203	0.8	KKVVVKVKDKEMTCGSY
y_{18}^{+2}	1033.5423	1033.5405	1.8	EKKVVVKVKDKEMTCGSY
y_{19}^{+2}	1090.5638	1090.5655	1.6	NEKKVVVKVKDKEMTCGSY
y_{20}^{+2}	1154.6113	1154.6049	5.5	KNEKKVVVKVKDKEMTCGSY
y_{21}^{+2}	1220.1315	Not Obs.	n/a	MKNEKKVVVKVKDKEMTCGSY

Table S20. NMR assignments for linear, MovBC-modified, and MovXBC-modified MovA trypsin fragments. Abbreviations: “n.d.” for signals not determined, “n.f.” for signals not found, and “–” for signals not expected.

		Linear substrate		MovBC product		MovXBC product	
		δH	δC	δH	δC	δH	δC
E	C	–	169.4	–	169.6	–	n.f.
	α	4.09	52.5	4.08	52.7	n.f.	n.f.
	β	2.15	26.3	2.13	27.5	1.95, 2.01	30.1
	γ	2.52	29.3	2.39	32.8	2.31	33.0
	δ	–	176.2	–	180.3	–	n.f.
M	C	–	173.4	–	n.f.	–	172.8
	α	4.58	53.3	4.59	52.9	4.53	52.9
	β	2.01, 2.08	30.8	2.06	30.2	2.02	30.1
	γ	2.56	29.5	2.57	29.4	2.52	29.2
	ε	2.06	14.6	2.08	14.3	2.04	14.2
T	C	–	171.8	–	157.2	–	156.9
	α	4.37	59.4	4.93	53.5	4.91	53.4
	β	4.19	67.5	4.33	67.3	4.28	67.3
	γ	1.18	19.2	1.19	18.6	1.15	18.5
C	C	–	172.4	–	n.d.	–	n.d.
	α	4.52	56.0	–	–	–	–
	β	2.92	25.7	–	165.6	–	165.5
G	C	–	171.4	–	172.6	–	172.4
	α	3.95	43.0	4.13	42.5	4.09	42.6
S	C	–	171.6	–	171.5	–	171.2
	α	4.39	55.8	4.44	55.5	4.41	55.5
	β	3.75	61.4	3.77	60.7	3.67, 3.72	60.6
Y	C	–	172.8	–	172.7	–	175.5
	α	4.55	55.5	4.59	55.0	4.51	54.9
	β	2.93, 3.04	36.3	2.97, 3.12	35.8	2.91, 3.12	35.9
	γ	–	128.0	–	128.1	–	128.1
	δ	7.09	131.0	7.11	130.5	7.08	130.5
	ε	6.79	115.8	6.81	115.6	6.77	115.4
	ζ	–	154.6	–	154.5	–	154.1
N	C	–	172.0	–	171.1	–	–
	α	4.63	50.6	4.70	50.5	–	–
	β	2.64, 2.74	36.7	2.68, 2.81	36.1	–	–
	γ	–	174.4	–	174.5	–	–
K	C	–	175.4	–	178.4	–	–
	α	4.30	53.0	4.17	54.9	–	–
	β	1.74, 1.89	30.2	1.71, 1.83	31.0	–	–
	γ	1.40	22.4	1.39	22.0	–	–
	δ	1.66	26.6	1.68	26.2	–	–
	ε	2.96	39.6	3.00	39.2	–	–

Table S21. HR-MS data for unlabeled and ^{15}N-labeled MovA peptides following *in vitro* reactions with MovX or MovXBC in the presence of ascorbate and DTT.

Substrate	Enzyme	Ion	Calc *m/z*	Obs *m/z*	Δppm
MovA	No Enzyme	$[M+2H]^{2+}$	1343.7081	1343.7091	0.7
		$[M+3H]^{3+}$	896.1412	896.1401	1.2
		$[M+4H]^{4+}$	672.3577	672.3590	1.9
MovA	MovX (-243 Da)	$[M+2H]^{2+}$	1222.1472	1222.1479	0.6
		$[M+3H]^{3+}$	815.1006	815.0999	0.9
		$[M+4H]^{4+}$	611.5773	611.5796	3.8
MovA	MovXBC (-247 Da)	$[M+2H]^{2+}$	1220.1315	1220.1327	1.0
		$[M+3H]^{3+}$	813.7568	813.7564	0.5
		$[M+4H]^{4+}$	610.5694	610.5720	4.3
^{15}Nβ-Asn-MovA	No Enzyme	$[M+2H]^{2+}$	1344.2066	1344.2071	0.4
		$[M+3H]^{3+}$	896.4735	896.4720	1.7
		$[M+4H]^{4+}$	672.6070	672.6082	1.8
^{15}Nβ-Asn-MovA	MovX (-243 Da)	$[M+3H]^{2+}$	1222.1472	1222.1468	0.3
		$[M+4H]^{3+}$	815.1006	815.0999	0.9
		$[M+5H]^{4+}$	611.5773	611.5793	3.3
^{15}Nβ-Asn-MovA	MovXBC (-247 Da)	$[M+3H]^{2+}$	1220.1315	1220.1337	1.8
		$[M+4H]^{3+}$	813.7568	813.7573	0.6
		$[M+5H]^{4+}$	610.5694	610.5719	4.1
$^{15}N_2$-Asn-MovA	No Enzyme	$[M+3H]^{3+}$	1344.7051	1344.7054	0.2
		$[M+4H]^{4+}$	896.8059	896.8044	1.7
		$[M+5H]^{5+}$	672.8562	672.8572	1.5
$^{15}N_2$-Asn-MovA	MovX (-242 Da)	$[M+3H]^{3+}$	1222.6457	1222.6450	0.6
		$[M+4H]^{4+}$	815.4329	815.4318	1.3
		$[M+5H]^{5+}$	611.8265	611.8284	3.1
$^{15}N_2$-Asn-MovA	MovXBC (-246 Da)	$[M+3H]^{3+}$	1220.6300	1220.6309	0.7
		$[M+4H]^{4+}$	814.0891	814.0887	0.5
		$[M+5H]^{5+}$	610.8187	610.8213	4.3

Table S22. HR-MS/MS data for trypsin-cleaved $^{15}N_2$-Asn-MovA peptide following the *in vitro* reaction with MovX in the presence of ascorbate and DTT. The observed species lacks the two *C*-terminal residues and is 0.0130 Da heavier than the substrate.

Ion	Calc *m/z*	Obs *m/z*	Δppm	Sequence
b_1^{+1}	130.0499	Not Obs.	n/a	E
b_2^{+1}	261.0904	Not Obs.	n/a	EM
b_3^{+1}	362.1381	362.1402	5.9	EMT
b_4^{+1}	465.1473	465.1507	7.4	EMTC
b_5^{+1}	522.1687	522.1695	1.5	EMTCG
b_6^{+1}	609.2008	609.2034	4.3	EMTCGS
b_7^{+1}	772.2641	772.2667	3.4	EMTCGSY
y_1^{+1}	182.0942	Not Obs.	n/a	Y
y_2^{+1}	269.1262	269.1267	1.9	SY
y_3^{+1}	326.1477	326.1487	3.1	GSY
y_4^{+1}	429.1569	Not Obs.	n/a	CGSY
y_5^{+1}	530.2046	530.2072	4.8	TCGSY
y_6^{+1}	661.2451	661.2499	7.2	MTCGSY
y_7^{+1}	790.2877	790.2884	0.9	EMTCGSY

Table S23. HR-MS/MS data for trypsin-cleaved $^{15}N_2$-Asn-MovA peptide following the *in vitro* reaction with MovXBC in the presence of ascorbate and DTT. The observed species lacks the two *C*-terminal residues and is 4.0183 Da lighter than the substrate.

Ion	Calc *m/z*	Obs *m/z*	Δppm	Sequence
b_1^{+1}	130.0499	Not Obs.	n/a	E
b_2^{+1}	261.0904	261.0904	0.0	EM
b_3^{+1}	362.1381	Not Obs.	n/a	EMT
b_4^{+1}	461.1160	461.1162	0.5	EMTC
b_5^{+1}	518.1374	518.1386	2.3	EMTCG
b_6^{+1}	605.1695	605.1669	4.2	EMTCGS
b_7^{+1}	768.2328	768.2344	2.1	EMTCGSY
y_1^{+1}	182.0942	182.0943	0.5	Y
y_2^{+1}	269.1262	269.1272	3.7	SY
y_3^{+1}	326.1478	326.1457	6.4	GSY
y_4^{+1}	425.1256	Not Obs.	n/a	CGSY
y_5^{+1}	526.1733	526.1720	2.5	TCGSY
y_6^{+1}	657.2138	657.2094	6.7	MTCGSY
y_7^{+1}	786.2564	786.2574	1.3	EMTCGSY

Figure S1 (page S34)**.** Methanobactin diversity and biosynthesis. (A) Structurally characterized methanobactins.[8–12] All methanobactins characterized to date contain two heterocyclic rings with associated enethiol groups through which they coordinate copper in a distorted tetrahedral geometry. All structures feature a *C*-terminal oxazolone, while the *N*-terminal ring is either an oxazolone, a pyrazinedione, or an imidazolone group (the latter has been called into question with a recent report suggesting the presence of a pyrazinedione instead[9]). Group I methanobactins have been isolated from *Methylosinus* species and feature a disulfide bridge, while Group II methanobactins have been isolated from *Methylocystis* species and harbor a sulfonated threonine residue. Oxazolone, pyrazinedione, and imidazolone moieties are highlighted in red, blue, and green, respectively. (B) Schematic representation of Group I–V operons. Clusters were initially categorized based on phylogenetic analyses of the precursor peptide MbnA and biosynthetic enzymes MbnB and MbnC, and then refined using conservation of genomic neighborhoods.[13] (C) Alignment of select precursor peptides from Groups I–V. Apart from Group V peptides, which contain only one Cys residue, the remaining precursors contain two conserved Cys residues (marked with a star); the *N*-terminal Cys is usually followed by a small hydrophobic residue (Gly or Ala) and then a slightly larger, polar residue (Ser or Thr). Group I peptides contain an additional pair of cysteine residues, which undergoes disulfide bond formation.

A

Group I

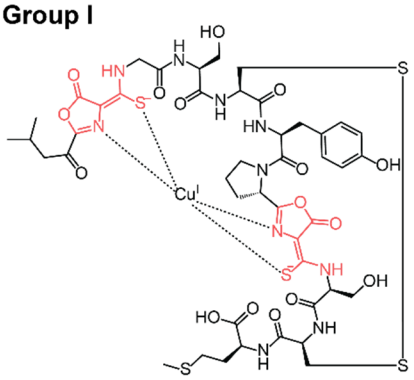

Methylosinus trichosporium OB3b

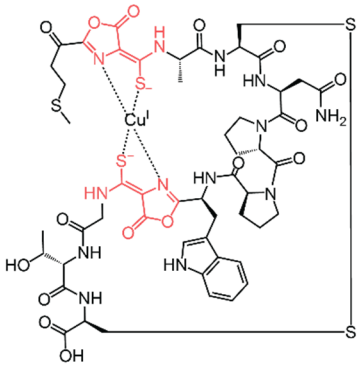

Methylosinus sp. LW4

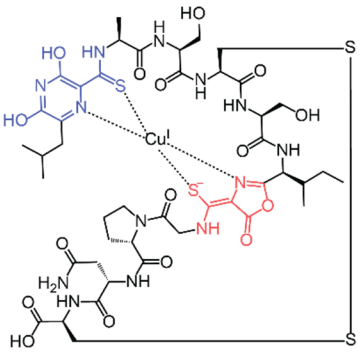

Methylosporium sporium NR3K

Group II

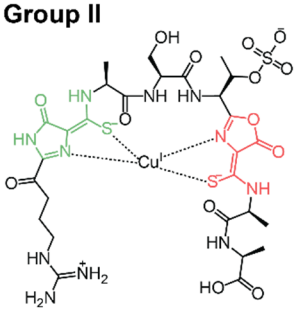

Methylocystis sp. SB2

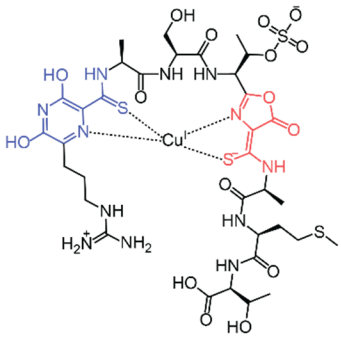

Methylocystis sp. M

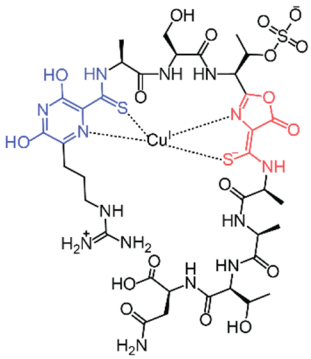

Methylocystis rosea SV97

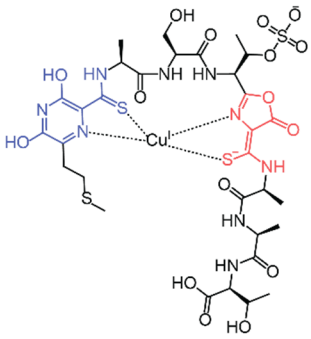

Methylocystis hirsuta CSC1

B

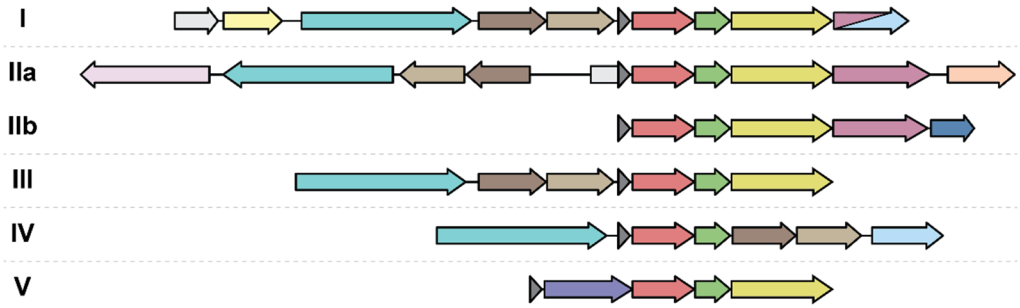

mbnI (ECF sigma factor)
mbnR (anti-sigma factor)
mbnT (TonB transporter)
mbnP (partner of MbnH)
mbnH (cytochrome c peroxidase)
mbnA (precursor peptide)
mbnB (DUF692)
mbnC (partner of MbnB)
mbnM (MATE efflux pump)
mbnF (FAD-dependent oxidoreductase)
mbnN (aminotransferase)
mbnE (periplasmic binding protein)
mbnS (sulfotransferase)
mbnD (dioxygenase)
mbnX (DUF692)

C

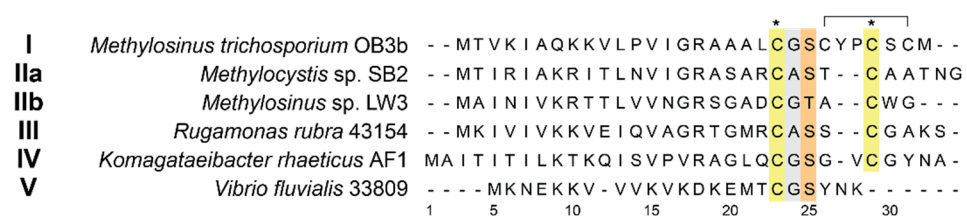

Figure S2. Multiple sequence alignment of MovA homologs present in Proteobacteria. In most cases, precursor sequences were identified through manual search of the genome region upstream of the MovX homolog. Sequence alignment reveals a conserved Thr-Cys-Gly triad and a Tyr-Asn dipeptide motif. Conserved residues within the core region are marked with a star.

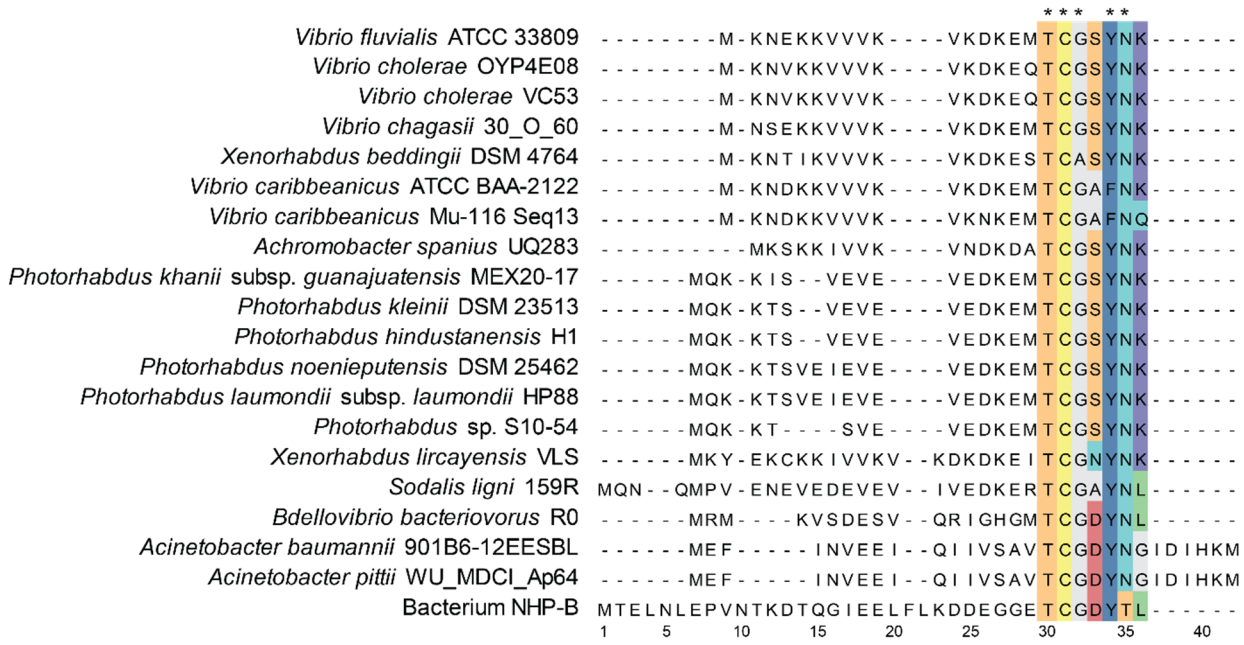

Figure S3. Retention time comparison of trypsin-cleaved unmodified, MovBC-, MovX-, and MovXBC-modified MovA. MovBC- and MovX-modified MovA peptides were obtained via heterologous co-expression of either MovBC or MovX with 6HMBP-MovA, followed by 6HMBP tag cleavage and trypsin digestion. MovXBC-modified MovA was obtained by incubating MovX with MovBC-modified MovA followed by trypsin digestion. Analysis was carried out using an analytical Phenomenex Jupiter C18 column (300 Å, 5 µm, 4.6 mm × 100 mm) operating at 0.6 mL/min. Elution was performed with an isocratic step of 5% acetonitrile in water (+ 0.1% formic acid) for 5 min, followed by a gradient step of 5-35% acetonitrile in water (+ 0.1% formic acid) over 20 min.

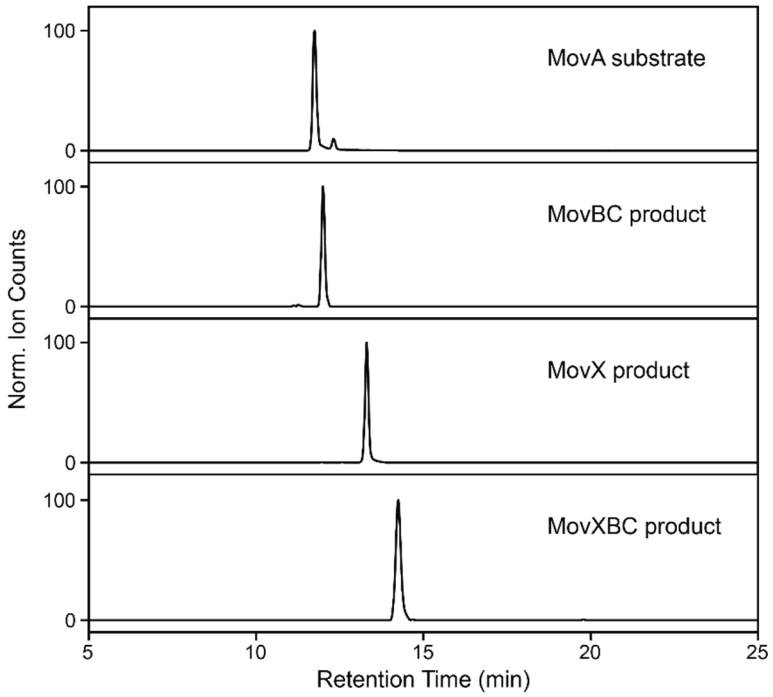

Figure S4. Side products of the MovBC-catalyzed reaction. (A) The MovBC complex catalyzes the formation of an oxazolone-thioamide moiety in product **1**, which can undergo acidic hydrolysis to yield side product **2**, followed by decarboxylation to yield side product **3**.[14] The *m/z* difference of each species relative to the linear substrate is provided. (B) Heterologous co-expression of 6HMBP-MovA with MovBC and subsequent 6HMBP tag cleavage affords species **1a** (calc *m/z* of 814.9096, Δppm = 0.8), **2a** (calc *m/z* of 819.4122, Δppm = 0.6), and **3a** (calc *m/z* of 808.4148, Δppm = 1.0). (C) Similarly, incubation of synthetic MovA with MovBC affords species **1b** (calc *m/z* of 671.3499, Δppm = 1.8), **2b** (calc *m/z* of 675.8525, Δppm = 1.8), and **3b** (calc *m/z* of 664.8551, Δppm = 2.1).

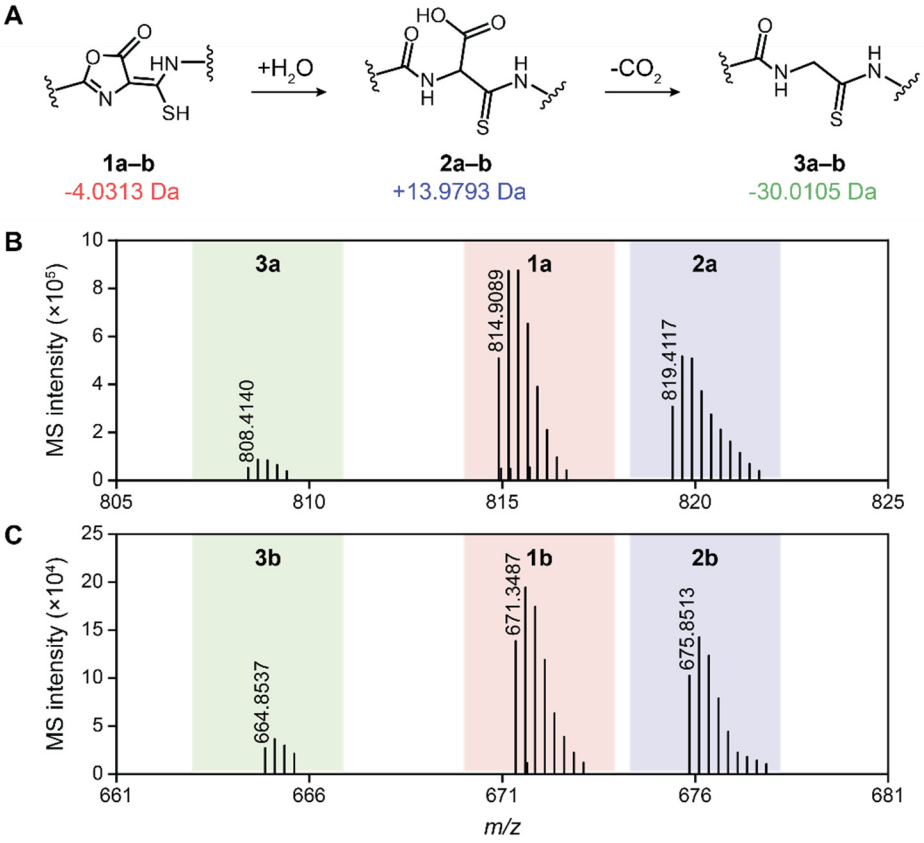

Figure S5. Purified proteins for *in vitro* activity assays. UV-Vis spectra of (A) MovX, (B) MovB, and (C) MovC. (D) SDS-PAGE analysis of purified proteins.

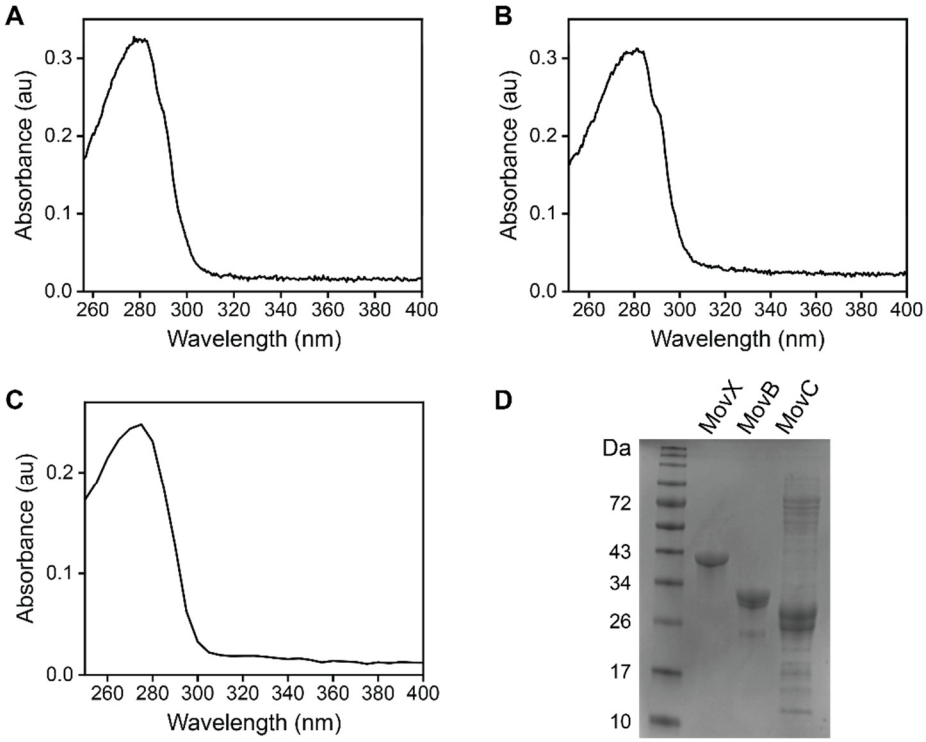

Figure S6. Predicted structure of MovX from *V. fluvialis* 33809. (A) MovX structure predicted by AlphaFold. (B) Predicted structure of MovX (purple) superimposed with crystal structure of an MbnB homolog from *V. caribbeanicus* BAA-2122 (red, PDB 7DZ9). (C) MbnB active site featuring three Fe atoms coordinated by nearby residues and water molecules. (D) Conserved residues that likely coordinate Fe ions in MovX based on the crystal structure of MbnB.

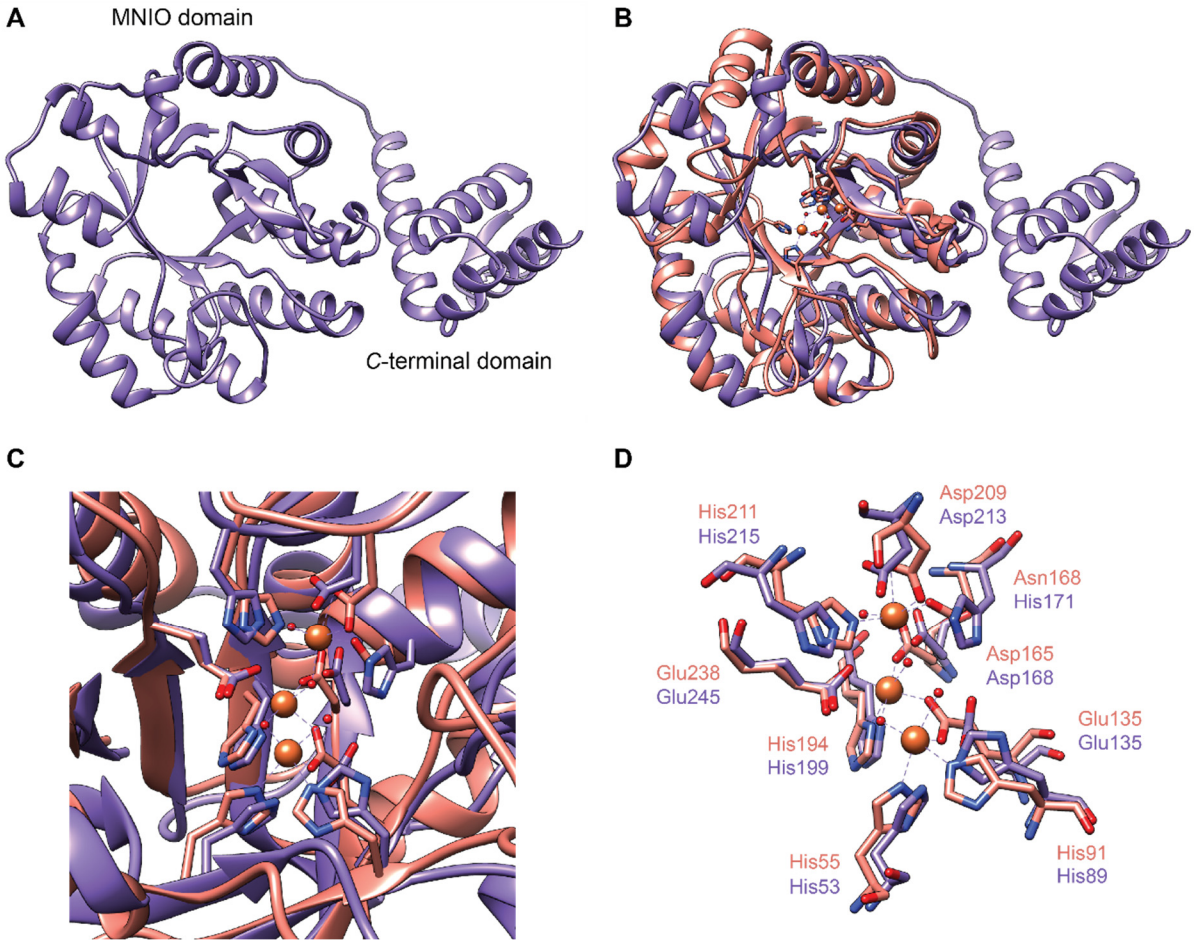

Figure S7. Purified unlabeled, ^{15}Nβ- and $^{15}N_2$-labeled MovA peptides. Purified peptides were analyzed using an analytical Phenomenex Jupiter C18 column (300 Å, 5 µm, 4.6 mm × 100 mm) operating at 0.6 mL/min. Elution was performed with an isocratic step of 5% acetonitrile in water (+ 0.1% formic acid) for 3 min, followed by a gradient step of 5-100% acetonitrile in water (+ 0.1% formic acid) over 8 min and an isocratic step of 100% acetonitrile in water (+ 0.1% formic acid) for 4 min.

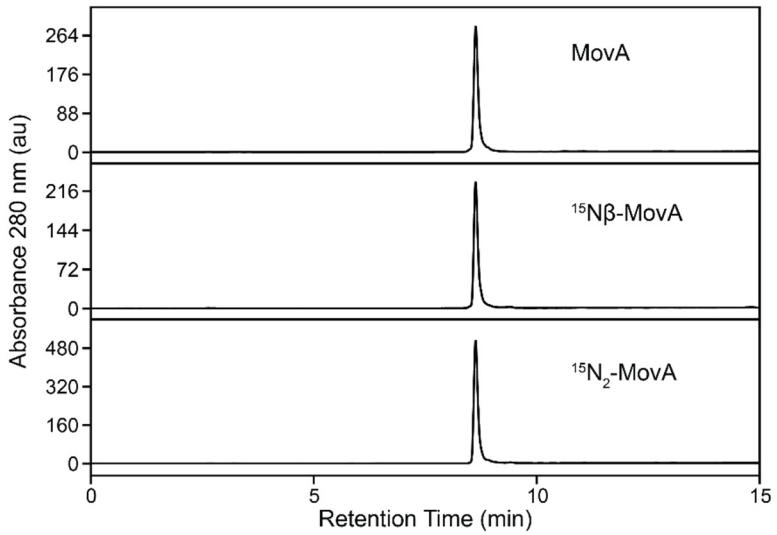

Figure S8. Time-dependent formation of reaction products by (A) MovBC and (B) MovX. Plotted are the integrated extracted ion peaks of each product at different time points. The averages of duplicate reactions are shown.

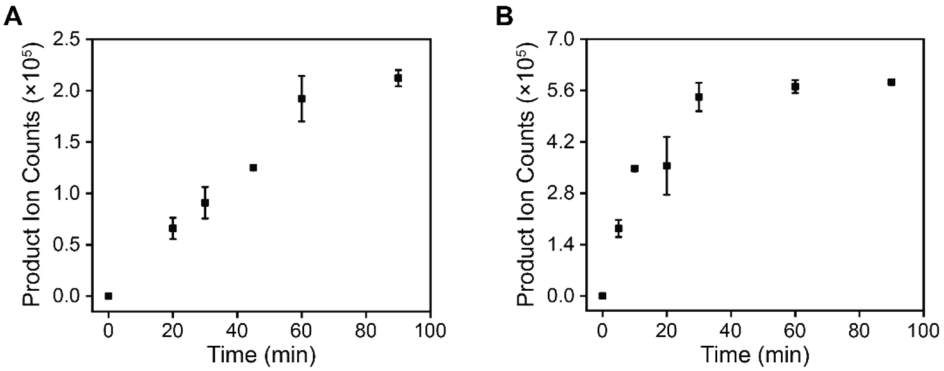

Figure S9. NMR spectra of linear MovA fragment in D_2O. Shown are in order: ^1H, COSY, TOCSY, ROESY, HSQC, and HMBC spectra.

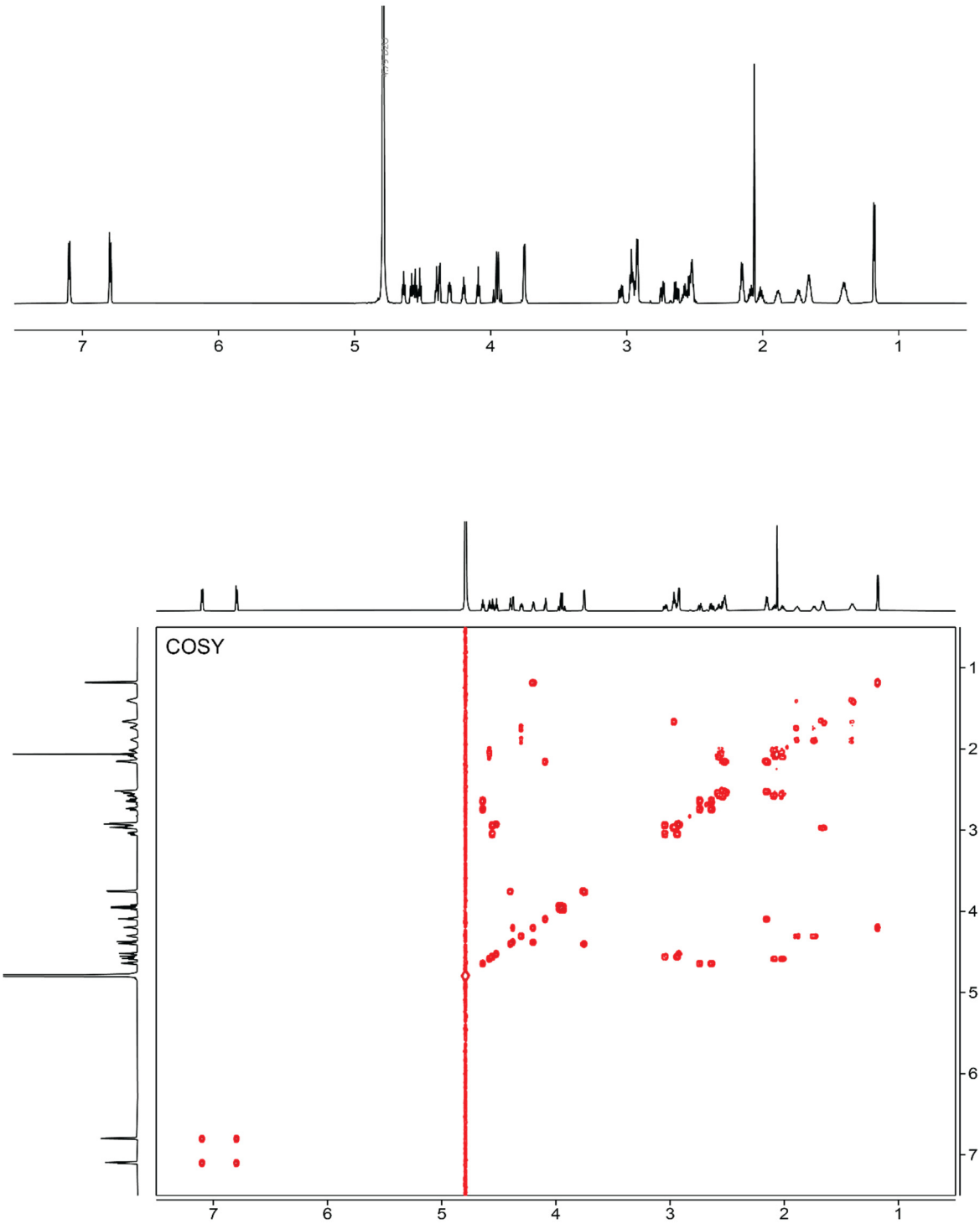

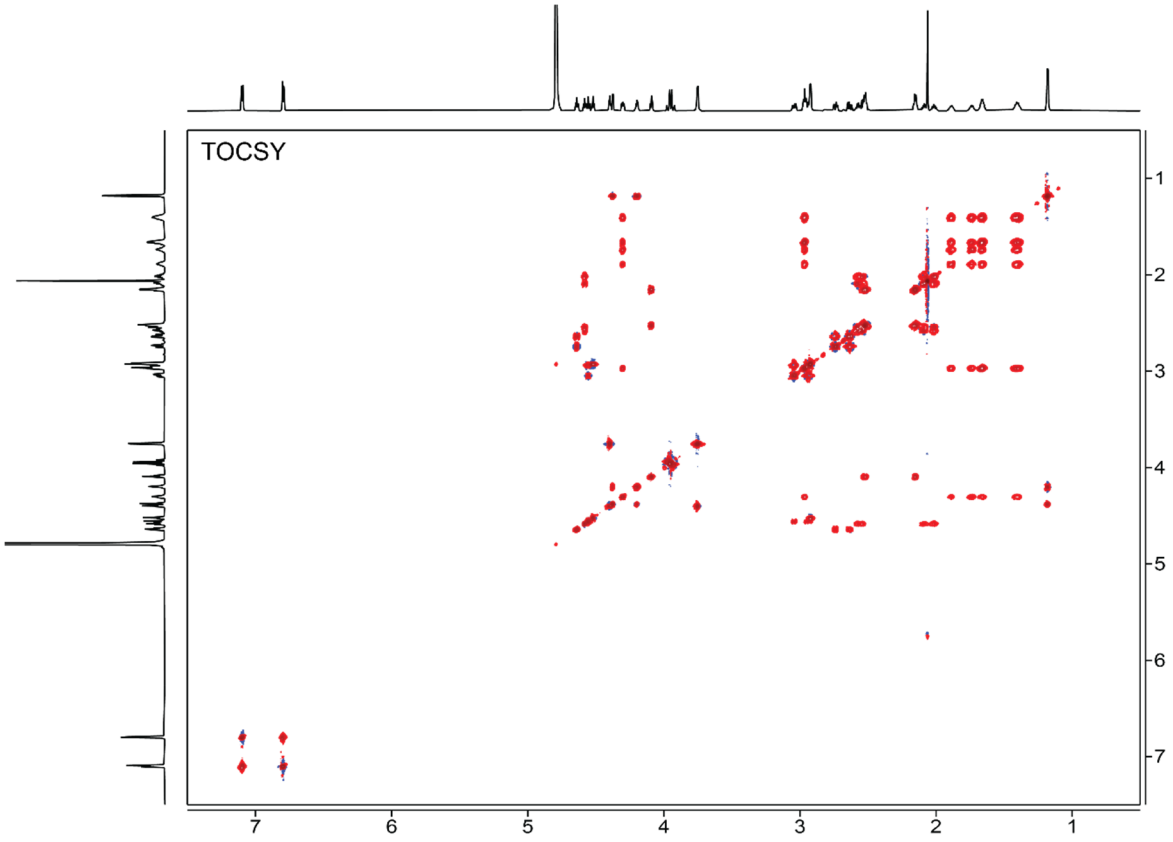

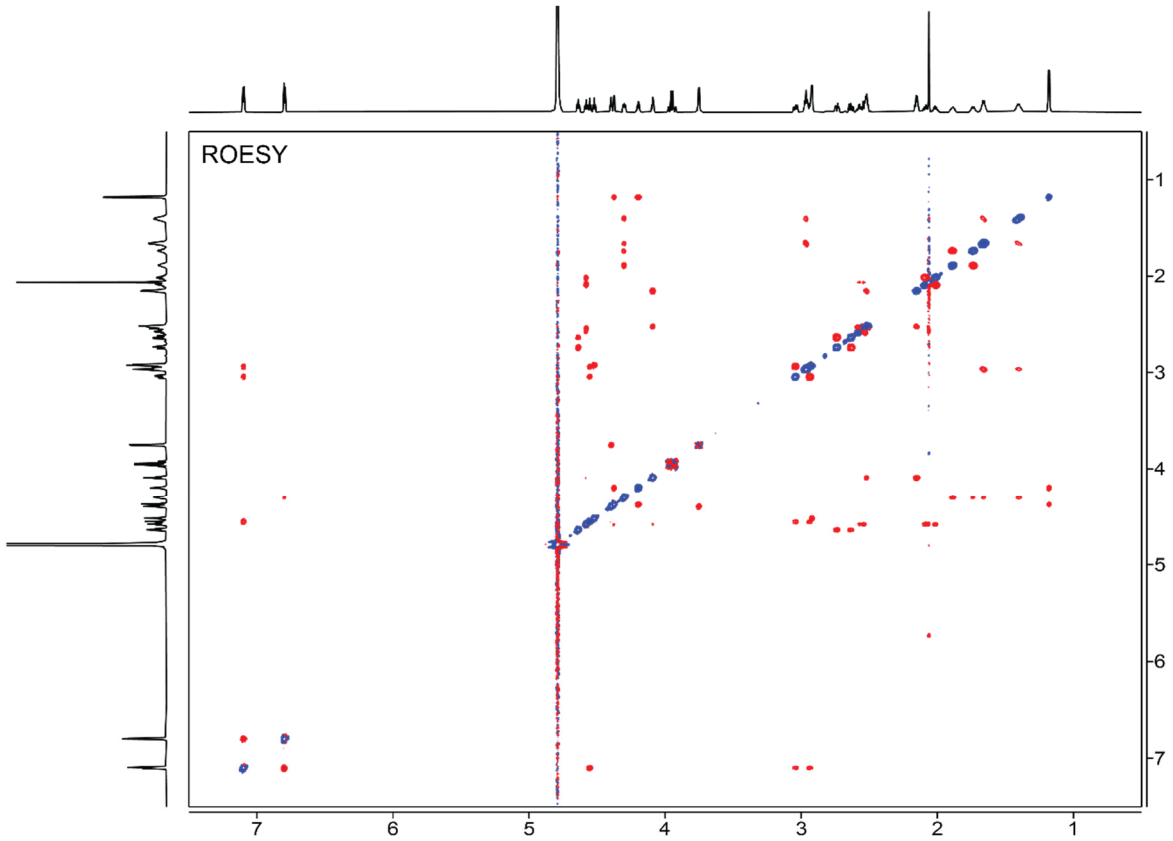

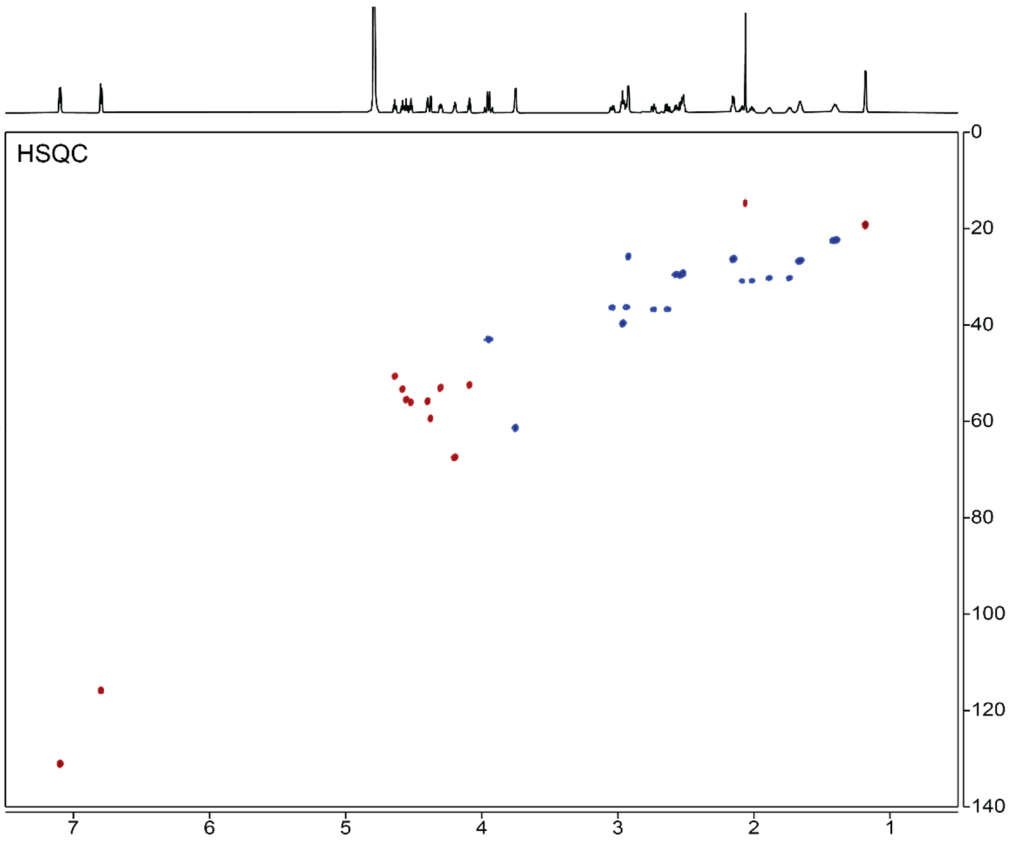

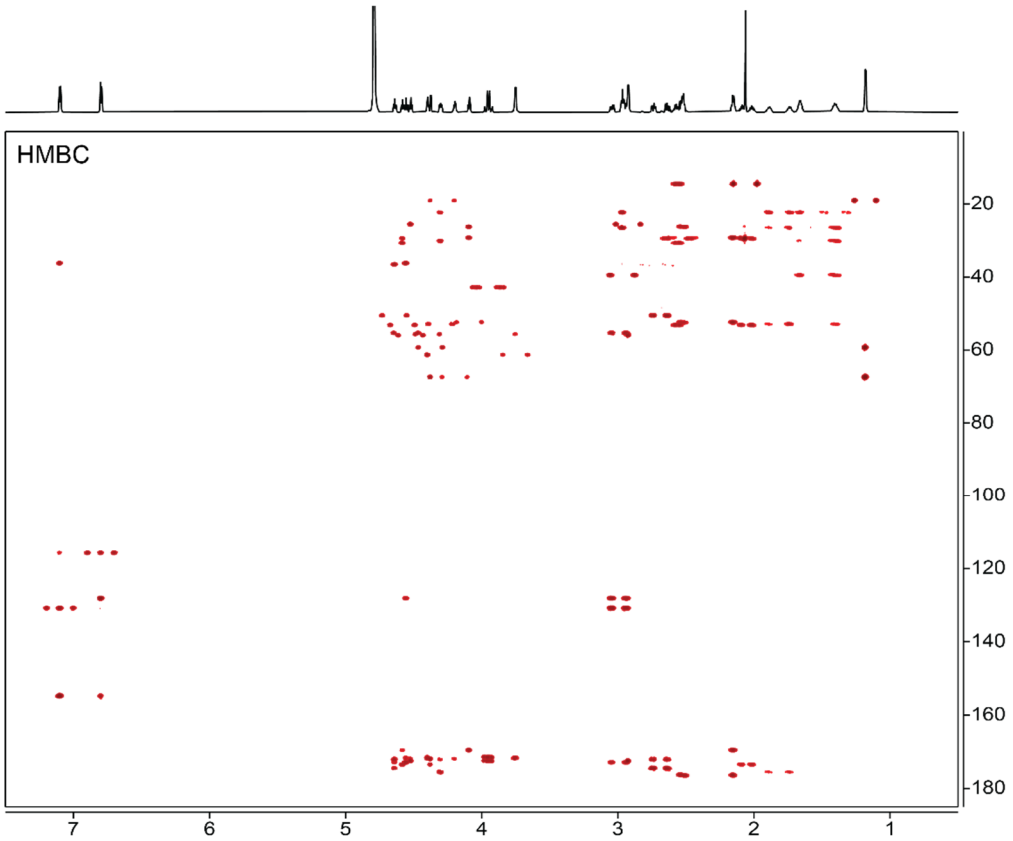

Figure S10. NMR spectra of trypsin-cleaved, MovBC-modified MovA fragment in D_2O. Shown are in order: ^1H, COSY, TOCSY, ROESY, HSQC, and HMBC spectra.

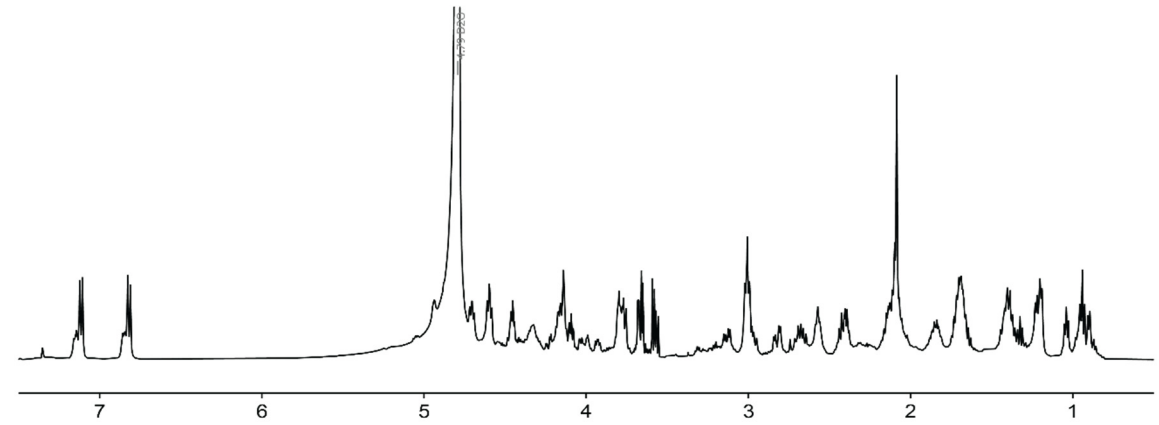

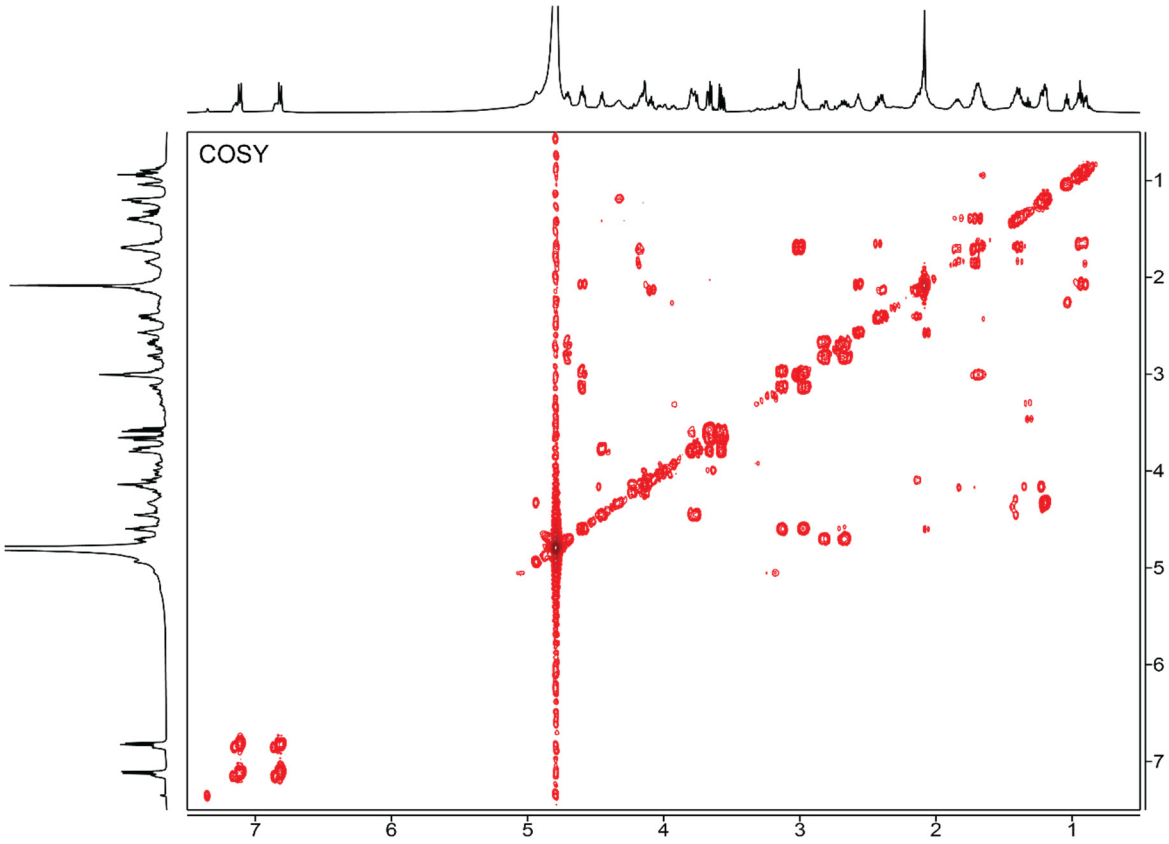

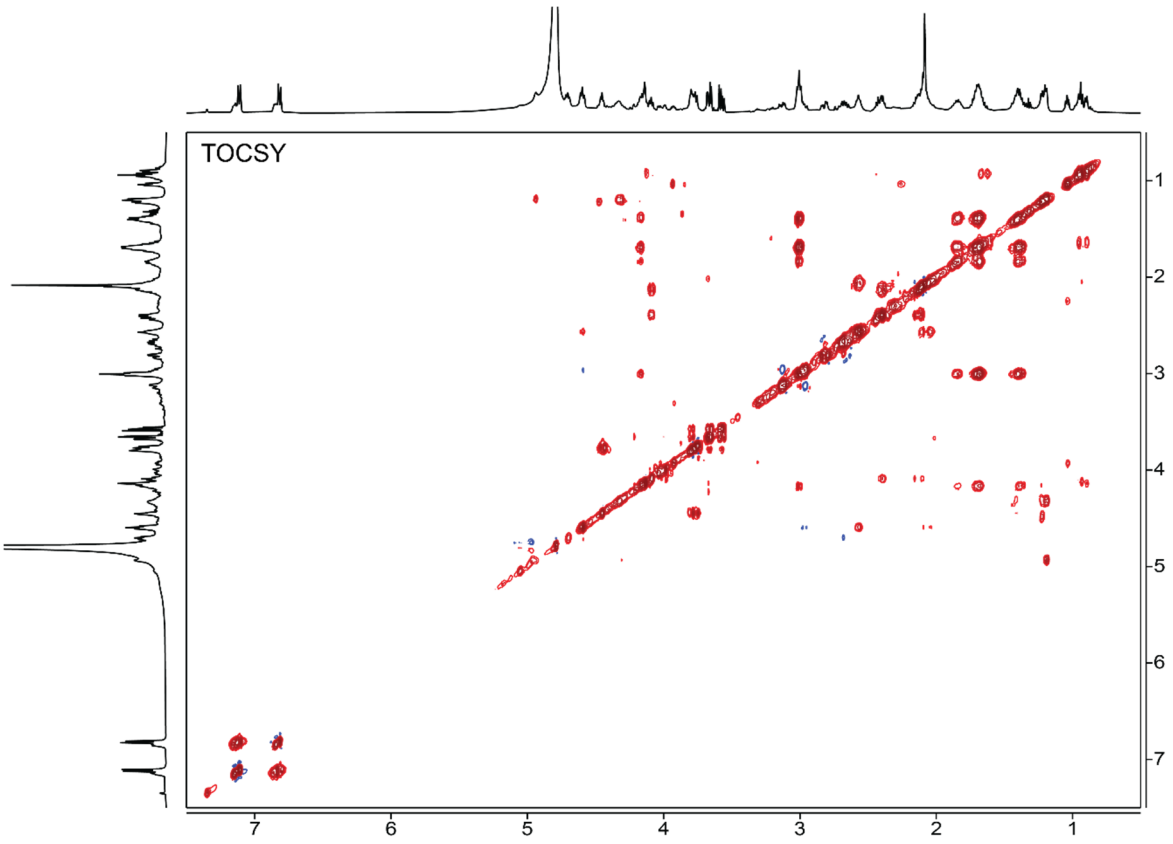

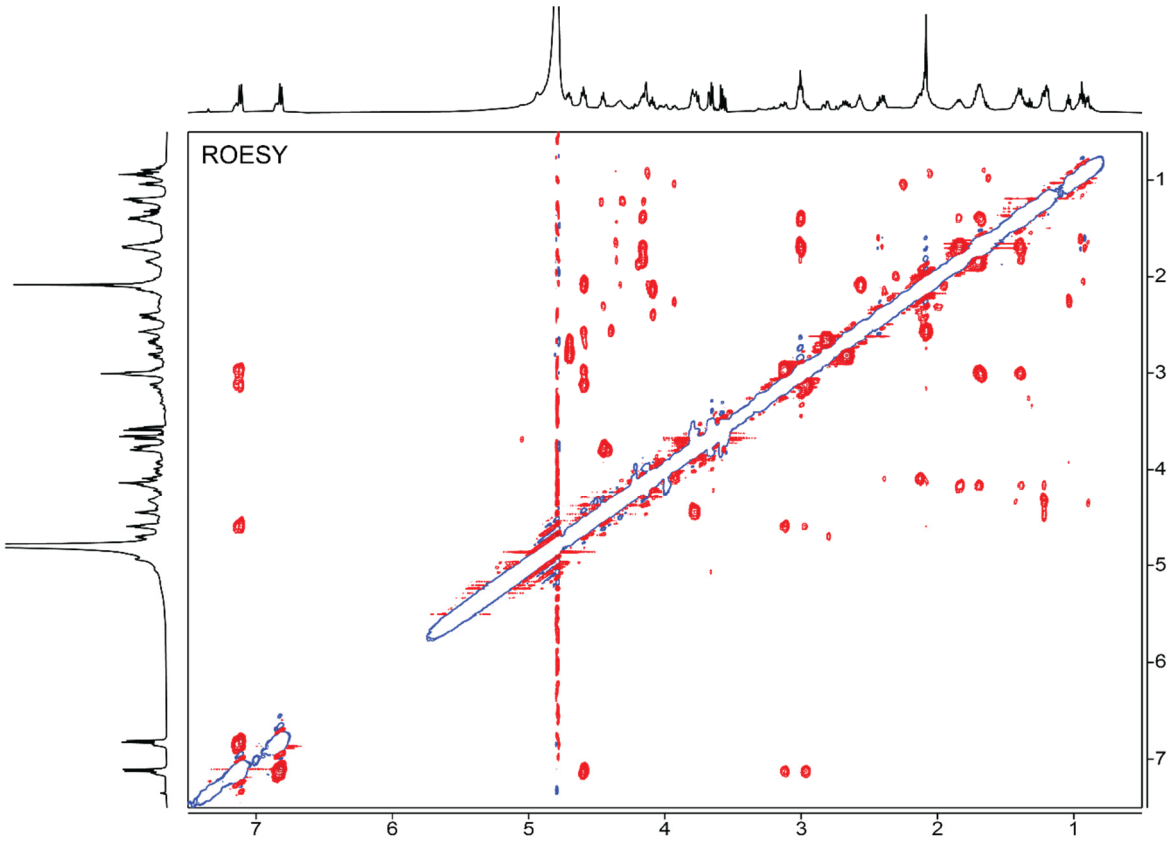

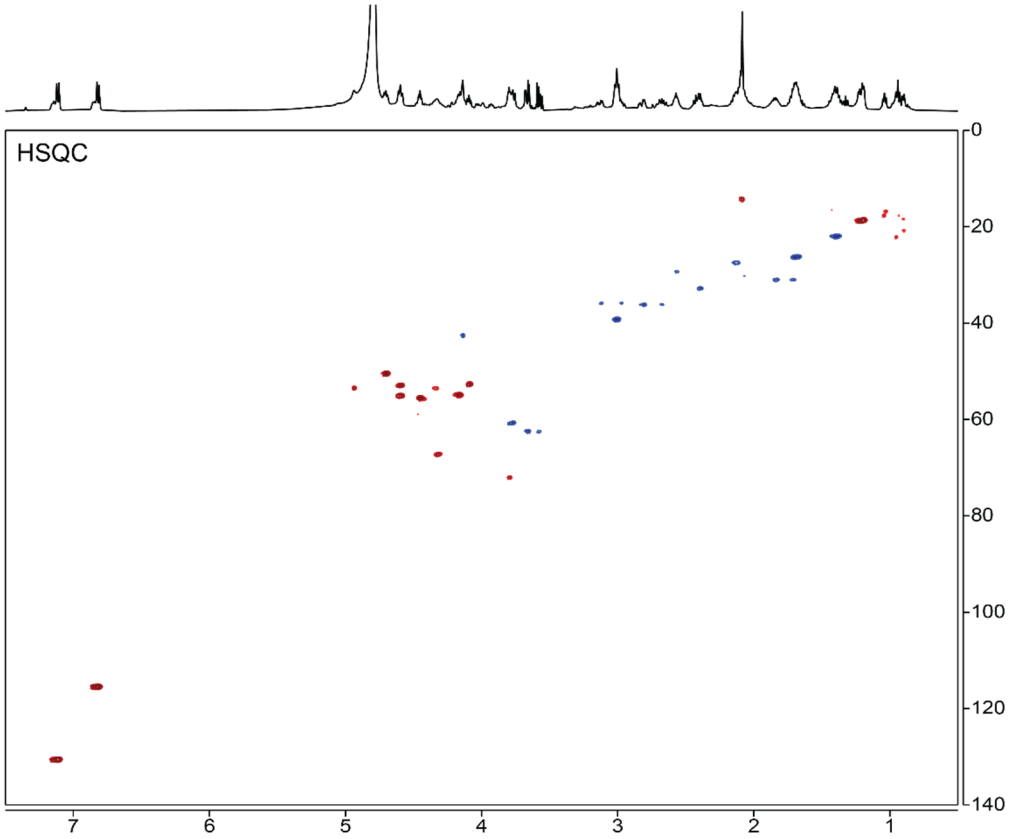

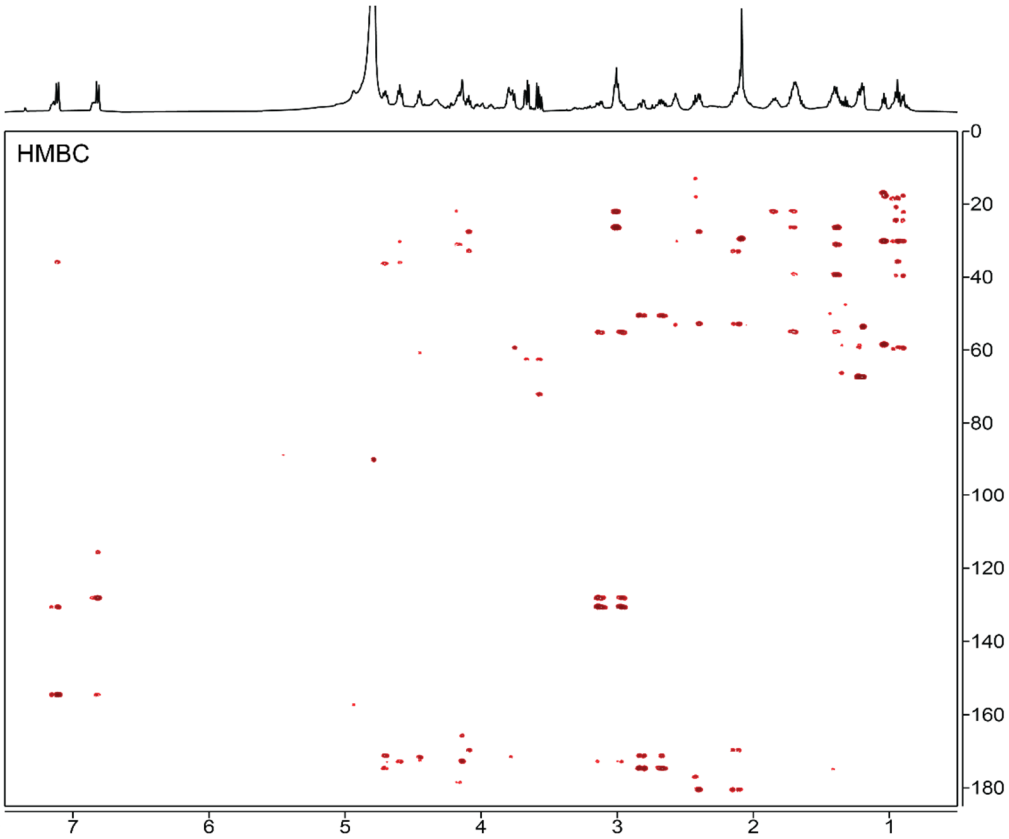

Figure S11. NMR spectra of trypsin-cleaved, MovXBC-modified MovA fragment in D_2O. Shown are in order: ^1H, COSY, TOCSY, ROESY, HSQC, and HMBC spectra.

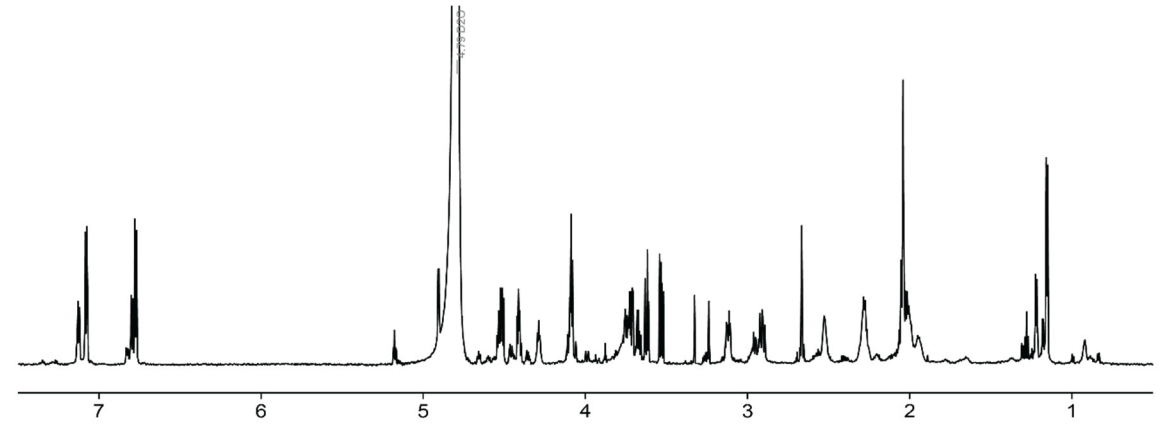

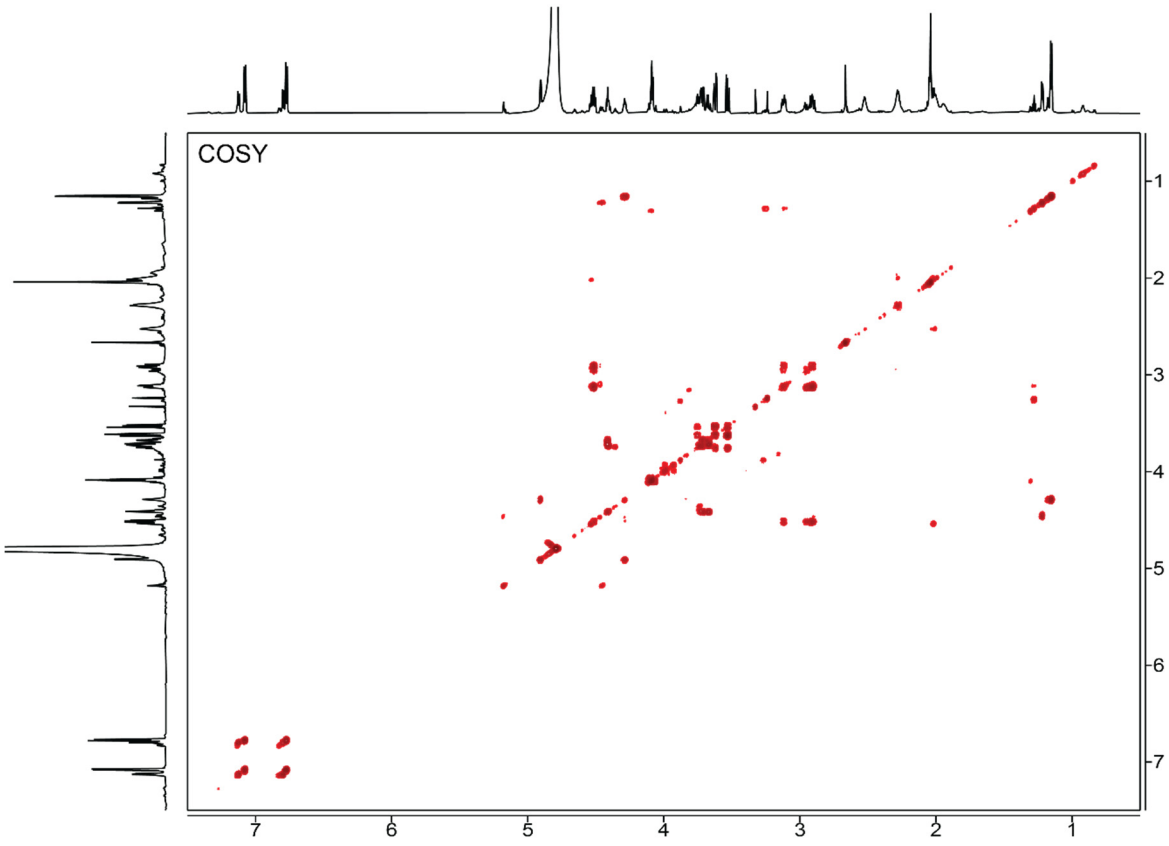

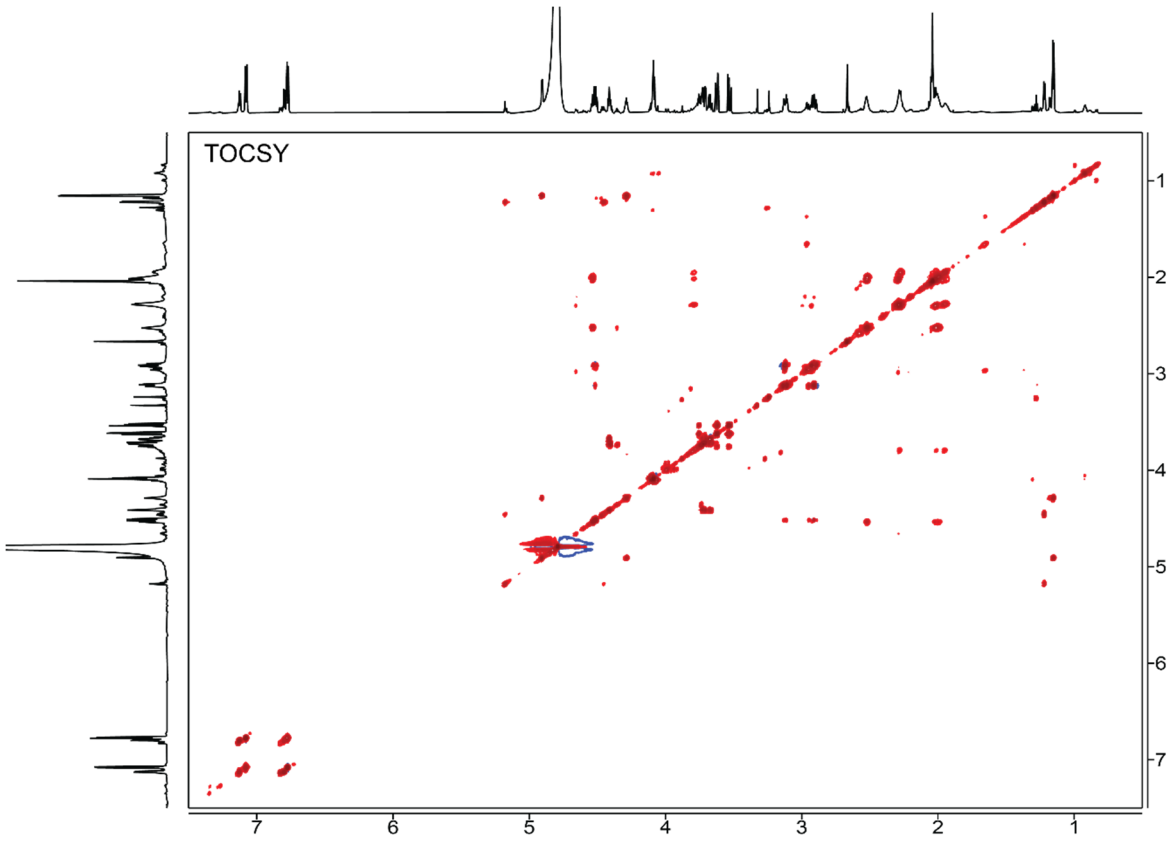

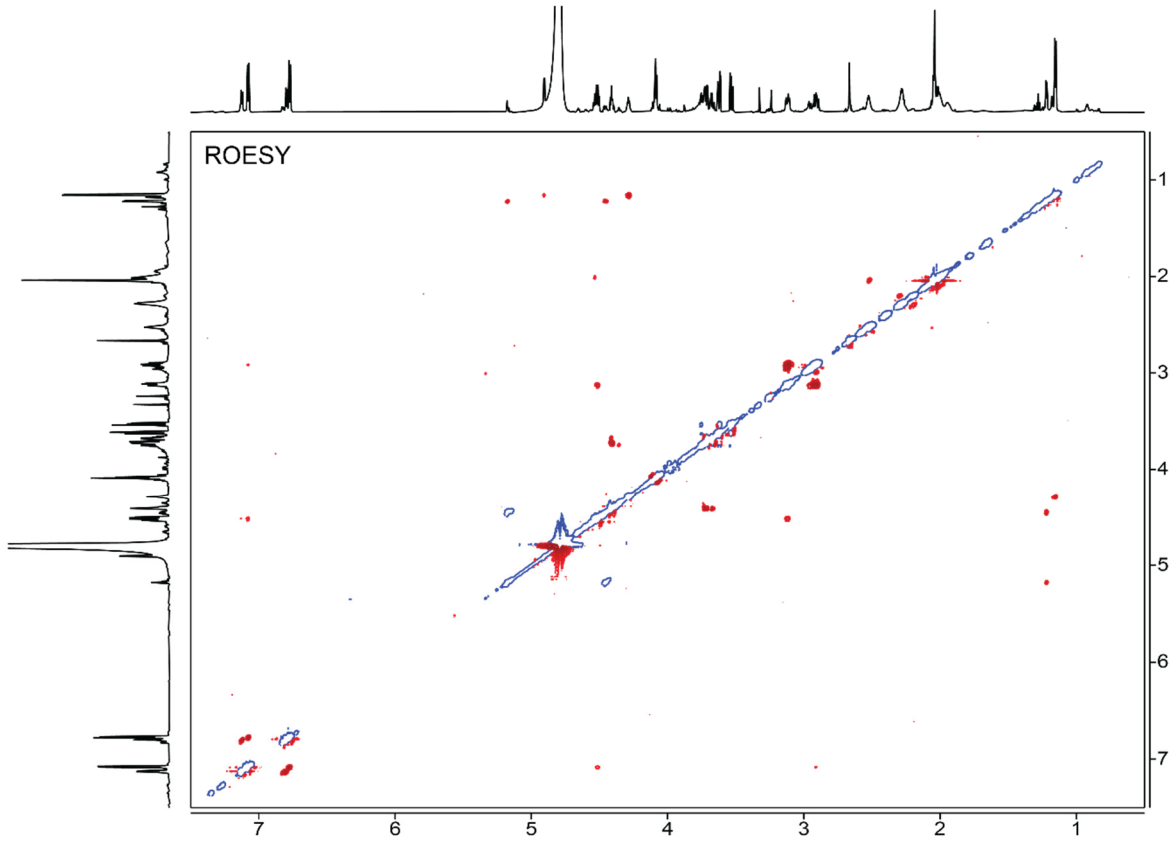

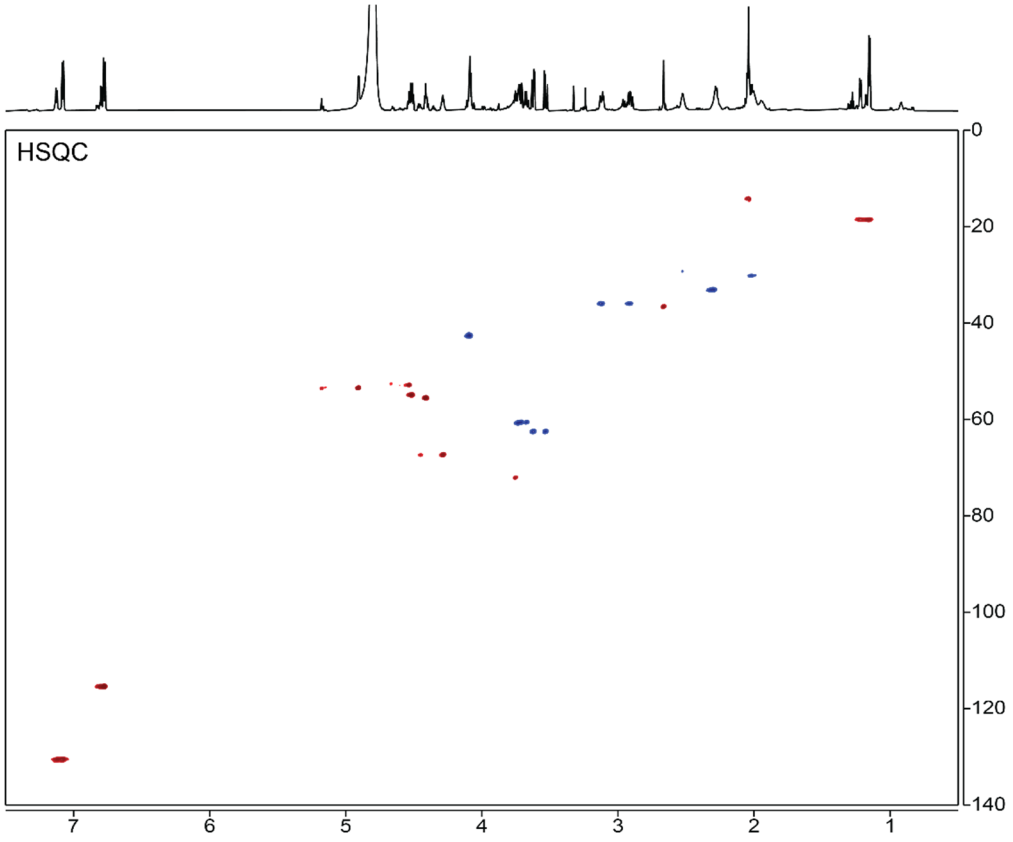

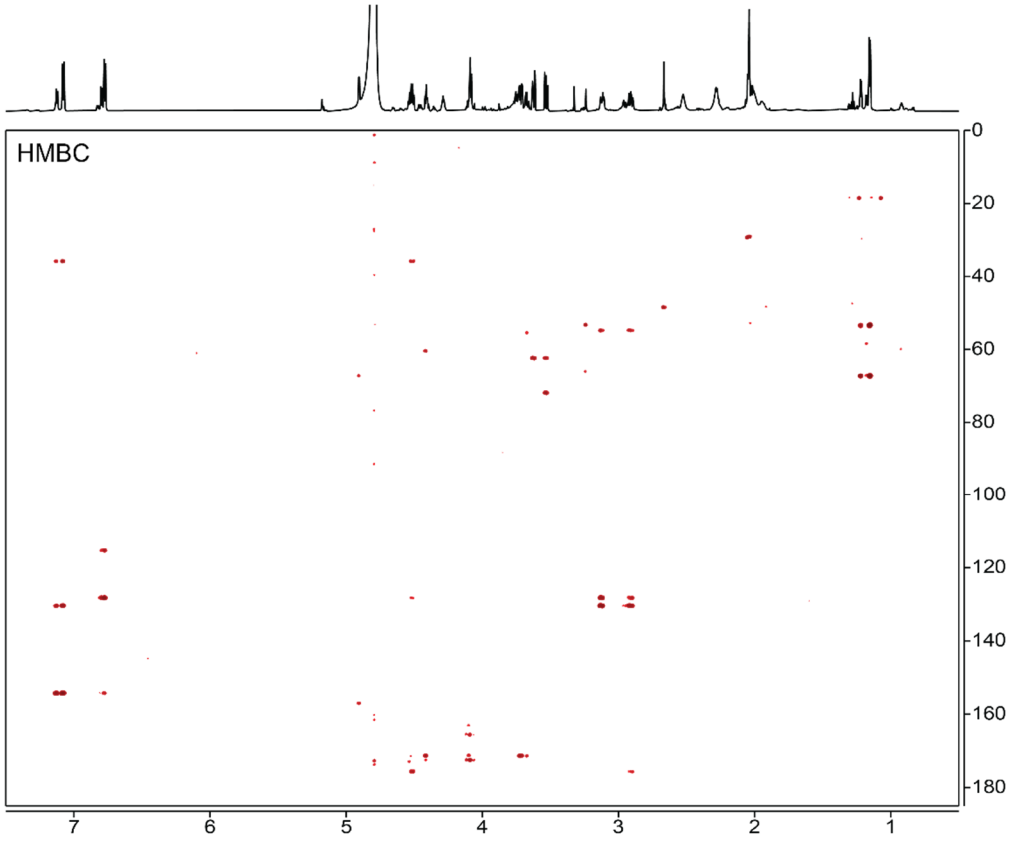

Figure S12. ^{1}H and ^{13}C spectra for *N*β-trityl-L-asparagine ($^{15}N_2$).

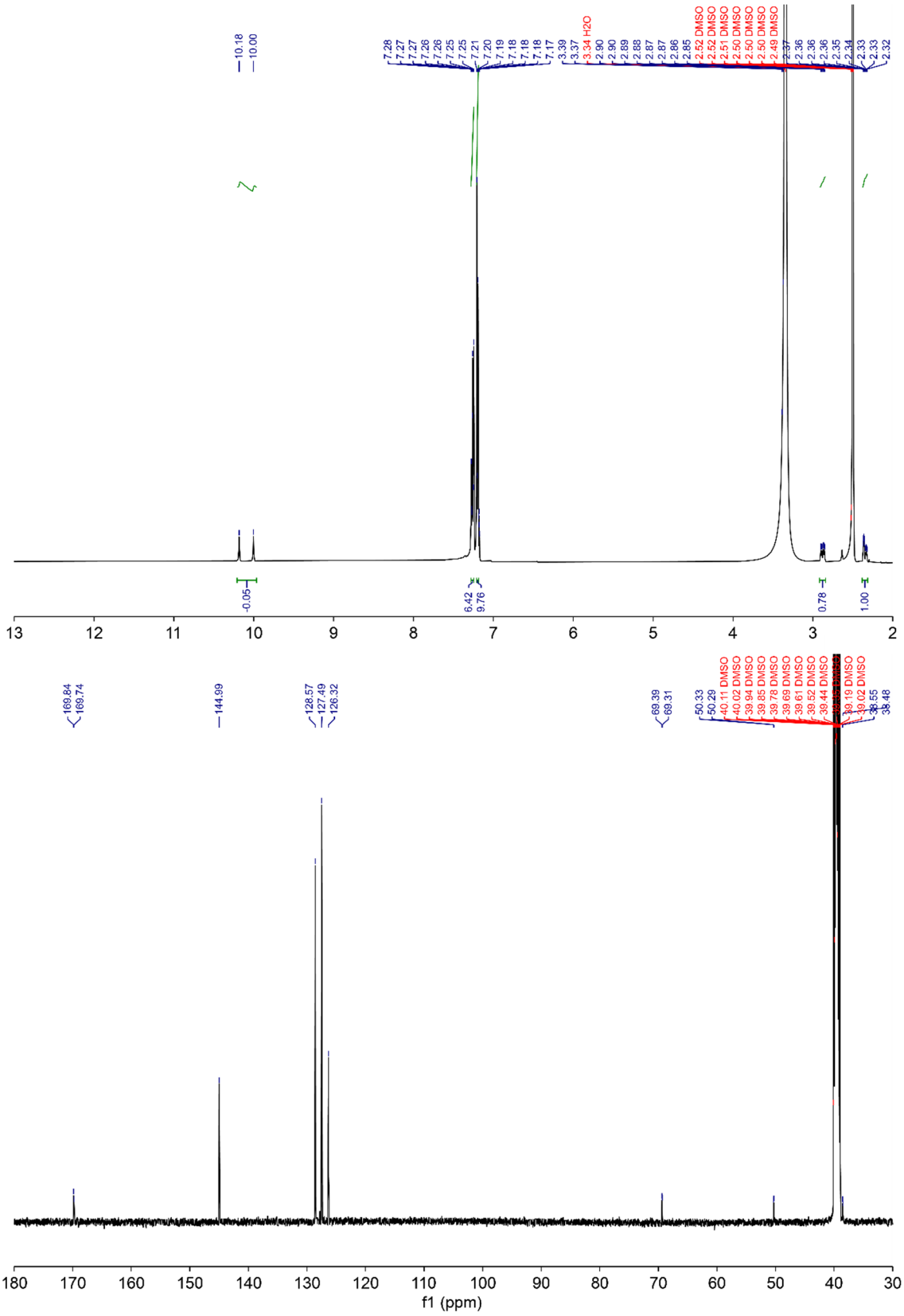

Figure S13. ^{1}H and ^{13}C spectra for *N*α-Fmoc-*N*β-trityl-L-asparagine ($^{15}N_2$).

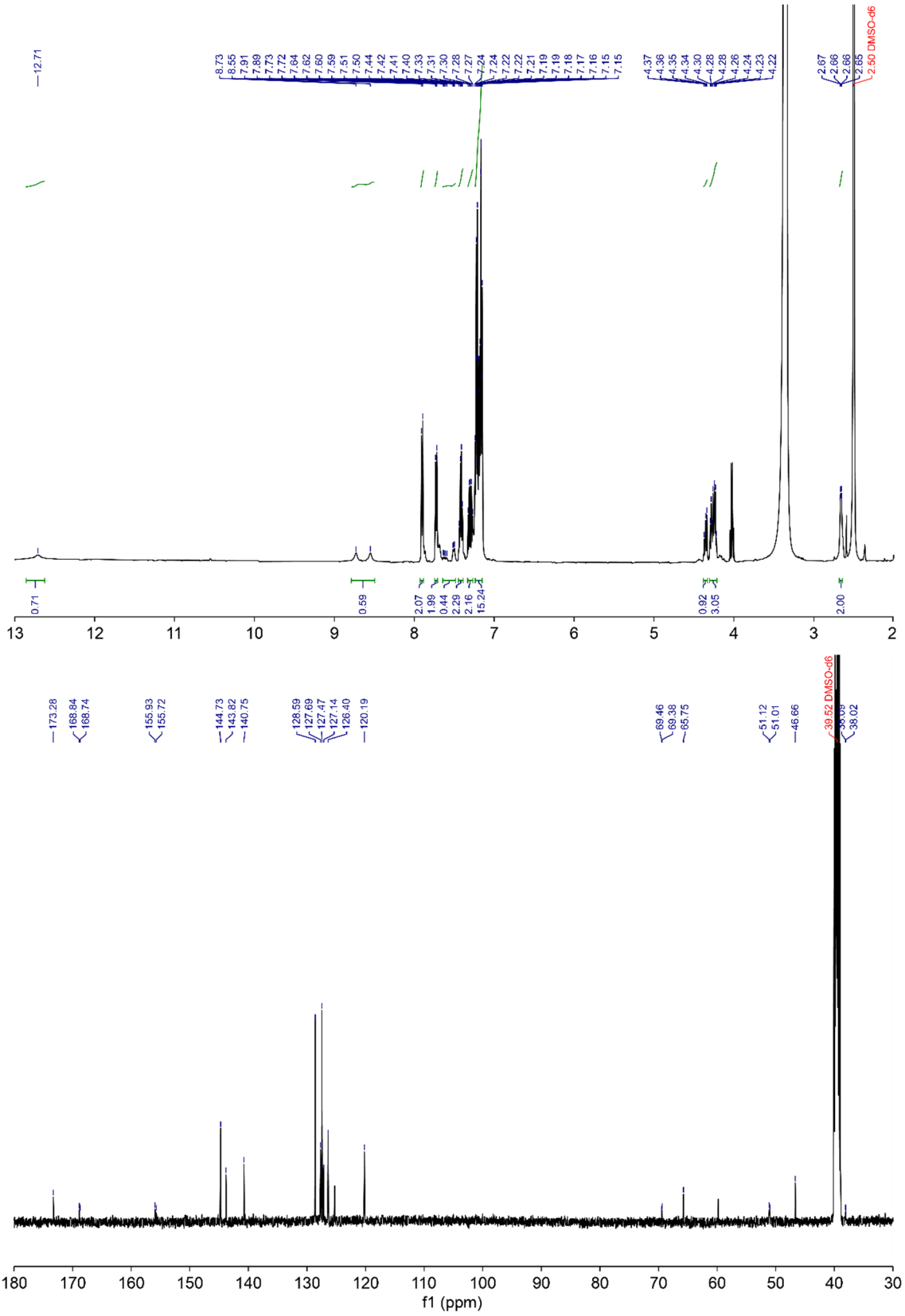

Figure S14. ^{1}H and ^{13}C spectra for *N*β-trityl-L-asparagine ($^{15}N\beta$).

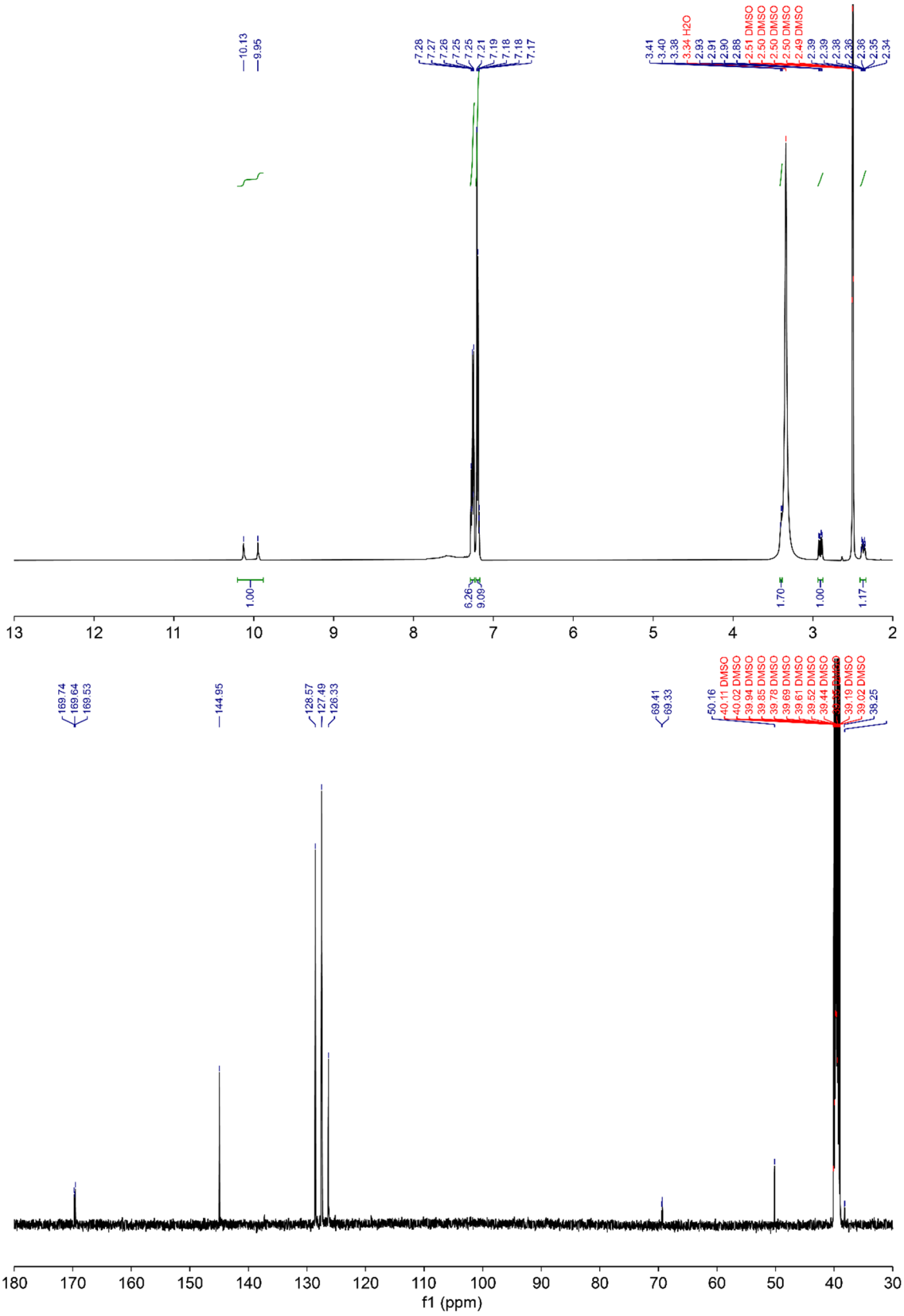

Figure S15. ^{1}H and ^{13}C spectra for *N*α-Fmoc-*N*β-trityl-L-asparagine ($^{15}N\beta$).

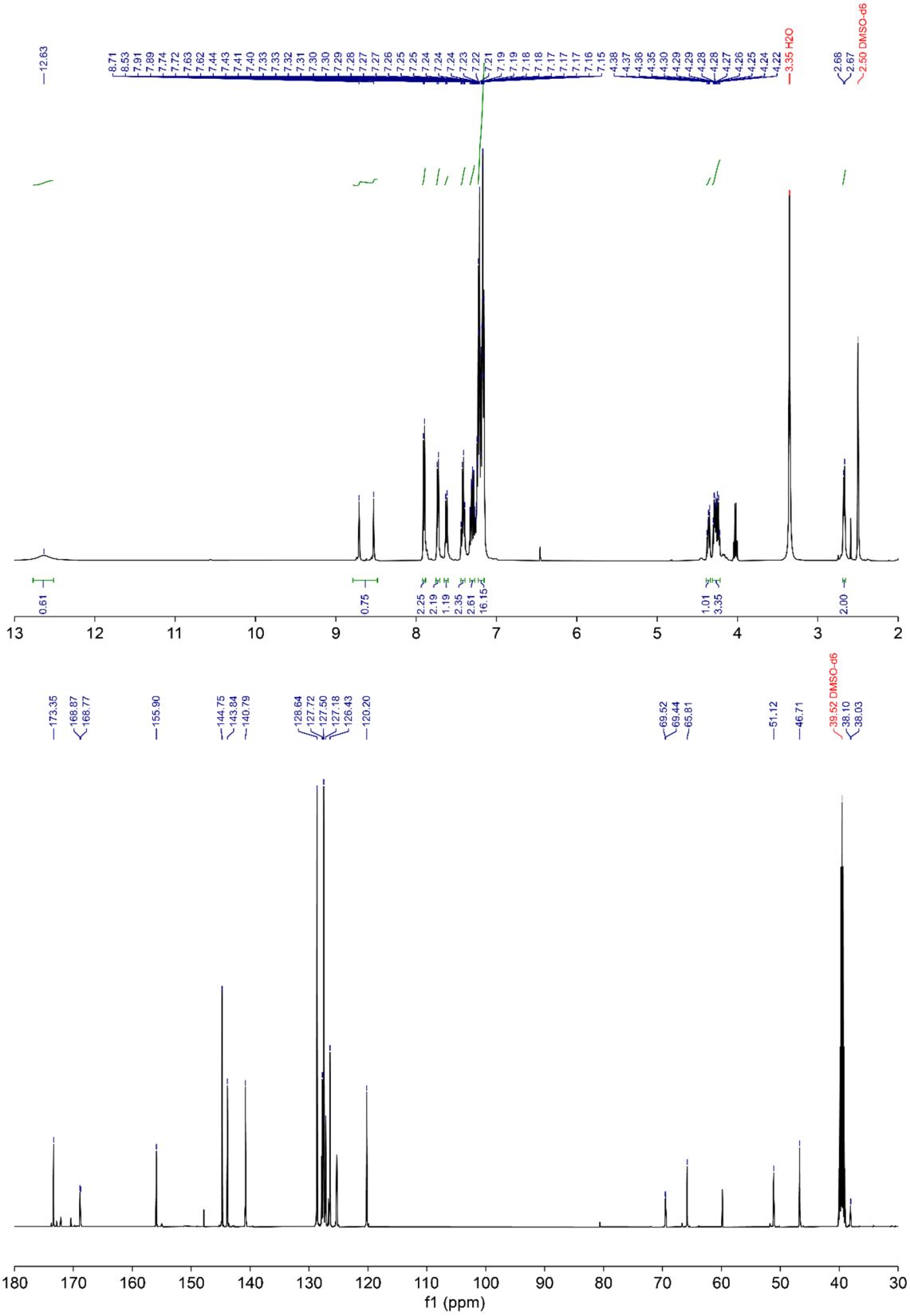

Figure S16. Detection of H_2O_2 using the Amplex Red assay. (A) In the presence of H_2O_2, horseradish peroxidase (HRP) reacts with the Amplex Red reagent to produce resorufin, a fluorescent product. Coupling the Amplex Red assay to the MovX reaction allows for the detection of MovX-dependent H_2O_2 production. (B) Time-dependent formation of resorufin in the presence of MovX. Reactions contained 100 µM Amplex Red reagent, 1 U/mL HRP, 200 µM MovA, and varying concentrations of MovX (0, 2, and 5 µM) in assay buffer. Fluorescence was measured at excitation/emission 530/590 nm using a Biotek Synergy H1 plate reader (BioTek). The averages of duplicate reactions are shown. The fluorescent product accumulates only in the presence of MovX and displays a dose-dependent behavior with regards to MovX concentration, suggesting that MovX generates H_2O_2 during catalysis or through uncoupling pathways.

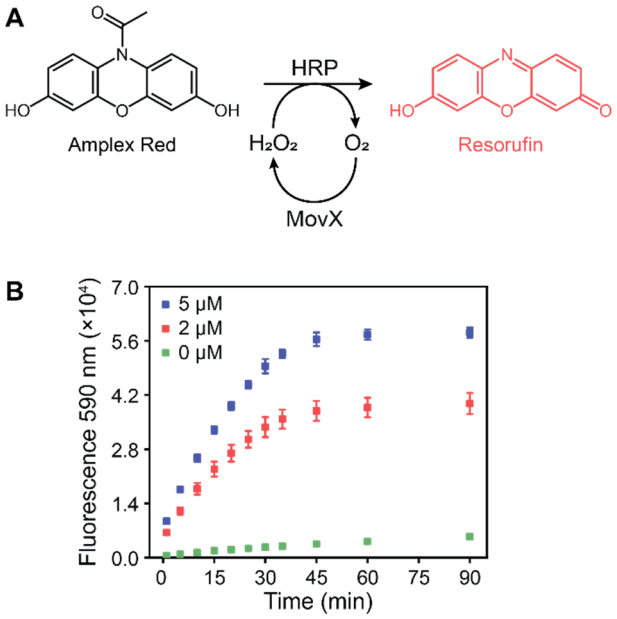

Supporting References

(1) Salis, H. M.; Mirsky, E. A.; Voigt, C. A. Automated Design of Synthetic Ribosome Binding Sites to Control Protein Expression. *Nat. Biotechnol.* **2009**, *27*, 946–950.

(2) Azem, A.; Kessel, M.; Goloubinoff, P. Characterization of a Functional GroEL14(GroES7)2 Chaperonin Hetero-Oligomer. *Science* **1994**, *265*, 653–656.

(3) Bushin, L. B.; Covington, B. C.; Rued, B. E.; Federle, M. J.; Seyedsayamdost, M. R. Discovery and Biosynthesis of Streptosactin, a Sactipeptide with an Alternative Topology Encoded by Commensal Bacteria in the Human Microbiome. *J. Am. Chem. Soc.* **2020**, *142*, 16265–16275.

(4) Kenney, G. E.; Dassama, L. M. K.; Pandelia, M.-E.; Gizzi, A. S.; Martinie, R. J.; Gao, P.; DeHart, C. J.; Schachner, L. F.; Skinner, O. S.; Ro, S. Y.; Zhu, X.; Sadek, M.; Thomas, P. M.; Almo, S. C.; Bollinger, J. M.; Krebs, C.; Kelleher, N. L.; Rosenzweig, A. C. The Biosynthesis of Methanobactin. *Science* **2018**, *359*, 1411–1416.

(5) Park, Y. J.; Jodts, R. J.; Slater, J. W.; Reyes, R. M.; Winton, V. J.; Montaser, R. A.; Thomas, P. M.; Dowdle, W. B.; Ruiz, A.; Kelleher, N. L.; Bollinger, J. M.; Krebs, C.; Hoffman, B. M.; Rosenzweig, A. C. A Mixed-Valent Fe(II)Fe(III) Species Converts Cysteine to an Oxazolone/Thioamide Pair in Methanobactin Biosynthesis. *Proc. Natl. Acad. Sci. USA* **2022**, *119*, e2123566119.

(6) Hennessy, D. J.; Reid, G. R.; Smith, F. E.; Thompson, S. L. Ferene — a New Spectrophotometric Reagent for Iron. *Can. J. Chem.* **1984**, *62*, 721–724.

(7) Elgaher, W. A. M.; Hamed, M. M.; Baumann, S.; Herrmann, J.; Siebenbürger, L.; Krull, J.; Cirnski, K.; Kirschning, A.; Brönstrup, M.; Müller, R.; Hartmann, R. W. Cystobactamid 507: Concise Synthesis, Mode of Action, and Optimization toward More Potent Antibiotics. *Chem. Eur. J.* **2020**, *26*, 7219–7225.

(8) Behling, L. A.; Hartsel, S. C.; Lewis, D. E.; DiSpirito, A. A.; Choi, D. W.; Masterson, L. R.; Veglia, G.; Gallagher, W. H. NMR, Mass Spectrometry and Chemical Evidence Reveal a Different Chemical Structure for Methanobactin That Contains Oxazolone Rings. *J. Am. Chem. Soc.* **2008**, *130*, 12604–12605.

(9) Kenney, G. E.; Goering, A. W.; Ross, M. O.; DeHart, C. J.; Thomas, P. M.; Hoffman, B. M.; Kelleher, N. L.; Rosenzweig, A. C. Characterization of Methanobactin from Methylosinus Sp. LW4. *J. Am. Chem. Soc.* **2016**, *138*, 11124–11127.

(10) Baslé, A.; El Ghazouani, A.; Lee, J.; Dennison, C. Insight into Metal Removal from Peptides That Sequester Copper for Methane Oxidation. *Chem. Eur. J.* **2018**, *24*, 4515–4518.

(11) Krentz, B. D.; Mulheron, H. J.; Semrau, J. D.; Dispirito, A. A.; Bandow, N. L.; Haft, D. H.; Vuilleumier, S.; Murrell, J. C.; McEllistrem, M. T.; Hartsel, S. C.; Gallagher, W. H. A Comparison of Methanobactins from Methylosinus Trichosporium OB3b and Methylocystis Strain Sb2 Predicts Methanobactins Are Synthesized from Diverse Peptide Precursors Modified to Create a Common Core for Binding and Reducing Copper Ions. *Biochemistry* **2010**, *49*, 10117–10130.

(12) El Ghazouani, A.; Baslé, A.; Gray, J.; Graham, D. W.; Firbank, S. J.; Dennison, C. Variations in Methanobactin Structure Influences Copper Utilization by Methane-Oxidizing Bacteria. *Proc. Natl. Acad. Sci. USA* **2012**, *109*, 8400–8404.

(13) Kenney, G. E.; Rosenzweig, A. C. Genome Mining for Methanobactins. *BMC Biol.* **2013**, *11*, 1–17.

(14) Dou, C.; Long, Z.; Li, S.; Zhou, D.; Jin, Y.; Zhang, L.; Zhang, X.; Zheng, Y.; Li, L.; Zhu, X.; Liu, Z.; He, S.; Yan, W.; Yang, L.; Xiong, J.; Fu, X.; Qi, S.; Ren, H.; Chen, S.; Dai, L.; Wang, B.; Cheng, W. Crystal Structure and Catalytic Mechanism of the MbnBC Holoenzyme Required for Methanobactin Biosynthesis. *Cell Res.* **2022**, *32*, 302–314.